UNIVERSITY OF CALIFORNIA

Los Angeles

# On the Genome Release Dynamics of Single-Stranded RNA Viruses.

A dissertation submitted in partial satisfaction of the

requirements for the degree Doctor of Philosophy

in Chemistry

by

Richard William Sportsman

2020

ABSTRACT OF THE DISSERTATION

On the Genome Release Dynamics of Single-Stranded RNA Viruses.

By

Richard William Sportsman

Doctor of Philosophy in Chemistry

University of California, Los Angeles, 2020

Professor William M. Gelbart, Chair

Measurements are described that begin to elucidate the mechanism by which some RNA viruses deliver their genetic information to their hosts. The work focuses on two closely related icosahedral viruses, Cowpea Chlorotic Mottle Virus and Brome Mosaic Virus. Each consists of a 28-nm diameter icosahedral protein shell, the capsid, containing an approximately 3000-nt long single-stranded RNA. We hypothesize that the RNA inside the capsid is delivered to the host's ribosomes by a thermal fluctuation of an end of the RNA being made available in a process called co-translational delivery. In this process, an end of the RNA fluctuates out of an intact capsid, is captured by the ribosomal machinery and is pulled out of the capsid under force.

We conducted studies to characterize RNA fluctuations that occur through capsid pores by capturing an RNA end. To realize this capture we have utilized ribosomes and purified eukaryotic initiation factor complex eIF4F. This complex is known to initiate the cap-dependent translation process of mRNA by eukaryotic ribosomes. In other studies, the fluctuations of the RNA outside of the capsid were captured by utilizing biotinylated fluorescent RNA which were caught by streptavidin-coated surfaces or nanoparticles.

Additionally we obtained preliminary data using magnetic tweezers to measure the forces required to extract RNA from a capsid with a protruding RNA end. Rather than capture a fluctuation in this force measurement work, we designed a virus like particle construct dubbed a “cherry bomb”. We produced this construct by packaging, in vitro, an RNA where its 5’ terminus had been made rigid by hybridizing to it a length of complementary DNA that is sufficiently long, such that it cannot be accommodated within the virus capsid.

Finally, we investigated how RNA can be condensed at the single-molecule level using polyvalent cations and observe changes in how a condensed RNA can be packaged into virus like particles by viral capsid protein.

Our results hint at the inherent dynamics of the viral RNA genome and its capsid shell, and the complex processes involved in a virus interacting with its host, processes that have been difficult to measure using other structural biological or physical chemical techniques.

The dissertation of Richard William Sportsman is approved.

Giovanni Zocchi

Shimon Weiss

William M. Gelbart, Committee Chair

University of California, Los Angeles

2020

# Table of Contents

# List of Figures

**Acknowledgments**

I would like to thank my two mentors Professor William M. Gelbart and Professor Charles M. Knobler for the opportunity to work in the laboratory. Getting the chance to talk “shop” with them everyday in the lab has been a truly unique experience. Both are wonderful mentors, writers, scientists, and *people* among many other admirable qualities. Our group’s members have been an incredible group of scientists and friends to get to know and work with. Without their charity, tenacity, brilliance, skepticism and warmth this work would have been very difficult to start and complete. I have learned a lot from members of the group over the years, and hopefully, I have been helpful in some of their endeavors. I would like to thank my committee members Professors Todd Yeates, Shimon Weiss, Sri Kosuri, and Giovanni Zocchi for stimulating discussions and helpful advice. I would like to thank Nati Alcaraz, Dr. Jenette Kropat, Elida Escalante, Dr. Martin L. Phillips, Ricky Ruiz, Dr. William Silkworth, Dr. Stacie Nakamoto, Ivo Atanasov and others who have been so wonderful to work with and have contributed a lot to keeping Young Hall and the CNSI a welcoming place to work.

I would like to acknowledge permission granted to reprint figure 6 from the following journal article reference, as figure 1 in the introduction of this dissertation: Florence Tama, Charles L. Brooks, The Mechanism and Pathway of pH Induced Swelling in Cowpea Chlorotic Mottle Virus, Journal of Molecular Biology, Volume 318,

Issue 3, 2002, Pages 733-747, https://doi.org/10.1016/S0022-2836(02)00135-3.

I would like to acknowledge my co-authors on the 2015 Journal of American Chemical Society paper Professors William M. Gelbart, Charles M. Knobler, Vinothan Manoharan, Dr. Rees F Garmann and Dr. Christian E. Beren. Chapter 4 is a pre-published draft of the final manuscript. Citation below.

Garmann RF, Sportsman R, Beren C, Manoharan VN, Knobler CM, Gelbart WM. A Simple RNA-DNA Scaffold Templates the Assembly of Monofunctional Virus-Like Particles. *J. Am. Chem. Soc*. 2015;137(24):7584-7587. doi:10.1021/jacs.5b03770

Chapter 6 is a draft of a work to be submitted, so I would like to acknowledge my furture co-authors, Liya Oster, Ana Luisa Duran-Meza, Martin L. Phillips, and Professors William M. Gelbart and Charles M. Knobler. Much of this work was funded by an NSF research grant provided to the Gelbart lab during much of our time at UCLA.

I would like to acknowledge a three year NIH Chemistry and Biology Interface (CBI) training grant I received. In this acknowledgement, I would also like to thank Professor Heather Maynard, who directed the CBI program during my time at UCLA, peers, and staff, who were all instrumental in keeping this program strong. Therefore to acknowledge that program, I have included the award number here; USPHS National Research Service Award 5T32GM008496.

I would like to thank Professors David Bensimon and Vincent Croquette and the ABCD Biophysics group, especially Martin Rieu, from the Ecole Normale Superieure for hosting me to complete the magnetic tweezer experiments. Also a special thanks to Professor James Bowie and Dr. Duyoung Min for collaborating with me to repeat these magnetic tweezer experiments at UCLA. This material is based upon research

supported by the Chateaubriand Fellowship of the Office for Science & Technology of the Embassy of France in the United States.

I had a lucky break to work with very talented peers, including many undergraduates, post docs, researchers, graduate students, and professors, who contributed or offered advice in the process of producing this work. This dissertation is dedicated to their persistence, brilliance, kindness and advice over the years.

I am greatly indebted to my family and close friends who have made this journey fulfilling. They have kept me inspired and focused and so I owe a lot of gratitude for them nudging me on. A special thanks to my housemates who have helped us all stay grounded and balanced through the sometimes arduous path of doing science. Finally, to Cathy, for being a thoughtful, kind and patient mentor, a friend and a partner on all of the switchback trails.

**Vita**

**Richard W. Sportsman**

**Education**
University of California, Los Angeles, Department of Chemistry & Biochemistry
Ph.D. Chemistry, Areas of Focus: Biophysics & Virology April 2020

University of California, Santa Cruz, Department of Chemistry
B.S. Biochemistry and Molecular Biology, with Honors June 2012

**Research Experience**
UCLA, Department of Chemistry & Biochemistry
Graduate Student Researcher, and Teaching Assistant 2013 – present

UCSC, Department of Chemistry, Undergraduate Researcher, 2009 – 2011

**Fellowships**
NIH Chemistry and Biology Interface Training Grant 2014 – 2017

Chateaubriand Graduate Student Fellow 2018 – 2019

**Publications**
Garmann RF, Sportsman R, Beren C, Manoharan VN, Knobler CM, Gelbart WM. A Simple RNA-DNA Scaffold Templates the Assembly of Monofunctional Virus-Like Particles. *J Am Chem Soc*. 2015;137(24):7584-7587. doi:10.1021/jacs.5b03770

Sportsman RW, Jin Y. A Personally Tailored RNA Cancer Immunotherapy*. AME Medical Journal. 2, (10), 2017*

# Chapter 1

## Introduction

Viruses offer ideal systems of study because they are a simplified biological entity with understandable, yet, astonishing complexity. A virus, and specifically its particle form – the virion – consists of *at least* two components, a nucleic acid and a protein coat, which together form a capsid, the container which protects and delivers the genetic cargo in its journey to its next host. The viruses that are the focus of this dissertation are Cowpea Chlorotic Mottle Virus (CCMV) and Brome Mosaic Virus (BMV); both are icosahedrally-symmetric viruses which contain single-stranded RNA (ssRNA) as their genetic cargo, enclosed by 180 identical copies of a capsid protein, forming the capsid shell of the virion.

Since there are many different types of viruses present on earth, we focus on classifying them into two types, a gross oversimplification, but nevertheless a valid one for purposes of the biophysical approach that we have taken to study them. The first group includes double-stranded viruses, whose pre-assembled *empty* capsid shells are

filled with double-stranded nucleic acid genomes, usually by a viral-derived DNA packaging motor that uses ATP of the host to package the DNA into the capsid; these viruses often have pressure-based genome release mechanisms, (e.g. T7, lambda, T4 phages or Herpes Simplex Virus-1)[1]. The second group with drastically different life cycles, consist of single-stranded nucleic acid viruses that usually rely on a spontaneous co-self-assembly process; here the single-stranded genome acts as a large negatively charged scaffold for positively-charged capsid protein to interact with and with proper cytosolic conditions, eventually the capsid proteins can re-organize around the RNA to form a symmetric shell (e.g., many of the alphaviruses, HIV, Hepatitis C virus, picornaviruses like poliomyelitis and others).

Our group has recently focused on the bromovirus family, specifically Brome Mosaic Virus (BMV), the type species, and Cowpea Chlorotic Mottle Virus (CCMV). These two icosahedral viruses have served as models for virus self-assembly since the mid-1960's, when the first demonstration of an icosahedral virus *in vitro* reconstitution was reported[2,3]. This came only a few years after the first reconstitution of a helical, rod-shaped, virus capsid, Tobacco Mosaic Virus, from its component RNA and capsid protein parts by Fraenkel-Conrat & Williams[4], which was in turn a follow-up of the work by Takahashi and Ishii[5,6] wherein empty TMV rods and other assembly products were produced upon dropping the pH of the purified TMV capsid protein solution. These viruses are excellent models for viral self-assembly as they can be easily reconstituted from only two purified components, the capsid protein of the virus and an RNA of sufficient length. 180 copies of the selected bromovirus capsid protein - through largely electrostatic attractions to the RNA and a variety of interactions between proteins -

forms a protective truncated icosahedron protein shell around the RNA. The icosahedron is one of the “Platonic solids”, a regular, convex polyhedron, with twenty triangular faces, and twelve vertices, described in depth by the Greek philosopher Plato and expounded upon by the Greek geometer Euclid in the *Elements*. As geometry and biology have intertwined, advancing our understanding of virus self-assembly and delivery for over 60 years, much has been revealed regarding viruses life cycles. How the process of viral self-assembly produces a symmetric capsid, has remained an active area of research, both in basic and applied studies, to better understand the kinetics of the process, develop gene therapies and potentially thwart the viral self-assembly process.[7,8]

In the natural infections of the bromoviruses the virion may be transported by a vector such as an aphid/beetle to a new host plant, such that the virus can be replicated again. As will be noted below, the virus must make contact with exposed cytoplasm of the host plant, and often this cytoplasm is made available by either plant abrasion or insects biting/damaging the plant and releasing the virus.

In many plant viruses, the viral genome is segmented, with multiple RNAs necessary for an active infection. In the case of the bromoviruses, these RNAs are packaged in separate virions, making them *multi-partite* viruses, each virion containing a different molecule of the genomic RNA, with the total amount of RNA per capsid being ~3000 nucleotides. While many studies have worked on the complex host-virus interactions that are necessary for the virus to survive[9–12], there remain many steps in the viral life cycle that are not well understood, especially regarding the disassembly of the virus.

We chose to focus on a question that has vexed virologists for over 50 years. *If a virus particle, particularly an icosahedrally symmetric one, can self-assemble spontaneously into a relatively stable capsid, then how does the genetic cargo initially get out of the capsid to access and take advantage of the host cell biochemical and genetic machinery?*

To study this question, we must first consider a few factors that may influence RNA structure within the capsid and how it may be able to release the genome once it enters the host cytoplasm. Many viruses change their conformational state upon being delivered to and interacting with a host cell's surface and during the process of being taken inside the cell[6]. A route that many plant viruses take is through delivery by insect carriers that take virus up from an infected plant and deliver it to another plant, usually by abrasion or biting into the plant, generating damaged cells with their cytoplasm exposed. Inside the insect's gut/mouth parts, solution conditions are typically slightly acidic (pH 4-5) and contain high concentrations (approximately millimolar) of divalent cations such as calcium, conditions that are known *in vitro* to favor the compact ("un-swollen") conformation of the virion as visualized by cryo-EM single-particle reconstructions and x-ray crystal structures.[13] Once the capsid has been transported and subsequently released into the host cell's cytoplasm – where it experiences a low free-divalent cation concentration along with a pH of ~7.4 – it is likely to promote the swelling of the capsid. This is suggested by the fact that under *in vitro* conditions of pH 7.4 along with low concentration of divalent cations the capsid is known to swell radially as much as 10 percent in diameter from the compact virion form; further, by cryo-EM

and x-ray crystallography, it has been observed that at the three fold axis of the virion pores increase in diameter from 0.5 nm to about 2 nm.[13]

A simple hypothesis, proposed by T.M.A. Wilson and colleagues,[14] is the idea that the viral RNA is made accessible to the host through this swelling transition observed *in vitro* and that RNA may be pulled out of the capsid shell by the host's ribosome. In fact, for purified systems of capsids and cell-free extracts, this has been observed for the bromoviruses and tobamoviruses that infect plants, and other alphaviruses that infect mammals such as semliki forest virus.[14,15] Following co-incubation of different viruses with ribosome extracts, density gradient centrifugation analysis and electron micrographs reveal the presence of poly-ribosome capsid complexes. From these studies it has been speculated that only one end of the RNA, the 5' end, may be necessary to be made available to the ribosome factors such that the RNA can be pulled out of the capsid by the mRNA translocating ribosome. This process, often referred to as co-translational disassembly, is dependent on ATP and GTP, charged tRNAs, amino acids and functional ribosomes and their associated protein factors. We prefer to modify the name of this process to be co-translational *delivery* as the capsid does not necessarily disassemble immediately upon the beginning of translation, at least as observed *in vitro*.[15] For CCMV, the capsid appears to be relatively intact until the time at which enough ribosomes have translocated, or pulled out, a sufficient amount of mRNA from within the capsid, in Roenhorst, et al. this appears to be about four ribosomes bound. Estimates for this critical amount of RNA removed from the inside of the capsid appear to be close to ~15% percent of the viral RNA, where it is predicted that due to changes in the amount of electrostatic charge balance between

the 180 of the viral capsid protein's 10 positive charges on their N terminus, which are known to interact with the RNA of the virus, and the loss of the negatively charged RNA inside the capsid, the capsid may begin destabilizing and come apart. Nevertheless, these studies, which do not benefit from high-resolution structure determination of the process of RNA being translocated out of the capsid, are not able to clarify the nature of how the RNA is made available in the first place to the host's ribosomes.

While this hypothesis has evolutionary arguments that the viral RNA genome is maximally protected until it is translated by its host's ribosomes, there may be other mechanisms that we need to consider and determine the likelihood of. For example it could be that the virus upon entering its host's cytoplasm undergoes partial capsid proteolysis, or a defect in the capsid can be formed through the involvement of host factors. While for some viruses, like Turnip Crinkle Virus (TCV), preferential proteolysis of the pentamers of the capsid has been suggested to promote the exposure of the viral RNA,[16] in the case of the bromoviruses this process may not be necessary, partly due to the fact that the capsid shell does not have as strong protein-protein interactions; but proteolysis in the cell cannot be ruled out. Could a capsid dimer or pentamer of dimers be removed by host factors before RNA is released? Indeed, this cannot be currently resolved because the resolution of the negative-stain images of ribosomes with CCMV (Roenhorst et al)[15] is limited and the capsid at least in those images seems relatively intact. Thus we aim to determine higher-resolution structures of this co-translational delivery process and learn about this process using structural, biophysical and biochemical techniques.

To discern how the RNA might make its way out of the capsid, we have begun studies that examine how an end is made accessible to the ribosomal apparatus. We have approached this in two different ways, one by use of *in vitro* self-assembled virus like particles with modified RNA ends[17], and second by use of purified initiation factors involved in the first stages of protein synthesis by the ribosome. In addition, we have begun to work with *in vitro* translation cell-free extracts to look at later stages of how the virion might interact with ribosomes.

**Capsid protein sequence and structure of the virus and its expanded forms**

BMV and CCMV capsids are dynamic particles that have nearly identical structural homology but differ substantially in amino acid sequence, with about ~70% sequence conservation at the protein level. The beta barrel jelly-roll fold is present in many capsids but the bromovirus capsid structure seems to have been evolutionarily separated from other types of capsids based on structural homology. An interesting aside: there is a possibility that BMV and CCMV capsid protein have more structural similarity to kexin-like proteases than to other capsid proteins found in nature and specifically to the P domain of these proteases,[18] based on a DALI server protein similiarity clustering. Interestingly, these proteases' P domain is thought to stabilize the catalytic domain of the protease when complexed with calcium: the P domains of the kexin-like proteases possess hydrophobic residues that promote association with the catalytic domains. This hydrophobic interaction from the P domains may be similar to the hydrophobic capsid protein-capsid protein interactions that are believed to be shared among the dimers of BMV and CCMV in solution and in the assembled capsid. If

a virus derived this from its host, or found access to this gene in still another way, it would be an interesting line of work to investigate in the evolutionary history of these viruses and their self-assembly properties.

Both BMV and CCMV capsids are believed to undergo swelling transitions *in vivo*, and this transition has been observed using density gradient analyses and more recently x-ray crystallography and cryo-EM reconstructions. The expansion results in major changes of the capsid at the quasi-three-fold and two-fold symmetry points of the capsid. As shown below, the virus can expand when in the presence of a neutral pH and low or no divalent cation solution (if EDTA or EGTA is added this maximally expands the capsid). This expansion has been proposed to allow for some of the RNA to be made accessible outside of the capsid, and perhaps, a 5' end of the RNA could fluctuate either by itself or with a flexible N-terminus to display the RNA outside of the capsid. There may be entropic gains to the system by having the genome partly outside the capsid upon entering the low concentration of free divalent cation within the cellular cytoplasm.

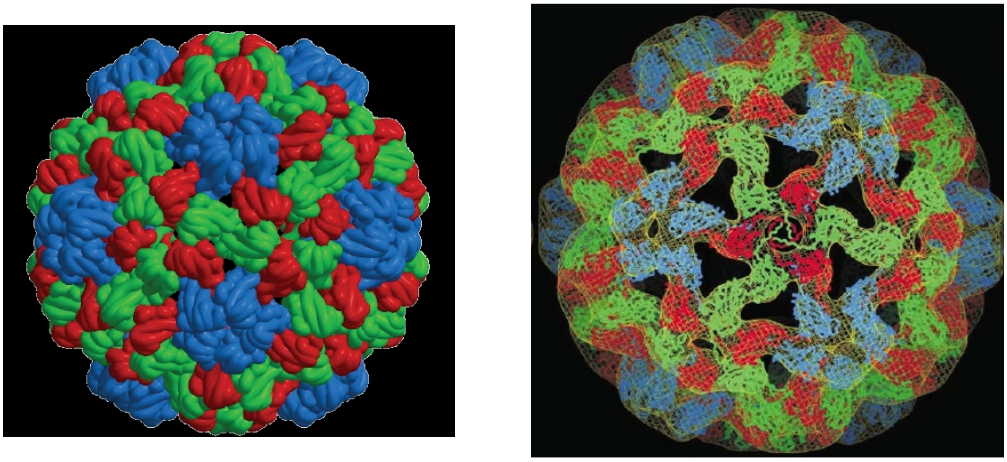

**Figure 1. a and b** a) Compact and b) expanded forms of CCMV are shown above. These images are generated from CryoEM reconstructions. The expanded form on the

right demonstrates approximately a 10% increase in diameter with the largest deformations of the capsid occurring at the quasi-three-fold axis where pores are expanded to approximately two nanometers. Figure 1A was generated from[20]. Figure 1b from Tama and Brooks, reprint with permission.[21]

**On the structure of the viral genome in and out of the capsid**

While the RNA secondary and tertiary structure is not entirely resolved inside the capsid in either the cryo-EM reconstructions or the deposited x-ray crystal structures, the RNA indeed must be deformed to some extent due to capsid protein RNA interactions, when compared to RNA structures in solution based on neutron scattering, cryo-EM,[22] chemical probing/sequencing (e.g. RNA SHAPE and related procedures) or algorithmic approaches (e.g. mFOLD and other free energy minimizing RNA folding software). In the Speir et. al.[13] cryo-EM reconstruction on CCMV, approximately 600 nucleotides of averaged electron density can be accounted for of the ~3000 nucleotides per capsid, but since these reconstructions were done on a sample that contained the three different capsids (each with a different genomic RNA) and icosahedral symmetry was imposed, it is currently technically difficult to determine exact sequence or structure of the RNA within the capsid. Recently, work from our group (Beren et al, 2019, under review by PNAS) has revealed some of the asymmetric nature of the RNA inside the capsid. These asymmetric reconstructions of a single BMV capsid, containing RNA 3 and RNA 4 only, suggest that there may not be only one structure of the RNA within the capsid, but instead an *ensemble* of RNA structures. Since the RNA within the capsid must accommodate its shape to the presence of the positively charged N-terminal tails

of CCMV and BMV capsid protein, its density is believed to be concentrated primarily across the capsid interior surface. Comparing the RNA to a “real” self-avoiding random walk polymer in three dimensions, which on average takes on an ellipsoidal structure, this negatively charged RNA inside the icosahedral capsid is constrained by being largely confined to the positively-charged interior capsid surface, making it more like a shell of RNA, with a minimal amount of RNA density found in the center of the capsid. Furthermore, if the capsid is put into a swelling buffer (pH > 7 and low divalent cation concentrations) its swollen or expanded form is approximately 10 percent larger in diameter. During this expansion, the RNA moves outward radially with the capsid shell. Since this expansion results in reorganizations primarily at the quasi-three-fold and two-fold axes, it may be that RNA in these regions is made more dynamic in ways that may allow for the single-stranded 5’ end of the RNA to be made accessible to the outside of the capsid, likely through the expanded-in-diameter pore at the center of the quasi-three-fold axis. This thesis investigates this fluctuation phenomenon through a variety of experimental approaches, in the following chapters.

## Chapter 2

### *in vitro* Translation & Ribosomal Initiation Factor Experiments

To catch a virus in the beginning stage of delivering its genome to the host is a focus of this dissertation. To learn a little about what is known and has been done in the past, we turn to experiments done by Brisco et al.[23] (in the lab of T.M.A. Wilson) and by the work of J.W. Roenhorst et al.[15], as their fundamental studies laid the foundation for this work.

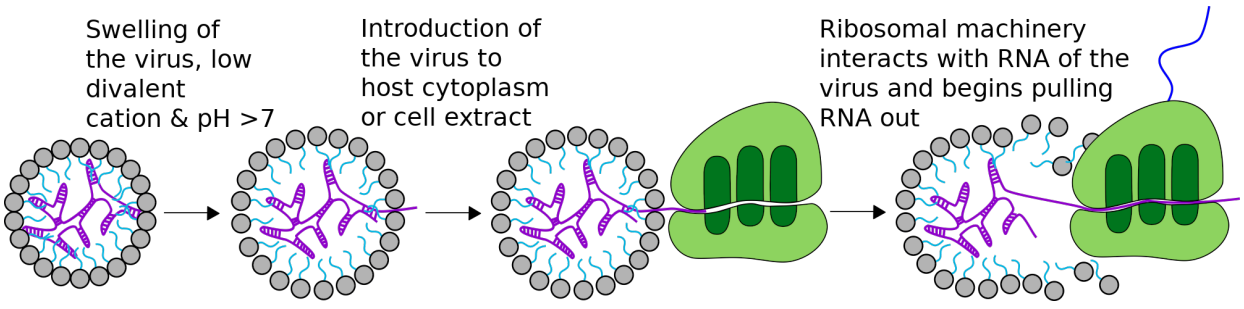


**Figure 1.** The co-translational delivery mechanism of a positive sense ssRNA virus. Virus is introduced into a neutral pH condition with low <0.5 mM free-divalent cation, condition, resulting in capsid swelling. This condition, similar to cytoplasmic conditions,

where free divalent cation is relatively low, contributes to viral RNA being made accessible to the host's ribosomes through a currently undetermined mechanism, but our hypothesis is that this is an RNA end fluctuation. Following the initiation steps of translation, the ribosome can assemble on the RNA and begin translation, translocating the RNA through its mRNA channel, and form viral-derived proteins. At some point in time, this results in the disassembly of the virus, but not until enough of the viral RNA message has been translated. *Figure credit:* Cheylene Tanimoto.

Since this early pioneering work of co-translational disassembly (or, the slightly modified name which we prefer, co-translational *delivery* – as the viral RNA is being handed over to the ribosome with the capsid remaining relatively intact), much has been learned about the structure and working of the actively translating ribosome/mRNA complex. Ribosomes translate messenger RNA (mRNA) using a variety of protein components including – arguably most notably – the *initiation factors*, which are believed to bind the mRNA before recruiting the ribosomal subunits. In eukaryotes, these proteins have been classified by the moniker of eIF (eukaryotic initiation factors) amalgamated with a number and sometimes a letter. How does mRNA get in contact with these initiation factors in the first place? In eukaryotes, the currently accepted paradigm is that mRNA is first transcribed in the nucleus by RNA polymerase (referred to in the literature as pol II) as a pre-mRNA. During transcription, the pre-mRNA is co-transcriptionally spliced by the spliceosome and simultaneously processed to add a 5' $m^7$Guanosine cap moiety, a 3' poly A tail and, in many cases, base modifications like the methylation of A or C nucleobases. During this process the RNA is bound by many co-factors including helicases that are involved in remodeling RNA secondary and tertiary

structure and in handing off the RNA to the nuclear pore complex for export into the cytoplasm. During this time, the proteins involved in the previous steps of mRNA processing and maturation may be exchanged for new cytoplasmic dominant proteins like the initiation factors of translation. One of the key points about this process to keep in mind is that mRNA is always bound to proteins such as ATP-dependent helicases, cap-binding proteins, and others from early synthesis stage to translation and export into the cytoplasm.

In the case of single-stranded RNA viruses like BMV or CCMV, these RNAs come into the cell bound up by capsid protein. mRNA, on the other hand, and shuttled from the nucleus to the cytoplasm and are bound up by many proteins including ATP dependent helicases, cap binding proteins and polyA binding proteins. Note, that each one of the molecules making up the viral genome is a ready-to-translate mRNA, meaning once it has made itself available to ribosomes, it can be translated without other preceding steps like the replication of the RNA. It is hypothesized that in the bromoviruses, upon entering the cytoplasm of its host plant from mechanical damage of the plant either by abrasion or through an insect's mouthparts (where the capsid may be in a lower pH and higher calcium concentration condition which causes the capsid to be in a compact form), the capsid is believed to expand radially about 10 percent, and a large part of that expansion comes with the enlargement of pores at the quasi-three-fold axis of the icosahedral capsid. This pore is ~20 angstroms in diameter according to CCMV's expanded-form cryo-EM reconstruction (Speir et al)[13]. Therefore, it may be possible that the viral RNA – and in particular its 5' end – can be made accessible to the outside of the capsid after expansion through this pore. To capture the RNA from the

pore, we suggest that the first step may be the binding to this exposed RNA of initiation factors that include eIF4E, eIF4A and eIF4G.As a first step, we have attempted to repeat the studies of Roenhorst et al[15], using BMV under these expansion/swelling conditions and have then explored how to capture these capsid-RNA-initiation factor complexes and determine how the RNA is making its way out of the capsid through a pore or defect.

**How do viral proteins get *initially* produced *in vitro*?**

Our initial studies involved using a western blot or similar system to measure the presence of nascent viral proteins produced after incubation of BMV capsids with wheat germ cell-free translation extract. We elected to use a fluorescently-labeled lysine-tRNA reagent, as it was incorporated relatively efficiently into proteins in the wheat germ system and produced a fluorescent signal determinable in a 8-12% SDS PAGE gel; this reporter on nascent polypeptide production is useful because of the low background fluorescent signal. One issue with this system is the presence of free fluorescently-labeled lysine-tRNA which overlaps with a number of the protein products on the SDS-page gel of the wheat germ cell-free protein synthesis extract. While there are some new studies underway to minimize this background fluorescence, most of the work of this thesis was concentrated on other measurements.

An alternative set of experiments were conducted using *in vitro* assembled virus like particles containing renilla luciferase molecules (~1,200 nucleotides long), and checking the relative efficiency of translation – in a wheat germ cell-free extract – of the mRNA according to whether it was contained in virus particles, free-in-solution, or

complexed with capsid protein but not assembled. In this experiment, viruses were assembled with CCMV capsid protein using the two-step dialysis procedure.[7] Briefly, *in vitro* transcribed 5' capped Renilla luciferase RNA was incubated in a 4.3 to 1 mass ratio of capsid protein to RNA in protein buffer (1 M Sodium Chloride, 50 mM Tris pH 7.2, 1 mM DTT, 1 mM PMSF), with final concentrations of capsid protein and RNA at 0.129 mg/mL and 0.03 mg/mL, respectively. This sample was dialyzed with 1000 volume equivalents of RNA Assembly buffer (RAB: 50 mM Tris-HCl pH 7.2, 50 mM NaCl, 5 mM $MgCl_2$, 1 mM DTT) for four hours at 4°C . Finally, the dialysate was added into a virus suspension buffer solution (VSB: 50 mM sodium acetate, pH 4.75, 8 mM magnesium acetate) and dialyzed again for 4 hours at 4°C. Samples were analyzed by native agarose gel electrophoresis and negative stain EM.

For the *in vitro* translation experiment, capsids were dialyzed into a neutral pH buffer containing solution, a combination of Hepes-KOH and Potassium acetate (HEKO: 40 mM HEPES-KOH, pH 7.6, 100 mM potassium acetate). Capsids were added with ~ 1 picomole of capsid, naked RNA or RNA-protein aggregate added to a 20 uL Wheat germ extract experiment which contained 10 uL of wheat germ (Promega), 2.4 uL of a concentrated solution of amino acids (varying from 1-10 mM final concentration of each of the canonical 20 amino acids), 1-5 uL of capsid/RNA in HEKO buffer and 0.8 uL of Protector RNase inhibitor (Sigma), and the remainder $ddH_2O$. Samples were incubated at 30°C for 2 hours. All samples were done in technical triplicate. Afterwards, the sample was measured using a luminometer. Results are in figure 2.

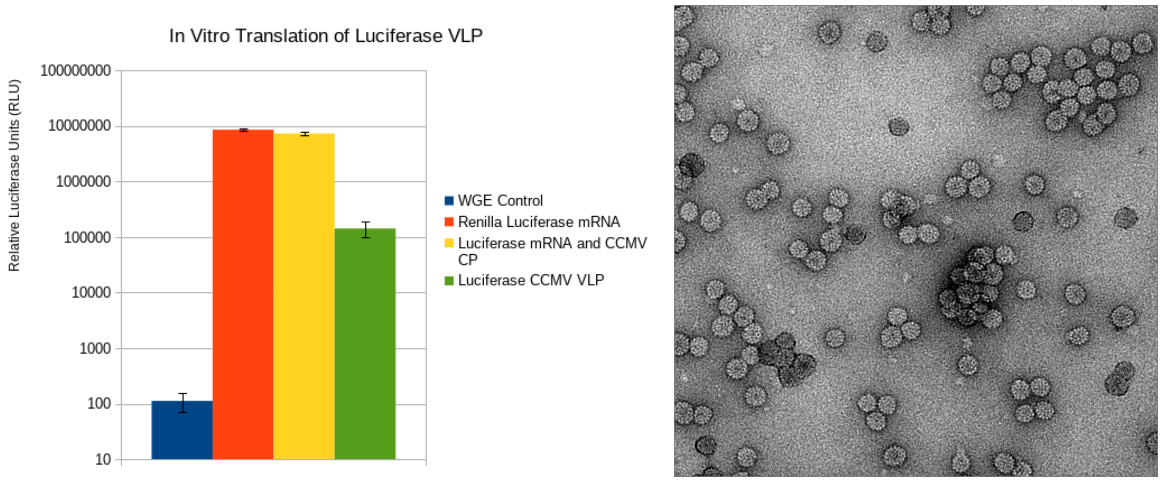


**Figure 2. a and b.** a) Renilla Luciferase mRNA *in vitro* translation assays for determining translation efficiency of luciferase mRNA alone, mRNA complexed with capsid protein, and in an intact, RNase resistant capsid. Bar graph displays the logarithm of Relative Luciferase Units associated with each of these three samples. b) Renilla-luciferase-mRNA-containing CCMV VLPs; capsids are approximately 24-28 nm in diameter.

These results demonstrate a stark difference between RNA and protein in an aggregate form, and capsids that have a fully-formed shell around the luciferase mRNA. There is approximately an 80 fold difference in the renilla luciferase photon counts which correlates with a proportional difference in renilla luciferase protein concentration generated from the *in vitro* translation experiment. We believe this could be due to two things, one, that the time it takes for an RNA to come out of the capsid in this assay is prohibitive. The other possibility is that some of these capsids are smaller than the canonical T=3 geometry of the CCMV virus. It has been shown that capsids that are formed around RNAs that are shorter than 2000 nucleotides long can be packaged into

particles[7] which possess non-Caspar-Klug geometries[24], including ellipisoidal particles with un-resolved symmetry. To make up for this later fact, a new set of assays using a different RNA construct, ~3500 nucleotides which should favor T=3 geometry preferentially.

**Ribosome & preliminary initiation factor complex incubation with capsids**

The ribosome can be paused on mRNA undergoing translation using a few approaches: either by adding only the first three amino acids to the wheat germ extract which are the first to be incorporated in the polypeptide from the protein encoding sequence of the mRNAs present in the viral genomes; or by using small-molecule inhibitors of translation elongation such as cycloheximide. In this way single ribosome/capsid complexes can be captured in relatively similar physicochemical states. This modified *in vitro* translation procedure, mixing pre-swollen BMV wild-type (WT) capsids with wheat germ extract containing all the necessary factors but with only methionine, serine and asparagine amino acids provided, resulted in a new species produced in an agarose gel electrophoresis experiment that highly suggests a ribosome-capsid intermediate has been formed. In a native 1% agarose TAE gel, BMV WT capsid runs toward the anode if the wells are formed at the top of a 10 cm by 15 cm mini-gel; the wheat germ extract, which has large and small ribosome subunits, both of which run toward the cathode; and the newly-formed complex runs approximately equidistant to these oppositely mobile species, which reflects the change in the mass and the electrostatic charge of this new complex, most likely a complex that occurs because of direct interaction of BMV with ribosome species. After careful gel electro-

elution of this newly formed band, a negative-stain electron microscope grid (using 2% uranyl acetate stain) was made of the sample and imaged on a JM-12 Jeol electron microscope (80kV accelerating voltage).

The images below show – see Figure 3 – the presence of capsid-ribosome interactions as compared to the work of Roenhorst et al[15]. The main two differences between the Roenhorst et al work and our studies was that they opted to use CCMV and we used BMV, and secondly, we opted to use in our *in vitro* translation assay only the first three amino acids of each of the three BMV RNA genome primary gene products (where RNA1 encodes the helicase, RNA 2 encodes the RNA dependent RNA polymerase, and RNA3, dicistronic, contains at the 5' proximal end the movement protein and the 3' proximal the capsid protein gene) to capture an early stage of the co-translational delivery process. In Roenhorst et al, their approach was to capture the ribosome-capsid complexes after a short period of time of starting the *in vitro* translation process, and freeze the experiment using cycloheximide, a ribosome elongation inhibitor. Following that process, they used glutaraldehyde crosslinking and sucrose gradients/cesium chloride gradients to separate out the different capsid ribosome species, where they observe a range of one to four ribosome shaped objects per intact CCMV capsid, but no more than four, while still maintaining an intact viral capsid. They suggest that after a certain amount of RNA has been pulled out of the capsid, a collapse or disassembly of the virus occurs, positing ~15 percent of the genome must be pulled out for this collapse to occur. We worked with limited number of amino acids and our observation in electron microscopy was that only single ribosome-capsid complexes were present.

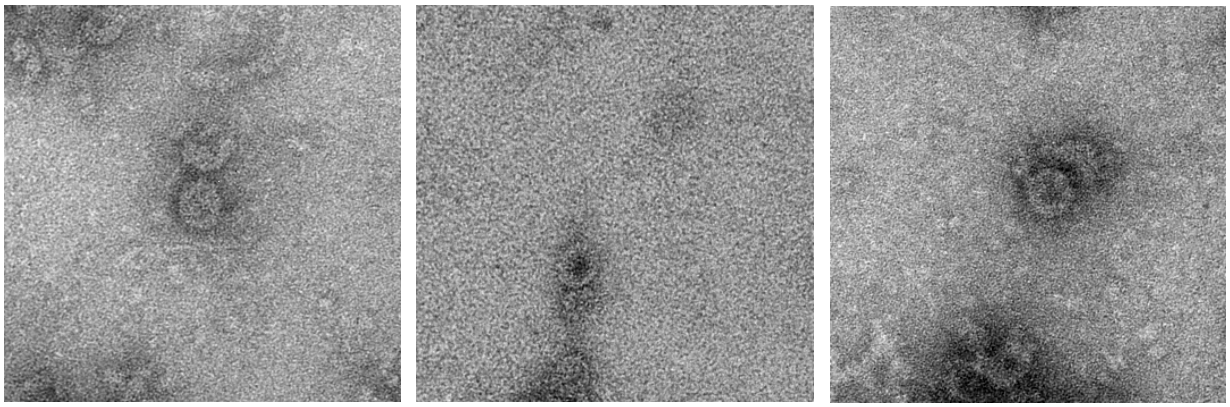

**Figure 3.** Ribosome-capsid complexes. BMV WT was incubated with wheat germ extract in the presence of an added solution containing only the three first amino acids present in the primary gene products of BMV. Samples were incubated for 15 minutes at 30°C, and then pipetted into a 1% agarose gel in 40 mM Tris Acetate, pH7.5; 2.5 mM $CaCl_2$ running buffer and run at 50 volts for 1 hour at 4°C. Gel slices were cut out and electro-eluted into a dialysis bag (1 hour at 50 volts and 4°C) and subsequently the electro-eluted sample was loaded onto a TEM grid and stained with 2% uranyl acetate.

**Purified initiation factors for incubation with BMV WT**

Eukaryotic translation requires a highly coordinated sequential set of initiation steps, often referred to as the scanning initiation model of translation. As mRNA is exported from the nucleus of the cell, the eukaryotic initiation factor 4E (eIF4E) complexed tightly with eIF4G binds the mRNA 5' cap structure, replacing nuclear protein factors involved in splicing, transcription and mRNA error checking. eIF4G, a scaffolding protein, together with eIF4E and eIF4A form the eIF4F complex. eIF4A is an ATP-dependent (and RNA-dependent) helicase, and is believed to unfold RNA secondary structure such that subunits of the ribosome can assemble on the mRNA. Once this

initiation mRNA complex has formed, the remaining 40S subunit can assemble along with eIF3, eIF2, the charged initiator methionine tRNA and other factors, which begin the ATP-dependent, 5'-to-3' linear search on the mRNA for, usually, the first AUG start codon that has a sequence context similar to the Kozak consensus sequence.[25] This dynamic complex, upon reaching the start codon, is often referred to as the 48S pre-initiation complex and it can recruit the 60S subunit of the ribosome, generating the mature ribosome complex, with the methionine-tRNA in the P site of the 60S subunit. At this point, polypeptide synthesis can begin.

To see if we could "fish the end" of the RNA out of the capsid with the initiation factors (or, put in another way, the RNA, whose end is fluctuating out of the capsid, is fishing for the initiation factors), we purified wheat (*triticum aestivum*) initiation factors from recombinantly expressed versions produced in E. coli (plasmids kindly provided to us from Professor Karen Browning of University of Texas, Austin)[26]. We then incubated these purified proteins with the swollen virus to look for association. Since initiation factors involved in the initial binding of messenger RNA are believed to consist of eIF4E, eIF4G, eIF4A and eIF4B, we concentrated on these factors first since we reasoned that they may be involved in the first contact of the fluctuating RNA coming out of the viral capsid.

Our first experiments were done by labeling eIF4F (the combination of eIF4G and eIF4E) with a fluorescent NHS-ester probe. We reasoned that if we were to observe association, we could observe it using a fluorescent gel assay. While results from this experiment were not conclusive, partly because background of the assay was high, and because we only had a limited amount of eIF4G to work with, we decided to employ a

more sensitive assay to observe the initiation factor binding to the capsid, i.e., negative stain electron microscopy. While the assay was relatively crude, since negative stain EM can have artifacts from grid preparation, there appears to be association with capsids with these initiation factors. Our observation of oval-shaped objects next to the capsid, of the size expected for the eIF4F complex (~5nm x 10 nm) was encouraging, and gave us more evidence that initiation factors may complex with intact virus particles.

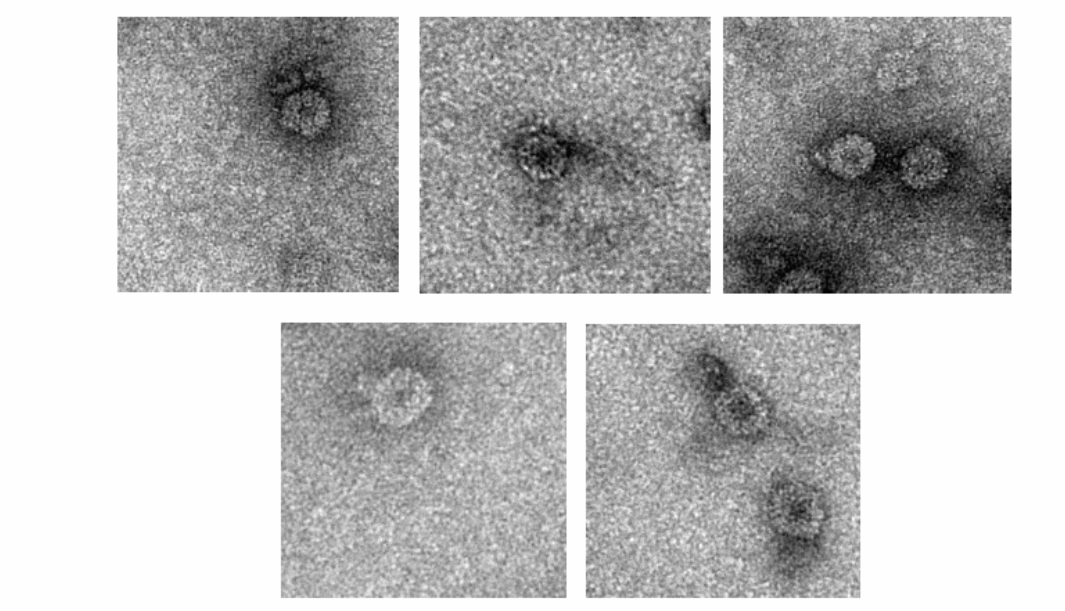

**Figure 4.** Initiation factor capsid experiments. Some representative negatively-stained electron micrographs of BMV WT capsids incubated with eIF4A, eIF4G, eIF4E in the presence of ATP and magnesium. All images were imaged at 200,000x magnification on a TF20 Tecnai microscope. Oval-shaped objects are observed next to the virus capsids. Capsid are 28 nm in diameter across, full initiation factor complexes should be

approximately 5nm x 10 nm, with eIF4F complex having an oblong cylindrical form based on prior crystallographic studies.

If we are indeed capturing a piece of RNA out of the capsid, we should be able to observe this RNA-helicase interaction, using either single-particle reconstruction or electron tomography, to see and incorporate into the bound proteins and model in the density of eIF4F's known structures. But most importantly, we may be able, for the first time, to see specific RNA sequence coming out of the capsid, and indicate where this RNA is coming from. Further verification using the initiation factor complexes is underway.

**Using tagged initiation factor fusion proteins to catch virus particles**

A variation of the experiments above was to capture viruses with eIF4E fused to a Glutathione-S-Transferase protein. This construct, GST-eIF4E K119A (from here on referred to simply as GST-eIF4E*), includes the K119A eIF4E mutant protein domain which has a remarkably high affinity for the 5' end of a viral RNA (low nanomolar $K_D$)[27] which has higher affinity than eIF4E alone[28], because of a removed competitive binding site for guanosine nucleotides adjacent to the primary cap binding site.

Using this GST-eIF4E* has a couple of advantages over just eIF4E or eIF4G/4F complexes. First, the fusion protein is ~50 kDa in size, making potential measurements of capsid-initiation factor interactions (namely by electron microscopy or pull-down assays/surface plasmon resonance) more easily done. Second, GST can be bound to surfaces/nanoparticles/microspheres that contain either covalently bound glutathione or gold via a cysteine-gold bond.[29]

These experiments had two versions, one of them using the protein alone, and the second with gold nanoparticles covalently bound to the GST-eIF4E* initiation factor. In the protein alone version, it was very difficult to discern if the protein is binding and how to interpret that interaction, so data is not shown, but the data obtained with the GST-eIF4E* gold nanoparticles is discussed and shown in figures 5 and 6 below.

The second type of experiment was done using gold particles that were made following a protocol[29] developed to make gold nanoparticles that bind specifically to GST, presumably through a covalent bond to a thiol residue by displacing the gold's surface bound citrate ligands. Purification was done using a sucrose gradient and subsequent pelleting at 10,000*g for 10 minutes at 10°C.

**Results of AuNP-GST-eIF4E interacting with the BMV WT**

Our results suggest that the capped-RNA virus-like-particle is interacting with the GST-eIF4E* gold nanoparticle. Studies done with *in vitro* assembled VLPs with uncapped RNA, containing B1 BMV RNA, were also done, and tests were conducted to detect interaction of the VLPs with the GST-eIF4E* gold nanoparticles, specifically looking for association of the gold with the capsids.

The issue with this assay was that significant aggregation was observed between capsids and virus particles. After reviewing the literature, it is possible that the 5' end, possessing a triphosphate terminus in the *in vitro* transcribed B1 RNA, could bind eIF4E with a similar affinity. Another possibility is that *in vitro* assembled capsids have some variability in their structure, perhaps making them more likely to aggregate on the GST-eIF4E* beads. One more experiment is underway to determine if the beads can interact

with capped RNA specifically over uncapped RNA along with using the non-triphosphate ends. We hope that these experiments could also offer higher-resolution structures to determine if the 5’ cap of the RNA is interacting specifically with the eIF4E protein while the capsid remains largely intact.

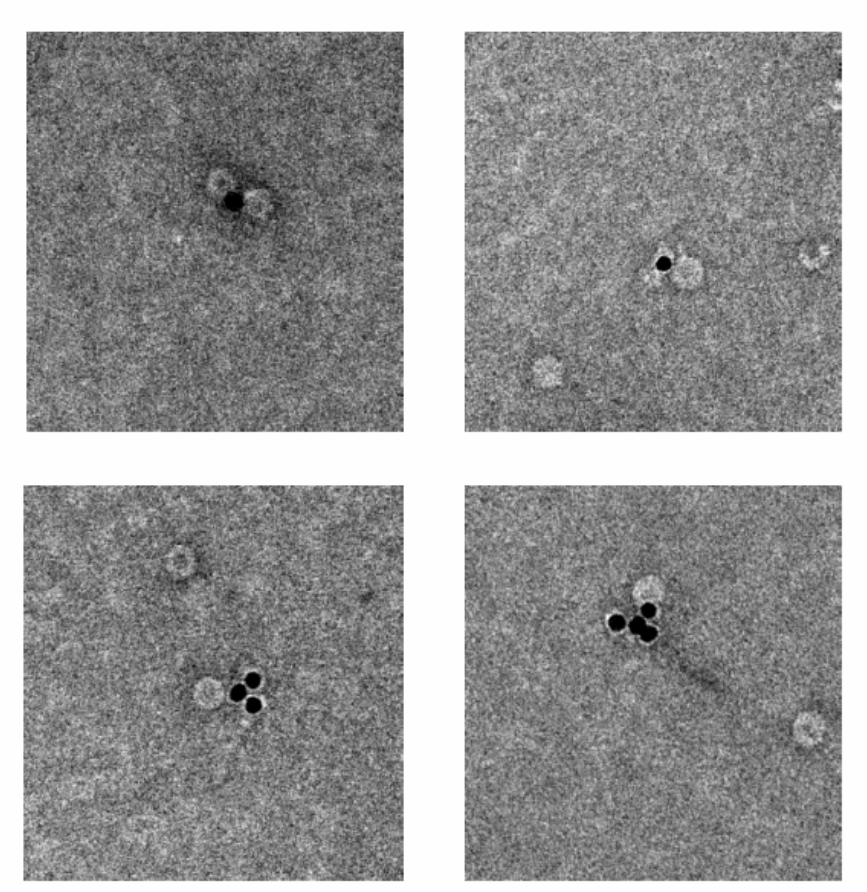

**Figure 5.** Negative stain electron microscopy images of BMV WT in complex with GST-eIF4E* gold particles. Capsids are 28 nm in diameter, gold ~20 nm in diameter which appear as solid black circles in the EM because of the gold’s inherent high electron density. The halo around the gold is interpreted to be the GST-eIF4E* protein as EM images with only 20 nm AuNP do not have a light colored halo around it, while the AuNP

activated with the addition of GST-eIF4E* look identical under EM as the gold nanoparticles present in the image.

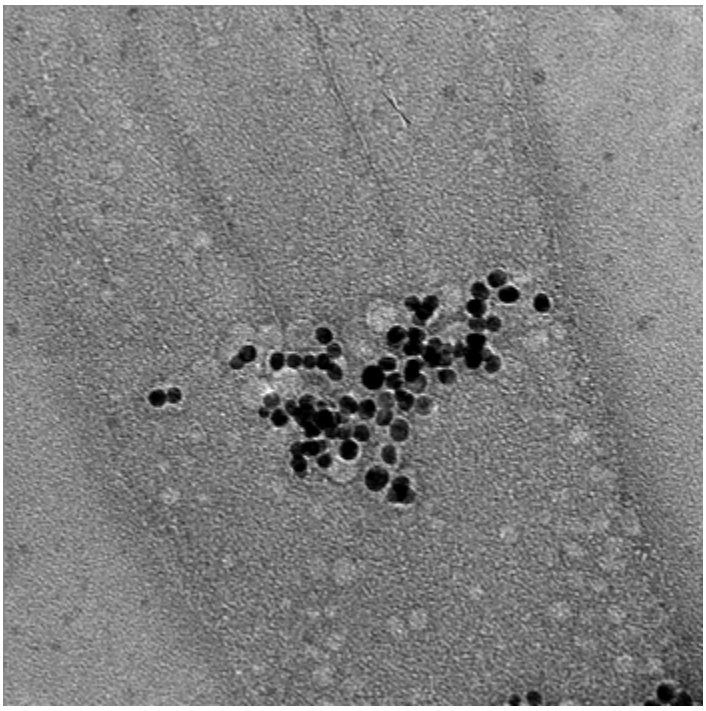

**Figure 6.** Aggregation with 5’ triphosphate-B1 RNA containing BMV VLP control assay for non-specific interactions of GST-eIF4E* AuNP. Aggregation of GST-eIF4E* 20 nm gold nanoparticles with or without capsids is frequently observed in this negative stain TEM data.

**Method for gold particle synthesis, protein labeling, and interaction with virus particles.**

20 nm citrate capped gold particles were synthesized by the Turkevich method. 11 mL of 20 nm AuNP at approximately 1 nM concentration were concentrated using centrifugation at 17,000g for 15 minutes at 10°C. Supernatant was removed and approximately 120 uL of concentrated gold was dialyzed overnight into 20 mL of 8 mM HEPES-KOH, pH 7.4; 20 mM Potassium Acetate 1 mM EDTA (0.2x HEKO buffer +1 mM EDTA). This sample was sonicated for 1 hour at ~10°C in a bath sonicator. The sample was then diluted into 12 mL of 0.2x HEKO. Then GST-eIF4E* was added at 120 nM concentration in 0.2x HEKO EDTA. To remove excess protein from the samples, a step sucrose gradient (14 mL of 30%,7 mL 40%,7 mL of 60%) was run at 25,000 rpm in a SW28 swinging bucket rotor for 25 minutes at 10°C (This is not an isopycnic gradient; equilibrium buoyant positions of the particle are not reached, since the densities of the hydrated gold particles surpass that of the most dense sucrose solutions present in the step gradient). Samples were collected mostly in between the 40% and 60% interface, but some particles had sedimented to the bottom and these samples were collected as well. To remove sucrose, samples were diluted three fold into 0.2x HEKO EDTA. Then samples were pelleted gently at 10,000g for 20 minutes at 10°C. This was repeated three times, but the volume remaining from pelleting was approximately 50 uL from originally 1,500 uL, therefore a 30 fold dilution was done using 0.2x HEKO buffer to bring the volume back up to 1,500 uL in these subsequent two pelleting steps, resulting in a ~2,700 fold dilution of sucrose in total (from an initial fraction containing ~60% sucrose down to ~0.02%). GST-eIF4E* AuNPs (16 nM AuNP), BMV WT virions (80 nM)

and uncapped B1 RNA containing BMV VLPs (~220 nM) were then separately dialyzed into HEKO EDTA buffer (20 mM HEPES pH 7.4; 100 mM Potassium Acetate, 1 mM EDTA). For the experiment, all samples were mixed with an approximate 1 to 1 ratio of gold to virus or VLP, resulting in ~13.33 nM AuNP and 6.666 nM capsid (10 uL of AuNP + 1 uL of virus/VLP). This ratio was chosen on the basis of how the stability of concentrated gold particles evolves in time, to minimize aggregation. It is estimated that ~100 protein equivalents can bind the surface of the gold particle, meaning that there are ~ 200 mole equivalents of initiation factor per virus in this experiment. This may be key to maximizing the chance of catching an RNA end fluctuation. Incubation times were selected to be 1 hour, 2 hours, 6 hours, 12 hours, 24 hours, 48 hours and 96 hours at 25°C. Immediately upon mixing virus/VLP with the GST-eIF4E** AuNPs, there seemed to be a shift to a purple color in the resultant solution indicating some form of aggregation may be occurring. Samples were analyzed using electron microscopy at a 1 to 20 and 1 to 200 dilution factor in HEKO EDTA (pH 7.4) on a TF20 FEI 200kV electron microscope.

## Chapter 3

### *in vitro* Self-Assembly of Biotinylated-RNA-Containing Virus-Like-Particles & Biotinylated-RNA-End Fluctuation Binding Experiments

To understand the genome delivery process of ssRNA viruses, our approach was to make a specific probe that could report on how RNA from inside an intact virus like particle (VLP) might make its way outside its host shell possibly through a fluctuating RNA end. A fluctuation, particularly a thermal fluctuation, is defined as a random deviation of an object or system from an average state occurring when a system is at thermodynamic equilibrium. Our experiments were designed to probe how a 5' end of an RNA may thermally fluctuate in and out of an intact capsid, perhaps through a pore in the capsid. Specifically, we take purified BMV or CCMV capsid protein which contain 9-10 positive charges on its N-terminus (depending on whether BMV or CCMV capsid protein is used, respectively), and mix it with an RNA of interest (the RNA of interest can be packaged in a single virus particle if the RNA length is anywhere in the range from

several hundred to ~4000 nt) at a pH of 7.2 and an ionic strength of ~ 0.1-0.3 (100-300 mM). An RNA-protein aggregate is formed within 30 minutes of mixing; usually, at this stage, the capsid is not completely formed, but may possess some elements of local icosahedral order (this can be observed by cryo-EM[30]). After this, the pH is lowered to 6 or below (from pH 4-6) by dialysis or mixing with a low pH solution, and capsids are formed. This assembly route may or may not correspond to what occurs *in vivo*, but many properties of this self-assembly process can be studied from this purified-components approach.

We utilized this approach to prepare BMV and CCMV VLPs to study the mechanism of how a virus forms and of how it may deliver its RNA to its host. As discussed in the preceding chapter, one aspect of this thesis work was to specifically determine the way in which an end of packaged viral RNA can be made accessible outside of the capsid without the capsid necessarily coming apart. Our hypothesis was that the 5' end of the viral RNA may be made available to the host via a fluctuation of the RNA end coming out of a ‘’hole” between capsid protein subunits making up the intact capsid. This possibility is further enhanced by the isometric expansion of the capsid following dialysis into a neutral-pH, low divalent-salt-concentration, swelling buffer, which results in hole sizes on the order of 2 nm in diameter at the quasi-three fold axis[13](see chapter 1 Figure 1 of this thesis). An alternative scenario is that the capsid begins to undergo disassembly before releasing its RNA to the host ribosomal factors necessary to pull the remaining parts of the RNA out of the capsid. It has been reported that Cucumber Necrosis Virus (family tombusviridae), for example, may be disassembled by binding of its capsid by chaperone proteins in the new host’s cell[31].

To test this fluctuation hypothesis we carried out *in vitro* self-assembly reactions with BMV viral RNA and capsid protein, but first modifying the 5' end of the RNA with a biotinylated residue; the self-assembled capsid is then swollen to increase pore size and thereby make the 5’ RNA end more accessible to the outside of the capsid. This biotinylated form of BMV's RNA 1 molecule was generated by *in vitro* transcription using a dinucleotide initiator, biotin-ApG – see Figure 1 below, with the biotin covalently attached to the adenine nucleotide as described in[32].To serve as the negative control, VLPs were also *in vitro* reconstituted with viral RNA whose 5’ ends were not biotinylated.

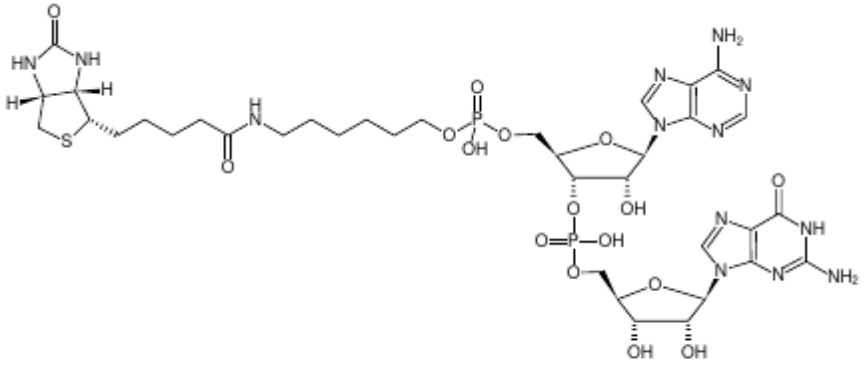

**Figure 1.** Biotin ApG dinucleotide structure adapted from [32].

The biotinylated or control B1 RNA was purified by an RNeasy column (Qiagen) and mixed with purified BMV capsid protein (BMV CP) in a super-stoichiometric 4.8 : 1 CP to RNA mass ratio, this ratio was experimentally determined by running a native agarose gel at different mass ratios, determining that 4.8:1 maximized encapsidation efficiency without forming larger aggregates that can occur at higher capsid protein to

RNA ratios. This ratio ensures the encapsidation of all the RNA in the solution when using pure BMV WT capsid protein[7]. After mixing, capsid protein, at a final concentration of 0.144 m/ml, associates with the RNA, at a final RNA concentration of 0.03 mg/ml in RNA Assembly Buffer (RAB; 50 mM Tris-HCL pH 7.2, 50 mM sodium chloride, 10 mM potassium chloride, 5 mM magnesium chloride, 1 mM DTT), by electrostatic attraction. This mix was incubated for 60 minutes at room temperature. At this point, the solution of partly-assembled capsid is subjected to a quick drop in pH by adding either one part 1.08M acetic acid solution into 100 parts RNA-protein assembly mix, or by diluting the assembly reaction 9-fold with a pH 4.75 Virus Suspension Buffer (VSB) solution, in both cases resulting in a pH of ~4.75. These assembled capsids were purified and analyzed using gel electrophoresis and negative-stain electron microscopy. The capsids were then RNase A treated for 1 hour at 4°C (RNase A at 4ng/uL final concentration) and extensively washed in VSB by spinning in a 100kDa Amicon filter at 4500*g for 5 minutes, filling up to a 500 uL volume with VSB, and spinning again, repeating this process a total of eight times. VLPs are recovered and dialyzed into a HEKOE swelling buffer (20 mM HEPES-KOH, pH 7.5 100 mM potassium acetate, 0.1 mM EDTA) and then incubated in either 96 well plates coated with streptavidin or with quantum dot nanoparticles also coated with streptavidin details, as explained in the following two sections.

**Catching a fluctuation using nanoparticles.**

After an initial "catch", capsid-nanoparticle complexes were subsequently diluted to ~0.02-0.04 mg/mL in HEKO buffer to be observed on negative stain EM grids. We

utilized streptavidin-coated quantum dots (approximately 5-8 nm in length, ellipsoidal particles, Invitrogen), and mixed them with biotinylated-B1-RNA-containing CCMV capsids in 4 to 1 ratio in HEKOE buffer and incubating at 25 °C as shown below. Typical micrographs are shown in Figure 2. We believe we are observing an interaction that is mediated by streptavidin – biotin coupling between the streptavidin functionalized quantum dots and the biotinylated RNA fluctuation outside of the CCMV VLP.

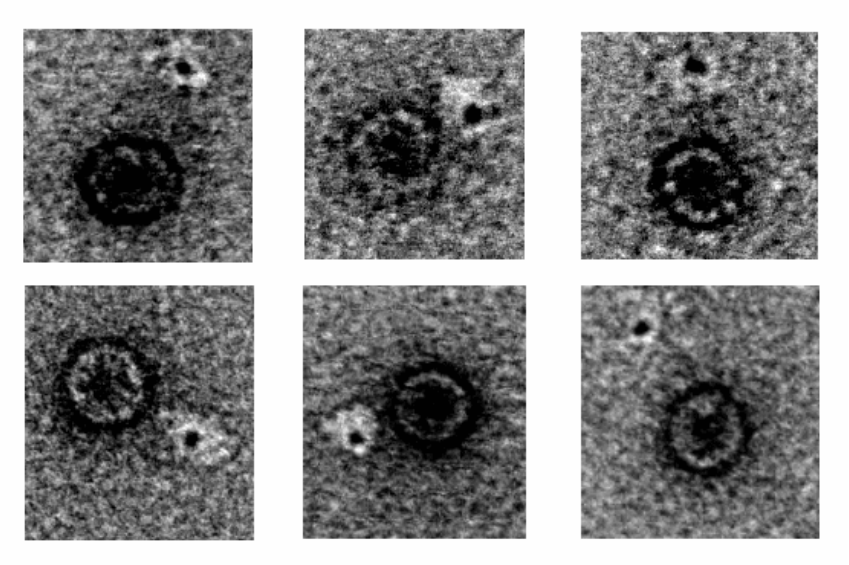

**Figure 2.** Streptavidin coated quantum dots (565 nm emission, Invitrogen) at a final 400 nM concentration were incubated with final concentration of 100 nM CCMV VLPs containing biotinylated RNA in a swelling buffer (20 mM HEPES-KOH, pH 7.5; 100 mM Potassium Acetate; 1 mM EDTA). After an overnight incubation at room temperature (~25°C), samples were diluted 50 fold and spotted onto carbon and parlodion coated copper TEM grids for one minute, then stained with 2% uranyl acetate to add contrast, blotted dry, and imaged using the FEI TF20 electron microscope at 200kV accelerating

voltage. For reference, capsids are measured to be ~26-28 nm in diameter, with variation due to staining effects.

These electron microscopy experiments proved difficult for observing *specific* interactions between the capsids and the quantum dots, partly because these small quantum dot particles were hard to detect in a large enough field of view to provide significant statistics in a reasonable amount of time while remaining at high enough dilution to insure real interactions and not just coincidental co-localization. Another issue was that when TEM was done in dilute conditions, namely when the average distance separating each particle is at least an order of magnitude greater than the size of the particles - a condition that is a requirement to determine specific interactions of these particles with the capsids - the capsids can become "positively stained" with the uranyl acetate. (Positive staining results in images where the capsids are dark and the background light, the inverse of what is found in negative stained TEM.) Because of this effect, capsids appear in the transmission electron microscope as dark spheres rather than more well defined icosahedral objects with clearly visible hexameric and pentameric units . Since the capsids appear as dark spheres, determining if another dark object that is four times smaller in diameter is co-localized with the capsid (namely the streptavidin-coated quantum dot nanoparticle) was somewhat difficult, especially at large fields of view that are better for gathering statistics on EM. Further experiments are underway to expand on these preliminary results, utilizing slightly larger nanoparticles functionalized with streptavdin.

**Catching an End Fluctuation Using Streptavidin Coated Plates**

While quantum dot particles allow for a direct visualization of the interaction with the biotinylated RNA fluctuating outside the capsid with streptavidin, and perhaps even allow for more sophisticated techniques like single-particle reconstructions of where and how the RNA capsid fluctuation is occurring in the capsid structure, we have found that a useful assay for determining if an RNA can fluctuate out of a capsid is by direct incubation with a streptavidin-coated surface, specifically, 96 well black plates with covalently bound streptavidin attached to the bottom of the wells. More explicitly, biotinylated BMV RNA 1 molecules (and the control BMV RNA 1 molecules without biotin) were fluorescently labeled by 488nm-UTP nucleotides randomly incorporated into the RNA during *in vitro* transcription, and then were mixed with BMV capsid protein in an *in vitro* self-assembly reaction, forming VLPs following the acetic acid pH drop. After RNase A treatment for 1 hour at 4° C, to remove non-encapsidated RNA (RNase A at a final concentration of 4 ng/uL with capsids that were at 0.15 ug/uL in VSB buffer, pH 4.75), the VLPs were washed with (filtered and autoclaved) VSB buffer in a 100 kDa Amicon filter at 4500*g for 5 minutes and this process repeated a total of 8 times, resulting in a ~100,000,000-fold dilution of RNase A (RNase A, 13 kDa, is significantly small enough to go through the 100 kDa molecular weight cutoff amicon filter membrane). Capsids were recovered from the amicon filtration unit and were approximately 7 fold more concentrated than from assembly conditions (~1 mg/ml versus ~0.15 mg/mL); they were then immediately dialyzed into HEKOE buffer (20 mM Hepes KOH, pH 7.6, 100 mM potassium acetate, 0.2 mM EDTA) such that capsids would be in a swollen state.

For the fluorescence plate assay, the sample was then mixed into a filtered HEKOE buffer that included, 5% DMSO, 0.1% Bovine Serum albumin (BSA), 0.002% tween-20 and 40 units of Protector RNase inhibitor (Roche). DMSO has been shown to be helpful for promoting single-stranded nucleic acid dynamics, which is important for enhancing a fluctuation of the RNA out of the capsid.[33] Tween-20 is used as a surfactant to prevent surface interactions with the capsid and preventing their denaturation. BSA is present to prevent any non-specific binding of the capsids to the 96 well plate. Using the streptavidin-coated plates required the washing of the wells with 200 uL of high-salt HEKOE buffer (200 mM potassium acetate rather than 100mM) as many as five times, because the plates provided by the manufacturer,Sigma Aldrich were coated with a proprietary preservative that is suggested to be washed away by the manufacturer. These plates were then incubated for increasing amounts of time with a solution of biotinylated-B1RNA-containing VLPs (and a solution of the non-biotinylated-RNA control VLPs) – that had been previously RNaseA-treated and dialyzed in the HEKOE buffer as noted above – at a standard *in vitro* self-assembly concentration (0.15 mg/mL). Each time point was measured in triplicate with 1 picomole of virus particle per well. Each plate was gently rocked in the dark at 30°C, and time points were taken after washing five times with high-salt HEKOE buffer.

Remarkably, following this streptavidin-coated plate incubated either with biotinylated B1 RNA VLPs or the control B1 RNA VLPs, a specific interaction could be measured. In the figure below, there appears to be approximately a three-fold difference of fluorescence intensity due to binding of the streptavidin coated plate between the biotinylated-RNA VLP and the control VLP at 24 hours and maintained at 96 hours. Our

interpretation of this is that – while both samples involve non-specific binding of the capsids to the plates, and both sets of viral-RNA-containing VLPs involve fluctuation of the RNA 5-end outside the capsid -- only the biotinylated-RNA capsids can be *specifically* bound by their RNA ends being caught by the streptavidin-coated plates.

The control VLP with the non-biotinylated RNA and its non-specific binding is what we should consider "background" and is used to compare to the specific binding of the biotinylated RNA containing VLP. We hypothesized that we would see a linear increase of fluorescence with time from the biotinylated-B1 VLPs because biotinylated-end fluctuations should be caught by the streptavidin surface i*rreversibly*, and *at a constant rate,* so that the number of caught VLPs is simply proportional to the time. Then number of non-specifically-bound VLPs, on the other hand, is expected to level off to an equilibrium adsorption value – corresponding to an asymptotic, sigmoid-like. fluorescence intensity response – in a manner consistent with a langmuir isotherm model. There should also be a non-specific binding effect of the biotinylated-RNA VLPs, and the fluorescence intensity measurement due to this effect should be similar to the B1 control VLPs as well. We could then expect to subtract this background non-specific binding contribution and see a linear increase in fluorescence intensity.

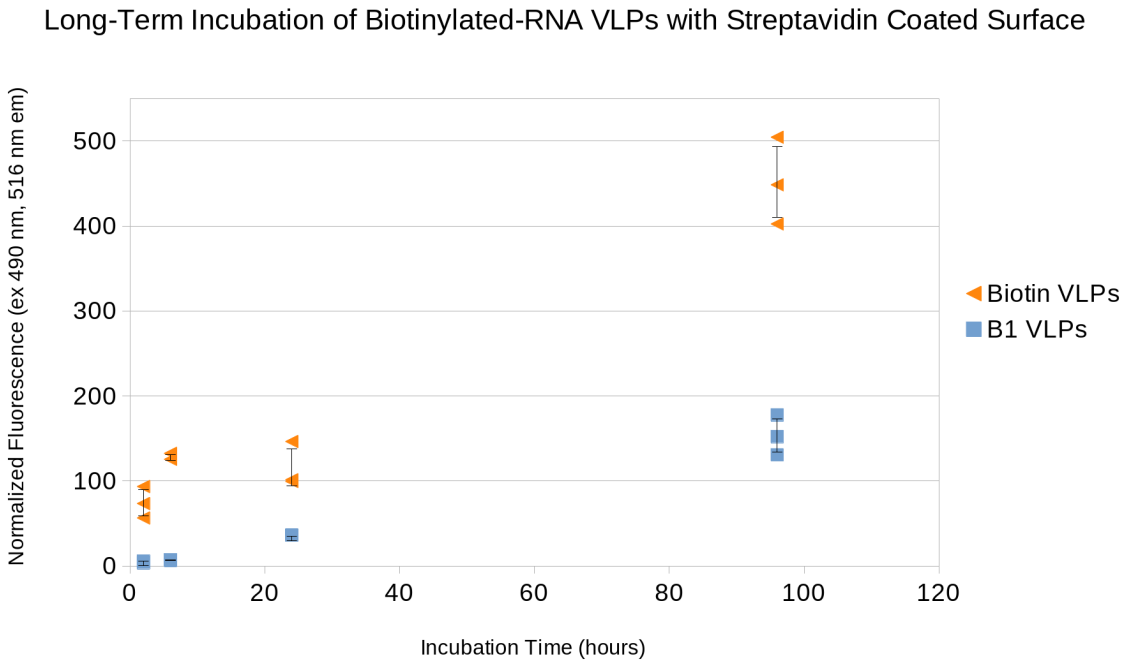


**Figure 3.** Plot of fluorescently labeled and bound biotin and B1 RNA containing virus like particles to a streptavidin coated 96 well plate. Measurements were taken with 488 nm excitation and 519 nm emission wavelengths (10 nm bandpass filters). Data is displayed in fluorescence units normalized to fluorescence differences between control and experimental VLP samples. Each RNA was fluorescently labeled to a similar extent by random incorporation of fluorescently labeled uridine nucleotides during *in vitro* transcription. Measurements were taken in triplicate and displayed with error bars indicating one standard deviation from the mean. An average of the triplicate values from the four time points, involving 50 uL samples (BMV VLPs containing biotinylated-B1 RNA or non-biotinylated-B1 RNA) were taken at the different times indicated. All incubations were done at ~30° C. At each time point, the sample solution was removed and five washes were performed with high salt HEKOE buffer pH 7.6 + 0.02% tween-20.

The ratio of fluorescence intensity between biotinylated RNA containing VLPs to non-biotinylated RNA containing VLP) binding is observed to be ~3 for the 24 hour and 96 hour incubated time points. Assays are underway to extend this time reference out to about 144 hours to see if a relationship, which is expected to be linear in catching a fluctuation specifically, versus a non-specific interaction with the non-biotinylated B1 RNA containing VLP control.

Furthermore assays were done to analyze the stability of the capsids at the later two time points in the B1 and Biotin B1 VLP incubation on the streptavidin plate. Samples were pipetted off of the 96 well plate and diluted by a factor of three to arrive at a dilution appropriate for negative stain EM analysis. This gel shows that these capsids are indeed still intact, at least to the level of visualization of the gel by eye, without apparent RNA degradation.

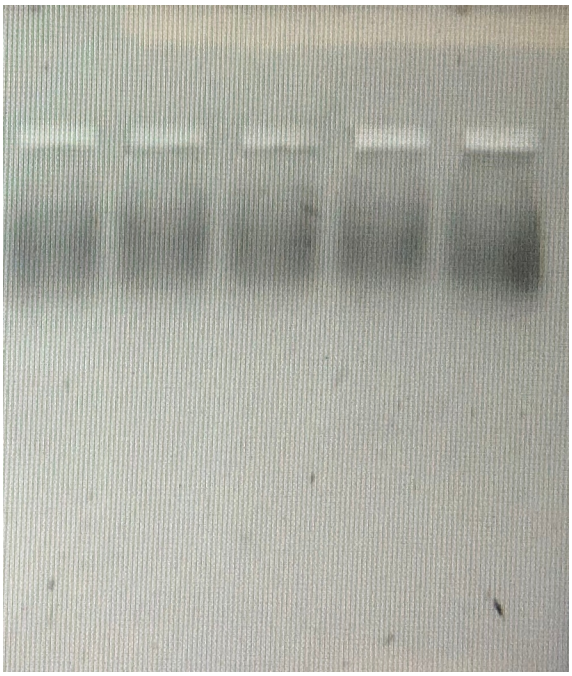

**Figure 4.** B1 and Biotin B1 RNA containing VLPs were run on a 1% agarose gel in OVB buffer pH 5.5 run at 50 volts for 1 hour at 4°C. Samples were further stained with 3x gel

red stain for 45 minutes at room temp and then images on a pharos FX plus gel scanner operated at the ethidium bromide default settings (medium sample intensity, 532 nm excitation, 605 nm emission bandpass filter). From left to right, lane 1 is Biotin B1 VLP without incubation on the streptavidin plate (control), lane 2 is B1 VLP after 24 hours, lane 3 B1 VLP after 96 hours, lane 4 is Biotin B1 VLP after 24 hours, lane 5 is Biotin B1 VLP after 96 hours.

**Discussion**

Our results suggest that a fluctuation of the 5’ end of RNA, outside the capsid, is occurring from an intact virus-like-particle based on gels of analyzing the capsid after they have been incubated with the streptavidin plate and that this may be a useful model to understand the first step of genome delivery in many single-stranded RNA viruses. One note that complicates this picture is in the experimental design. By using the 5’ biotinylated RNA as a probe, we have modified the viral RNA with a biotin attached with an 8-carbon-chain linker (see Figure 1). By contrast, in the wild-type virus the 5’ end of the capsid has a “linker” of a triphosphate and the cap is a methylated inverted guanosine residue, its linker length and charge is significantly different from the 8-carbon-chain biotinylated ApG residue. Therefore we must be cautious over-interpreting the results from this experiment and extrapolating to the WT virus’ genome release mechanism. But we believe it is still a useful set of assays that have informed our complementary studies using wheat germ extract cell-free *in vitro* translation assays and initiation factor protein incubations with capsids.

## Chapter 4

# A Simple RNA-DNA Scaffold Templates the Assembly of Functional Virus-Like-Particles

Rees F. Garmann, Richard W. Sportsman, Christian Beren, Vinothan N. Manoharan, Charles M. Knobler, and William M. Gelbart

**Abstract**

Using the components of a particularly well-studied plant virus, cowpea chlorotic mottle virus (CCMV), we demonstrate the synthesis of virus-like particles (VLPs) with one end of the packaged RNA extending out of the capsid and into the surrounding solution. This construct breaks the otherwise perfect symmetry of the capsid and provides a straightforward route for monofunctionalizing VLPs using the principles of DNA nanotechnology. It also allows physical manipulation of the packaged RNA, a previously inaccessible part of the viral architecture. Our synthesis does not involve covalent chemistry of any kind; rather, we trigger capsid assembly on a scaffold of viral

RNA that is hybridized at one end to a complementary DNA strand. Interaction of CCMV capsid protein with this RNA-DNA template leads to selective packaging of the RNA portion into a well-formed capsid, but leaves the hybridized portion poking out of the capsid through a small hole. We show that the RNA-DNA protruding from the capsid is capable of binding DNA and DNA-functionalized colloidal particles. Additionally, we show that the RNA-DNA scaffold can be used to nucleate virus formation on a DNA-functionalized surface. We believe this self-assembly strategy can be adapted to viruses other than CCMV.

**Graphical Abstract**

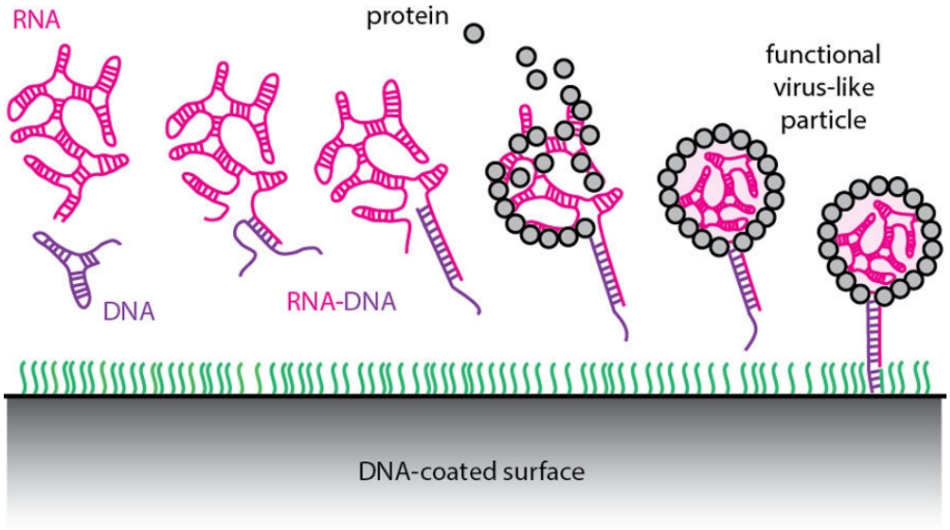


---

Small RNA viruses consist entirely of genomic RNA packaged inside a one-molecule-thick protective protein capsid (Fig.1). In addition to making up a large fraction of the world's viral pathogens, small RNA viruses are helping to define new fields of applied science through their use as functional nanoparticles[34]. For example, they have been exploited as contrast agents for biomedical imaging[35–38], as vectors for the delivery

of small molecules and genes to cells[39–44], and as nanoscale building blocks for the formation of superstructures with unique material, optical and dynamic properties[7,45–49].

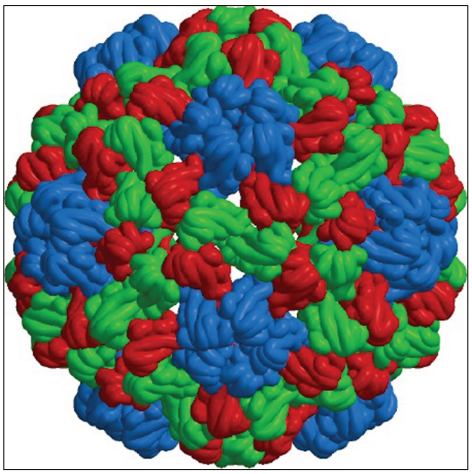

**Figure 1.** The capsid of cowpea chlorotic mottle virus (CCMV), like many small RNA viruses, has icosahedral symmetry and consists of 180 copies of its capsid protein. Diameter is 28 nm. Generated from PDB accession number 1CWP using NGL viewer[20]

Much of the utility of small RNA viruses derives from their symmetric capsids which can be engineered to display a high density of functional moieties. Indeed, an arsenal of functionalization strategies [33–43] have been developed that combine molecular biology (cloning) and/or selective covalent chemistries to isotropically label the various polyvalent surfaces (exterior, interior, and interfacial[34]) of the capsid. However, in situations where a high degree of labeling is not desired, monofunctional particles that display only a single copy (or a specific limited arrangement) of a particular functional group are needed. Mono-functional virus particles are difficult to produce[61–63] in a controlled way due to the inherent symmetry of the capsid and its abundance of equivalent binding sites.

Lying just beneath the capsid, the viral RNA contains a wealth of inequivalent binding sites that could in principle be selectively targeted using the methods of DNA nanotechnology[64–69]. Unfortunately, the capsid is impermeable to these techniques – the main evolutionary purpose of the capsid is to protect the RNA from unfavorable interactions with macromolecules from the outside world. Our work bypasses this inaccessibility through the synthesis of virus-like particles (VLPs) with a portion of one end of the RNA extending outside of the capsid (Fig. 2). With the symmetry of the particle broken by the exposed RNA, we generate robust monofunctionalization through the conjugation of desired moieties using only Watson-Crick basepairing.

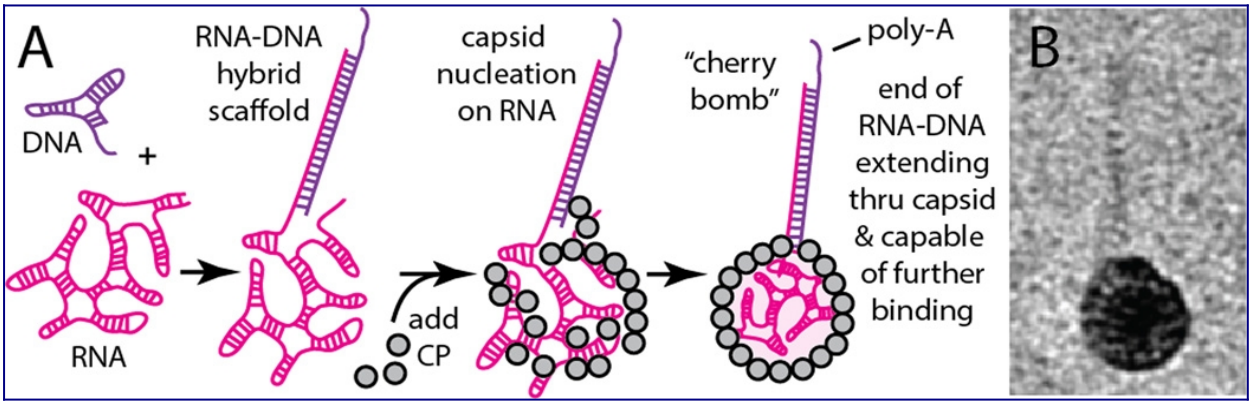


**Figure 2.** (A) Schematic illustration of assembly of the "cherry bomb". (B) Positive-stain transmission electron micrograph (TEM) of a cherry bomb capsid (dark sphere measuring 26 nm) and its RNA-DNA appendage (lighter strand extending upward).

Our synthesis (Fig. 2A) does not require genetic modification nor covalent chemistry, but instead relies on the ability of a particularly well-studied small RNA virus, CCMV, to be disassembled and reconstituted by self-assembly *in vitro*[3]. Additionally, we exploit the qualitative structural differences between single-stranded (ss) and double-stranded (ds) nucleic acid to reshape the viral RNA that templates the assembly. Due to

extensive intramolecular base pairing, ssRNA of the length naturally packaged by CCMV (about 3 knt) is a highly branched, flexible, compact object that has physical dimensions comparable to the capsid interior[55] (22-nm internal diameter). In contrast, the same length (3 kbp) of ds-DNA occupies a much larger volume due to its increased stiffness (~50 nm persistence length) and lack of branching. As a result, ds-DNA longer than about 75 bp cannot be accommodated within the interior volume of the CCMV capsid and does not function as a template for normal capsid assembly[70,71].

By hybridizing the first 185 bases at the 5′-end of a 3.2 kb ss-RNA with a complementary ss-DNA strand, we dramatically stiffen the 5′-end of the RNA. [We use the 5′-end of the 3234-base RNA molecule (“B1”) of the tripartite genome of brome mosaic virus (BMV), although either end of any similar-length sequence will likely do.] Here, the DNA strand (see SI) acts as a molecular splint. The resulting RNA-DNA hybrid can be expected to behave as a compact, flexible, branched 3-kb ss-RNA connected to a rigid, linear, 185-base ds-RNA-DNA appendage (see second-from-left cartoon in Figure 2A). The physical length of the ds portion is about 50 nm. It is very stable (85 °C melting temperature) owing to its perfect sequence complementarity. The *in vitro* packaging of this RNA-DNA hybrid by CCMV capsid protein (CCMV CP), using the same protocol developed earlier for pure RNA,[58–60] results in the selective encapsidation of the ss-RNA portion and leaves the ds-RNA-DNA appendage poking out of the capsid and into solution. We refer to this final construct as a “cherry bomb” because of its structural resemblance (Figure 2B, additional images shown in SI, Figure S1) to the well-known explosive firework.[72]

While the structure of the hole that passes the ds-RNA-DNA through the capsid is not known, previous *in vitro* packaging studies have shown ss and ds nucleic acid traversing the capsids of CCMV and the closely related BMV. We previously observed[7] that ss-RNA molecules significantly longer than wild-type are packaged by multiple CCMV capsids ("multiplets") that each share a portion of the overlong RNA (Figure 3). And a separate study[70] found that long ds-DNA is packaged by a contiguous string of many BMV capsids if ss-RNA fragments are also present. In both cases, nucleic acid is shared by connected capsids, passing through one or more holes in each capsid that are too small to be seen by negative-stain transmission electron micrograph (TEM). It is likely that the ds-RNA-DNA appendage of the cherry bomb exits the capsid through a similar hole.

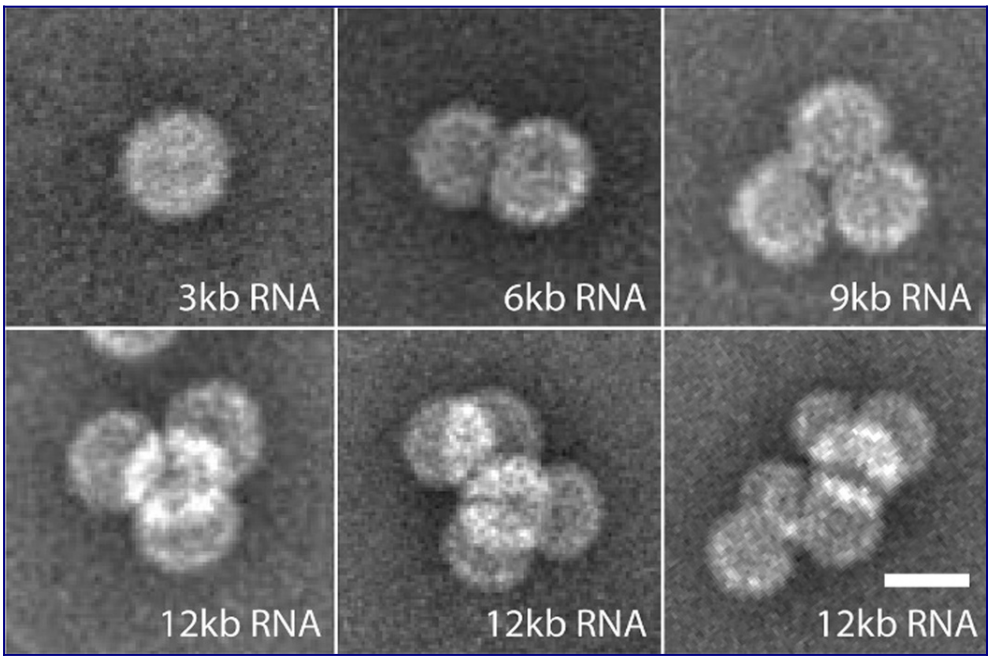


**Figure 3.** Single ss-RNA molecules progressively longer than wild-type (3 kb) are shared by two or more CCMV capsids; multiplets. Scale bar shows 25 nm. Adapted

from J. Virol. 2012, 86, 3322, doi: 10.1128/ JVI.06566-11. Copyright American Society for Microbiology.

To test whether the exposed RNA-DNA appendage can be used to bind nucleic acids in solution, we designed the DNA splint with a 3' poly-A15 overhang in addition to the 185 bases that complement the 5'-end of the RNA (see right-most cartoon in Fig. 2A). Once formed, cherry bombs were combined with fluorescent (green) poly-T15 DNA strands and analyzed by native agarose gel electrophoresis (Fig. 4). The capsids co-migrated with the fluorescent poly-T15 (Fig. 4, lane 3), confirming that the poly-$A_{15}$ sticky end of the RNA-DNA appendage binds its complementary strand in solution. Control experiments in which already-assembled VLPs containing only 3.2 kb RNA (B1) were added to the splint DNA and fluorescent poly-T15 showed no nonspecific binding (Fig. 4, lane 4).

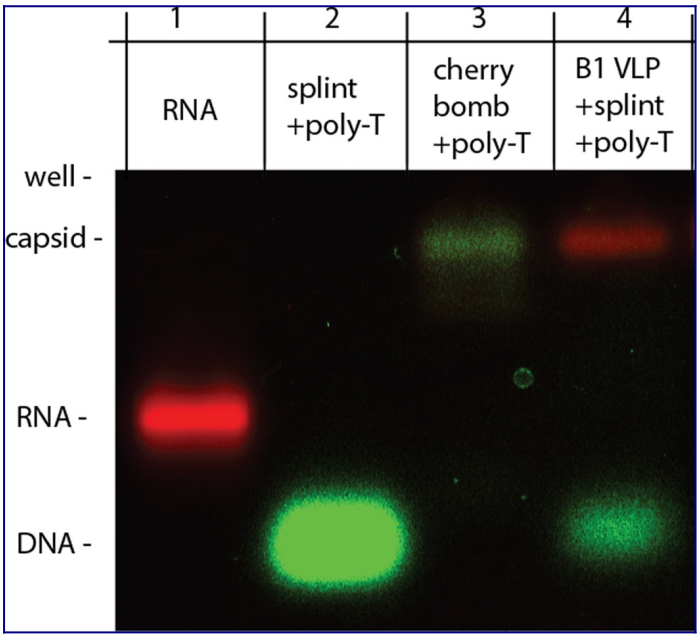

**Figure 4.** Native agarose gel electrophoresis shows cherry bombs selectively bind fluorescently labeled poly-$T_{15}$ DNA strands (green). Fluorescently labeled RNA shown in red.

The ability of the cherry bomb to bind a functionalized surface was demonstrated by direct imaging of a mixture of these capsids with 30-nm gold nanoparticles (AuNPs) that had been previously decorated with a high density of poly-$T_{25}$ DNA strands [73] (Fig. S2). Negative-stain TEM (Fig. 5) shows a high concentration of capsids at the AuNP surface, and an exceptionally well-stained image reveals the RNA-DNA appendage linking the capsids to the gold surface (Fig. 5, arrows). Control experiments between B1 VLPs and functionalized AuNPs showed no non-specific binding (Fig. S3).

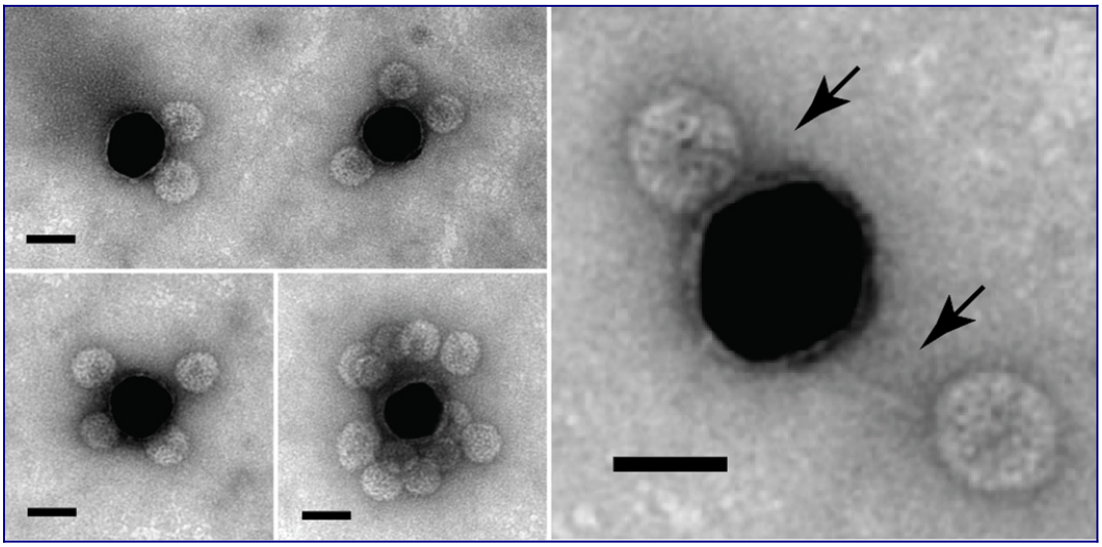

**Figure 5.** Cherry bomb capsids bind the surface of DNA-functionalized 30-nm AuNPs. A zoomed-in image resolves the RNA-DNA duplex (arrows) linking the capsids (light spheres) and the AuNPs (dark sphere). Scale bars show 25 nm.

Separately, we tested whether capsids could be assembled around RNAs that were already tethered to a functionalized surface (Fig. 6A). Here, the hybrid RNA-DNA

scaffold was prepared and equilibrated with 30-nm poly-T25-coated AuNPs at a molar ratio of 10:1 (RNA:AuNP). After hybridization of the RNA to the AuNPs, CP was added at a mass ratio of 10:1 (CP:RNA), equilibrated for 5 min on ice, and imaged by negative-stain TEM (Fig. 6B). The presence of well-defined capsids at the Au particle surface demonstrated assembly of cherry bomb capsids around the immobilized RNA-DNA. Some aggregation of CP in the presence of AuNPs was also observed (Fig. S4).

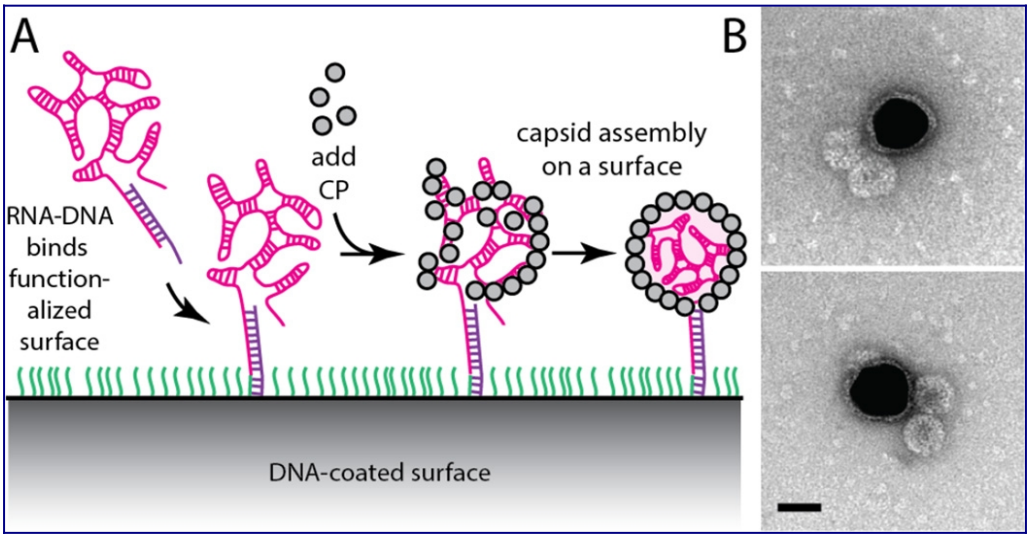


**Figure 6.** (A) Schematic showing the assembly of VLPs on a DNA-functionalized (green strands) surface. (B) Cherry bomb capsids (light spheres) were grown on 30-nm AuNPs (dark spheres) as shown in (A). Scale bar shows 25 nm.

While several elegant methods have recently been described for the mono-functionalization of tobacco mosaic virus particles,[74–76] they most likely cannot be applied to other viruses; they require either controlled disassembly of one end of the rod-like capsid or self-assembly of capsids on a substrate bound RNA that contains a specific packaging sequence. The homogeneous assembly pathway described here provides a general strategy for monofunctionalizing icosahedral particles. Here we note

that the ability to form cherry bomb structures is probably not limited to the plant virus CCMV; multiplet capsids have been observed in the packaging of overlong RNAs by the CP of the bacterial virus fr[77] and of the mammalian virus SV40[78], indicating that they too have the potential to form cherry bombs. In addition to offering a single, highly specific binding modality for building functional viral-based materials, our method for (i) physically binding and manipulating one end of the packaged genome and (ii) nucleating capsid assembly at a surface will enable new single-particle measurements that might reveal how RNA gets into and out of viral capsids during infection. Examples of such measurements include time-resolved studies of capsid assembly and force-pulling experiments[79,80] that measure the work required to pull viral RNA out of its capsid.

**Acknowledgments**

WMG and CMK acknowledge support from the NSF in the form of grant CHE 1051507. TEM images were obtained in the California NanoSystems Institute (CNSI) Electron Imaging Center for Nano-Machines, supported by NIH (1S10RR23057). Additional support provided by an NIH training grant for USPHS National Research Service Award 5T32GM008496.

**Supporting information**

**Synthesis of Capsid Protein**

Capsid protein (CP) was purified from wildtype cowpea chlorotic mottle virus (CCMV) grown in California cowpea plants (Vigna ungiculata cv Black Eye) as

described by Annamalai and Rao[81]. Briefly, virions were disrupted by 24-h dialysis against disassembly buffer (1M CaCl2, 50 mM Tris pH 7.5, 1 mM EDTA, 1 mM DTT, and 0.5 mM PMSF) at 4°C. The RNA was pelleted by ultracentrifugation at 4 x 105 g for 90 min and the CP was extracted from the supernatant in separate fractions. Each fraction was immediately dialyzed against protein buffer (1M NaCl, 20 mM Tris pH = 7.2, 1 mM EDTA, 1 mM DTT, and 1 mM PMSF). The protein concentration and its purity, with respect to RNA contamination, were measured by UV-Vis spectrophotometry – only protein samples with 280/260 ratios greater than 1.5 (less than 5% RNA contamination) were used for assembly. SDS-PAGE gel electrophoresis and MALDI-TOF showed no evidence of cleaved protein.

**Synthesis of RNA**

Fluorescently labeled brome mosaic virus genomic RNA1 (B1) was synthesized by *in vitro* transcription of a linearized DNA template by T7 RNA polymerase and fluorescent rUTP-AF488 (ChromaTide® Alexa Fluor® 488-5-UTP; Molecular Probes, U.S.A.). A rATP:rGTP:rCTP:rUTP:rUTP- AF488 molar ratio of 600:600:600:5.32:1 was used and resulted in a density of labeling of 0.5 rUTP- AF488s per RNA. After transcription, the template DNA was digested by DNase I (New England Bio-labs), and the resulting fragments removed by washing five times with a 20-fold excess of TE buffer (10mM Tris pH 7.5, 1 mM EDTA) using a 100-kDa MWCO centrifugal filter device (EMD Milipore) operated at 5,000 g.

**Design and Synthesis of DNA**

The DNA splint strand was purchased from Integrated DNA Technologies. The sequence is shown below:

5’AATCTGCGCAGATAACTGTTGCGCGACCTGATTGTCTACGATGTCTTGGGCACTC

TGGCTGGCAGCACCCTTCTCAGCAATCAACTTCAGCAAATCGATAGAACTTGACATT

TTGTTGGTGAAAAACAAAGAACAAGTAGCAGAACCGTGGTCGACAAGGGATTGAAC

CTCGTTCCGTGGTCTACAAAAAAAAAAAAAA-3’

This sequence consists of the reverse complement of the first 185 bases of the 5’ terminus of B1 RNA followed by poly-$A_{15}$.

We did not test whether DNA splints with complementary sequences shorter than 185 bases are capable of templating the assembly of cherry bombs, though we suspect this is the case. Assuming that the rise of hybridized dsRNA-DNA is intermediate between those of dsDNA (0.34 nm per bp) and dsRNA (0.25nm per bp), the physical length of a 185 bp hybrid strand measures about 55 nm, 2-3 times the inner diameter (22 nm) of the CCMV capsid. Therefore, we expect that much shorter DNA splints (as short as, say, 80 bases) should lead to hybrid ds-RNA-DNA portions that are too long to be packaged. However, these cherry bombs would have “fuses” that extend a shorter distance from the capsid. Alternatively, multiple short DNA splints designed to bind adjacent RNA sequences might be used to generate a more flexible fuse, due to the nicks between each pair of neighboring splints.

Fluorescent Poly-T15 was similarly purchased with 6-FAM conjugated to the 5’-terminus.

**Hybridization of the RNA-DNA Scaffold**

RNA-DNA hybridization was performed by mixing a 1:1 molar ratio of B1 RNA and splint DNA, each at 1 μM, in hybridization buffer (10mM Tris pH 7.5, 200 mM NaCl, 1 mM EDTA), heating to 90°C for 1 min, cooling to 55°C for 3 min, and cooling to 4°C indefinitely.

**Co-assembly of CCMV CP and the Hybrid RNA-DNA Scaffold – Assembling the Cherry Bomb**

Assembly was carried out as described in our earlier packaging studies involving CCMV CP and pure RNA[7,30,82]. Briefly, the RNA-DNA scaffold (final concentration 1nM) was mixed with purified CCMV CP in a ratio (wt/wt) of 4.4:1 in protein buffer and then dialyzed overnight at 4 °C against assembly buffer (50 mM NaCl, 10 mM KCl, 5 mM MgCl2, 1 mM DTT, 50 mM Tris-HCl pH 7.2). The samples were then dialyzed against virus suspension buffer (50 mM sodium acetate, 8 mM magnesium acetate pH 4.75) for at least 6 h to complete the assembly process. The products were then concentrated using a 100 kDa MWCO centrifugal filter device (EMD Milipore) operated at 3,000 g. The yield of cherry bombs – the fraction of RNA-DNA hybrids that are packaged by protein into capsids, with the ssDNA end accessible outside – was difficult to quantify by direct visualization by TEM because of the faint signal from the exposed RNA-DNA fuse. The majority of the assembly products appeared as well-formed capsids, but the number of capsids with a clearly visible fuse (Fig. S1) was low. However, native agarose gel electrophoresis showed that equilibrating roughly equal molar concentrations of cherry bombs and fluorescently labeled poly-dT (Fig. 4) resulted in all of the poly-dT signal comigrating with the cherry bombs (see lane 3 of Fig. 4) – suggesting that most

of the RNA-DNA hybrids were packaged and that the resulting cherry bombs had functional fuses.

**Decorating 30-nm gold nanoparticles with short DNA strands**

30-nm diameter gold nanoparticles (AuNPs) were functionalized following the protocol described by Hurst, Lytton-Jean, and Mirkin[73]. Briefly, 20 nmoles of 5' dithiol-terminated Poly-T25 DNA oligos (Integrated DNA Technologies) were incubated with DTT (0.1M DTT, 0.18M phosphate buffer, pH 8) for 1 h at room temperature. The DTT was then removed with a Nap-5 column (Sephadex G-25 DNA Grade), and the purified oligo concentration was determined by UV-visible spectroscopy. 2 nmoles of deprotected, thiolated Poly-T25 oligos (final concentration of 1 μM) were added to 1 ml of 30 nm citrate-stabilized gold nanoparticles (Nanopartz Inc., OD=1, 0.05 mg/ml, final concentration of 300 pM) and the mixture was brought to 0.01M phosphate buffer pH 7, 0.01% SDS. The reaction was mixed and sonicated thor- oughly, then incubated on a rotator for 2 h in the dark. The conjugation mix was incrementally introduced to higher salt conditions in the following way: 12.5 μL of 2M NaCl was mixed thoroughly into the reaction vessel, followed by sonication and a 1 h incubation. This procedure was repeated a total of 6 times, bringing the final concentration of NaCl to 0.1M. After salting, the reaction mix was left on a rotator overnight in the dark. To remove unbound DNA oligos, the solution was centrifuged at 10,000 g for 20 minutes, the supernatant was removed, and the gold nanoparticle pellet was resuspended in 1 ml 0.01M phosphate buffer pH 8, 0.1M NaCl, 0.01% SDS. This was repeated 3 times, and the final pellet resuspended in 0.01M phosphate buffer pH 8, 0.1M NaCl. The products were

imaged by negative-stain TEM (Fig. S2), which revealed a faint ring of material surrounding the electron-dense AuNP that most likely corresponds to the DNA coat. The number of Poly-T25 oligos coating the nanoparticles was not quantified, but oligo-coating was tested qualitatively using a salt-stability assay.

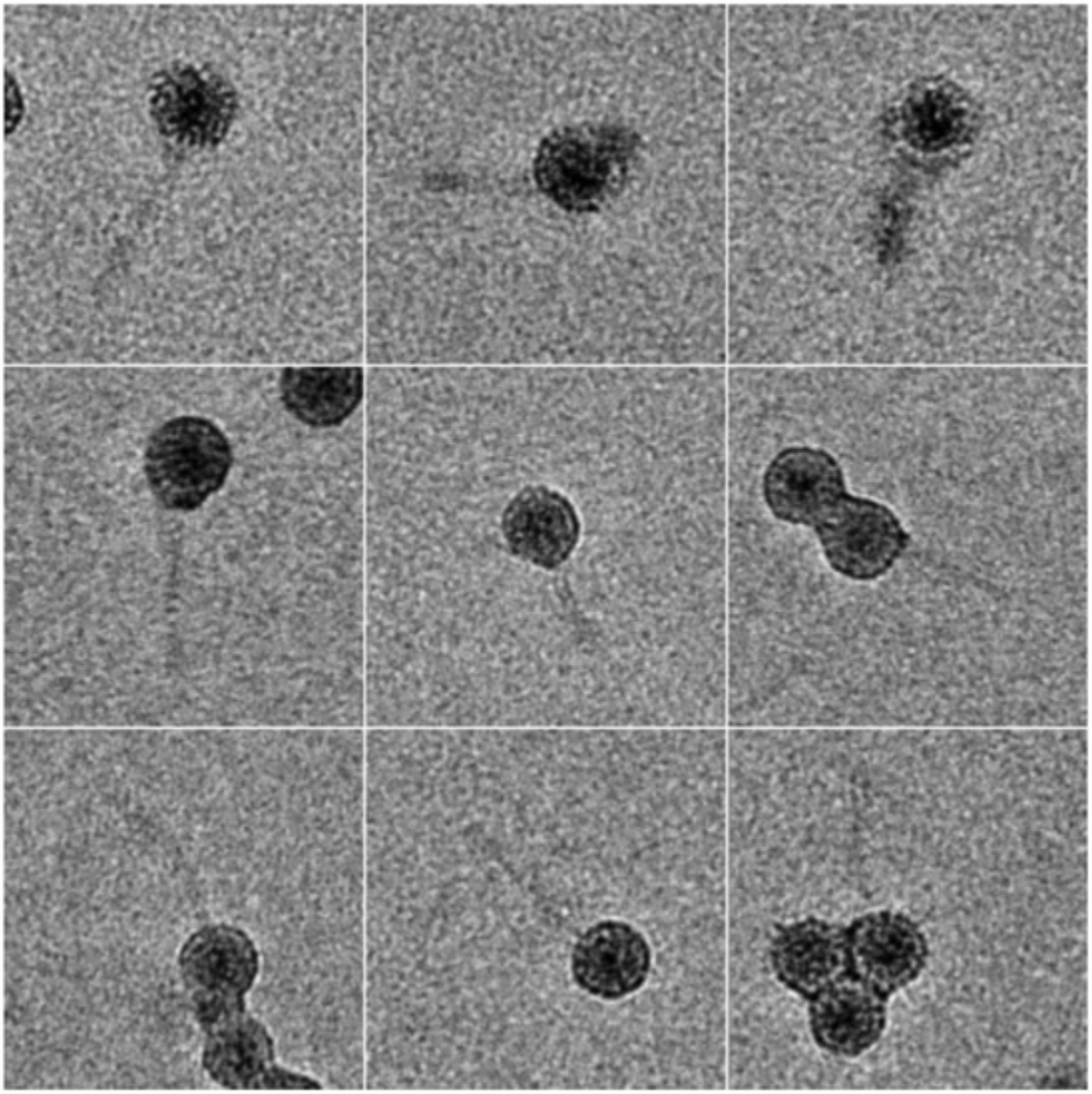

**Figure S1.** Positive stain TEM images of cherry bomb assembly products that show the ds-RNA-DNA “fuse”.

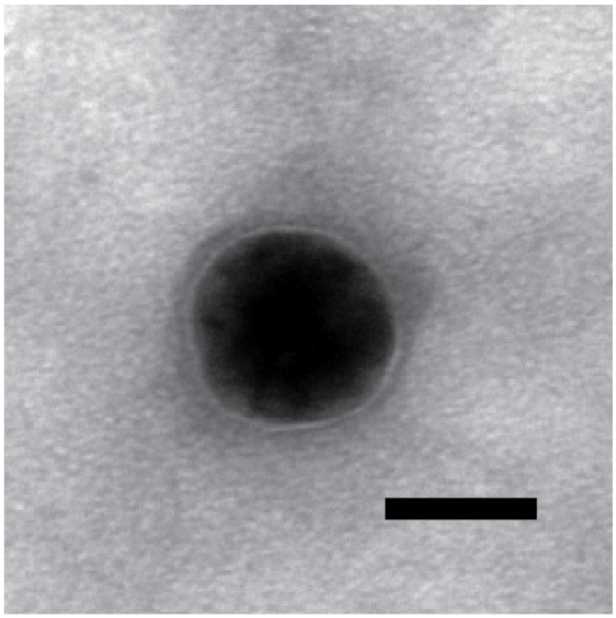

**Figure S2.** 30-nm AuNP coated with poly-T25 imaged by negative-stain TEM. Scale bar shows 25 nm.

**Testing for Non-Specific Binding Between CCMV VLPs and poly-$T_{25}$ -Coated AuNPs**

A control co-assembly reaction involving CCMV CP and pure B1 RNA was performed in parallel with the cherry bomb assembly reactions. The assembly products of the control reaction were then mixed with poly-T25-coated AuNPs, equilibrated for 5 min on ice, and imaged by negative-stain TEM (Fig. S3). The same conditions were used to assess the binding of cherry bomb capsids with the poly-T25- coated AuNPs. The control micrographs revealed no evidence of non-specific VLP-AuNP binding.

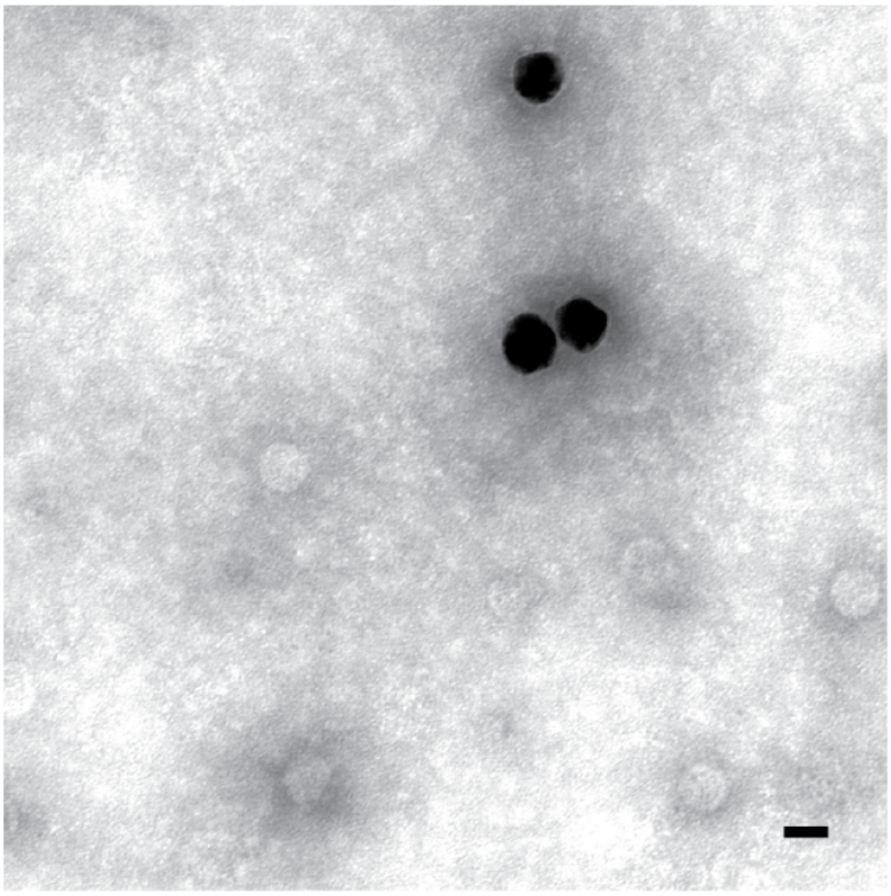

**Figure S3.** 30-nm AuNPs coated with poly-T25 (dark spheres) were incubated with VLPs containing pure B1 RNA (light spheres) and imaged by negative-stain TEM. There is no interaction between VLPs and AuNPs. Scale bar shows 25 nm.

**Aggregated assembly of CP around surface-bound RNA**

Hybridized RNA-DNA was prepared and equilibrated with 30-nm poly-T25-coated AuNPs at a molar ratio of 10:1 (RNA:AuNP) for 30 min on ice. After hybridization of the RNA to the AuNPs, CP was added at a mass ratio of 10:1 (CP:RNA), equilibrated for 5 min on ice, and imaged by negative-stain EM (Fig. 5B). We used a higher amount of CP (compared to the 4.4-fold mass ratio used to completely package unbound RNA[7,30]) in

case a fraction of the CP was bound by the excess of poly-T25 DNA oligos coating the surface of the AuNPs. Indeed, TEM images showing thickened layers of material coating the AuNP surface suggest that CP does bind the poly- T25-coating (Fig. S4). Earlier assembly studies[7] using pure RNA showed that CP:RNA mass ratios higher than 4.3:1 can result in aggregation. This phenomenon may contribute to the aggregation we see in the AuNP-bound assemblies (Fig. S4).

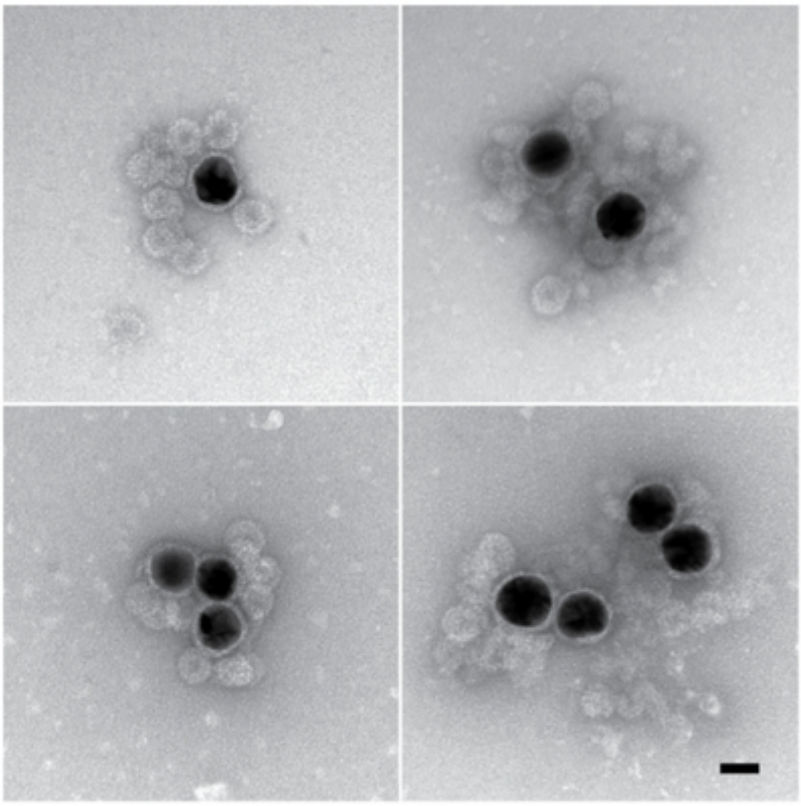

**Figure S4.** VLP assembly around RNA-DNA bound to the surface of 30-nm AuNPs coated with poly-T25 showed significant aggregation. The three types of aggregation seen are (i) an extra layer of material coating each AuNP (thick white halos surrounding electron- dense AuNP found in all images), (ii) extended capsid structures (upper-left image), and (iii) amorphous aggregation (upper-right and lower-right images). Scale bar shows 25 nm.

**Transmission Electron microscopy (TEM)**

Negative-stain: 6 µL of sample at a concentration of a few nM was deposited on glow- discharged copper grids (400-mesh) that previously had been coated with Parlodion and carbon. After 1 min, the grids were blotted and stained with 6 µL of 2% uranyl acetate for 1 min followed by blotting and storage in a desiccator overnight.

Positive stain: Inevitably, some regions of a negative-stained TEM grid exhibit positive staining. In these regions stain penetrates the sample particles, rather than coating them. We have found that certain structural features are sometimes better resolved through positive staining – in this case, the RNA- DNA hybrid appendage was more visible in positive- stained regions (Fig. S1).

**Native agarose gel electophoresis**

10 µL of sample was mixed with 3 µL of glycerol and loaded into a 1% native agarose gel in virus electrophoresis buffer (50 mM sodium acetate, 1 mM EDTA, pH 5.5). The samples were electrophoresed at 4°C at 50 V for 1 h and visualized with a FX Pro Plus Fluorimager/PhosphorImager (Bio-Rad) by ex- citing the UTP-AF488 of the B1 RNA and 6-FAM of the poly-T15, separately, and measuring the emitted fluorescence intensity. The emission intensity of UTP-AF488 (RNA) is shown in red, and that of 6-FAM (poly-T) is shown in green.

## Chapter 5

### Magnetic Tweezer Experiments of Capsid Disassembly

These studies are intended to discern, at a single-molecule level, details of the process of RNA being pulled out of a capsid by force. We expect that our force measurements may reveal how an RNA could be pulled out from inside an intact virus particle. Co-translational disassembly, a process by which a virus disassembled by its host's ribosomes, is a mechanism believed to be caused by the RNA being translocated by the host's ribosome as it translated the viral RNA. Studies done to measure this phenomenon have used cell free extracts and demonstrated evidence that the virus is not always disassembled immediately but requires a certain amount of RNA to be pulled out from the capsid before a collapse of the capsid is inferred. This disassembly process has been suggested to occur in systems such as tobacco mosaic virus, cowpea chlorotic mottle virus and human infecting viruses like Semliki Forest virus[83]. A single-molecule force microscopy technique could reveal if the forces required to

remove RNA from the capsid are similar to the forces the ribosome can pull[84]. While studies like this have been done on TMV using AFM,[79,85] we intend to use an icosahedral virus to better understand the dynamics of pulling RNA out of a spherical virus. In addition, the assays using AFM had issues with the force being non-biological (i.e. almost an order of magnitude beyond the ribosome pulling force). Overall, these single-molecule force-pulling assays may reveal physical aspects to the balance between a virus' particle stability and its dynamic fluctuating nature which both play an integral role in the virus life cycle.

We have developed two different constructs to study these phenomenon: one, a control, to understand pulling on large RNA alone, and the main experiment, which is to pull RNA out of an a virus-like particle with the 5' end of the RNA isolated outside of the capsid to provide an effective handle for magnetic tweezer single-molecule pulling.[86] In these experiments, using this RNA only unfolding experiment, we expect to see the difference between RNA being pulled apart from its respective ends, and the capsid being pulled apart with one end of its RNA tethered to a bead and its other end covalently attached to a surface.

**Magnetic Tweezer Principles**

A magnetic tweezer apparatus, diagrammed and photographed below in figure 2, fundamentally relies on an inverted microscope setup, with a bright LED, functionalized superparamagnetic beads ~0.5-5 micrometers in diameter which interact with the sample of interest to be pulled on, an immobilized sample (in our case the cherry bomb

VLP or naked RNA, both functionalized with a biotin at the 5’ end of the RNA) attached to a coverslip, and an actuated dual-magnet head which can be brought close or removed from the coverslip. The coverslip, which is in contact with the objective lens, is part of a flow cell, which allows for precise introduction of buffer solutions, samples and the magnetic beads by a syringe pump system. Super-paramagnetic beads which can have antibodies or other functional groups, can attach to the sample of interest, and can be manipulated by bringing the dual-magnet head closer, to increase the force felt on the magnetic beads, or moved away from the beads, to decrease the force. Magnetic beads are tracked using a CCD camera and recording software. Beads appear as large spheres, and to have accurate information about their precise position in Z-height (relative to the coverslip surface), the microscope’s focus is defocused to which result in observing a diffraction pattern (Airy disk and rings) of each magnetic bead. This Airy pattern, provides more information of the beads precise Z-height, and can also be used to calibrate the height of the magnetic beads relative to a bead that is fixed to the surface. As the magnet head can be manipulated by software, setting up an automated force pulling profile can be done on a region of interest within the flow cell. Key to the operation of these experiments is that the magnet can move at a millimeter length displacement, changing forces felt by the magnetic beads from a range of 0-200 piconewtons. In response to a quick change in force, the limiting factor of the displacement of the super-paramagnetic beads is largely due to the viscosity of the aqueous solution. Software allows for individual beads to be tracked with a precision of a few nanometers in lateral dimensions, x and y, and vertical direction normal to the surface of the flow cell, z. Figure 1 below displays multiple beads being tracked (with

the green reticules that indicate the software real time tracking of a bead along with an associated height of the bead from the surface of the coverslip in micrometers) overlain on the field of view. Note the Airy disks and rings present in the image below which have different thicknesses and distances from the center of the bead depending on the Z-height.

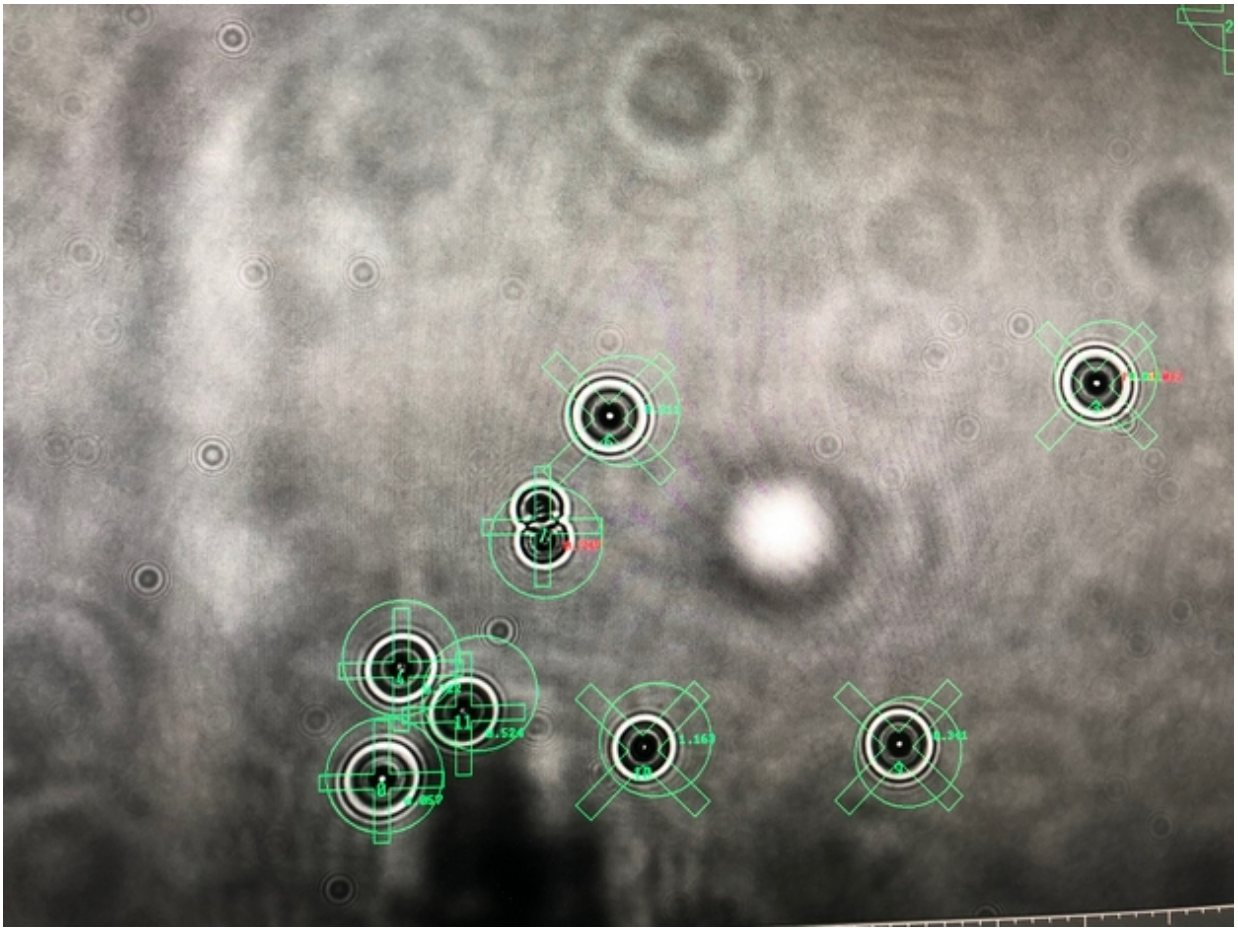

**Figure 1.** Magnetic beads in the field of view, are attached to the surface of the glass coverslip either through specific interactions with the capsid, or potentially non-specific interactions with the surface. In theory, multiple magnetic beads attached to a biomolecular sample could be probed at the same time, but often non-specific interactions can dominate a field of view.

**Pulling of naked RNA.**

First, we generated a functionalized single-stranded BMV RNA 1 (3200 nt long) with a biotin modification on the 5’ end. Magnetic tweezers, a nano-manipulation technique, allows for nucleic acids and proteins to be pulled on by piconewton forces with simultaneous measurement of the displacements associated with these forces. In this experiment, an iron-oxide super-paramagnetic bead, 3 μm in diameter, covalently functionalized with streptavidin can interact with the biotinylated RNA by its 5’ end. The 3’ end of the RNA is hybridized to a DNA linker, which can be further hybridized to an alkyne functionalized DNA oligo that is attached to an azide-coated glass coverslip, allowing for single-molecule pulling of the magnetic beads attached to the RNA that have been incubated with the presence of the DNA oligo on the surface.

**Experimental apparatus preparation**

We prepared glass coverslips for pulling experiments following protocols provided by Dr. Duyoung Min at UCLA and Professors Vincent Croquette and Professor David Bensimon at the Ecole Normale Superieure in Paris, France. We worked on optimizing glass slide cleaning and surface passivation/functionalization to maximize the chance of observing a pulling event. This was mostly an effort to make sure the glass coverslips were close to being atomically flat, and that the bound surface molecules would be efficiently chemisorbed onto the surface, such as epoxy-streptavidin functionalized coverslips or silane-PEG-DNA-tether functionalized coverslips.

For experiments done in Paris, pre-purchased epoxy coverslips PolyAn, 2d epoxy coverslips (size #1.5) were used to react with 0.1 mg/mL streptavidin in 20 mM

sodium bicarbonate buffer, pH 7.5 for 30 minutes, then washed extensively in water. Then a flow cell was constructed using precut double sided tape on top of the reacted glass coverslip and sealed with a mylar sheet with two precut holes for the inlet and outlet valves. With small square cut pieces of double sided tape with a hole through the center a inlet reservoir was attached along with a outlet piece which was attached to a long piece of plastic tubing and fitted to a 3 or 5 mL syringe.

For experiments done at UCLA, glass coverslips, Corning #1.5 24x60 mm, were cleaned with saturated potassium hydroxide in 100% ethanol in glass staining jars, which could fit ~15 slides.[87] Sonication with a bath sonicator was done after the cleaning, and washes with 100% ethanol, acetone and finally double deionzed water ($ddH_2O$) was done. These slides were then put into a flow cell construction as described above for the epoxy coated slides, then a 100% DMSO solution containing a 1% silane-PEG(2000dalton)-NHS molecules (w/v) solution was incubated in the flow cell for 1 hour at room temperature. DMSO was removed by pulling vacuum on the flow cell by a syringe. The flow cell was then washed with $ddH_2O$ then by a non-amine containing buffer (20 mM Sodium bicarbonate pH 7.2).

Covalently functionalized silane-PEG-NHS (~2500 daltons) coverslips were immediately covalently linked to an amine functionalized end of a 1 kb DNA tether through a N-hydroxy-succinimidyl ester (NHS-ester)-amine reaction. A majority of the PEG-NHS molecules on the glass coverslip did not react since a limitation of DNA in the solution (only 1 picomolar in the flow chamber) such that these DNA molecules were spatially separated from each other by a couple of micrometers apart on average, such that a single magnetic bead, approximately 3 micrometers in diameter, is unlikely to bind

more than one cherry bomb capsid per spot on the functionalized glass surface. The flow cell was again washed in 20 mM sodium bicarbonate buffer. The flow cell is then incubated with a 10 picomolar solution of streptavidin for 30 minutes.

Separately, cherry bomb VLPs were prepared as described elsewhere[17]. Briefly, *in vitro* transcribed B1 RNA with a biotin-ApG dinucleotide initiator was transcribed.[32] Biotin B1 RNA produced had a single biotin at the 5' end of the RNA. At 300 nM a 183 nucleotide DNA oligo complementary to the 5' end of the RNA was hybridized to 30 nM biotinylated B1 RNA in RAB* buffer (with 100 mM extra NaCl) incubated at 70°C for 5 minutes then decreased by 0.1 degree celsius per second to 4°C. This was mixed with purified BMV capsid protein, obtained from a disassembly of BMV WT virus grown in barley, in a 4.8 to 1 capsid protein to RNA mass ratio in RAB (at a final reaction concentration of 0.144 mg/mL capsid protein and 0.03 mg/mL biotin B1 RNA). After 30 minute incubation at room temperature, one part per 100 of 1.08M acetic acid was added to the reaction mixture (i.e. the remaining 99 parts). This formed biotinylated cherry bomb capsids which under electron microscopy were similar to the images shown in [17].

Finally a 10 picomolar biotinylated cherry bomb capsids with biotin at the end of the RNA in RNA assembly buffer* (50 mM Tris-HCl pH 7.2; 5 mM $MgCl_2$; 10 mM KCl; 50 mM NaCl, star indicates NO $MgCl_2$) are incubated allow for a strong-linkage to be made with the biotinylated cherry bomb constructs and the streptavidin functionalized 1 kbp DNA tethers.

The streptavidin in both cases interacts with the cherry bomb's biotin moiety at the end of the RNA-DNA handle, and then allows for a magnetic bead to interact either via conjugated antibodies that are specific for the capsid protein of BMV or covalently binding the magnetic beads to the capsid using EDC/sulfo-NHS chemistry, rolling the beads in over the sparsely coated cherry bomb glass slide such that they would react with the lysines present on the surface of the cherry bomb capsids in the flow cell forming a covalent tether.

Preliminary experiment were carried out that show promising results. Shown in Figure 3 and 4 but these experiments would likely benefit from using the DNA handle directly attached to the cherry bomb stem, removing the streptavidin linkage requirement and removing ambiguity on how the tether is lost. For our follow up experiments, we will make a glass coverslip with a PEGylated surface attached to a 1 kb DNA handle which has a poly T(30mer) sticky end accessible to hybridize to a PolyA (30 mer) of the cherry bomb capsid stem DNA. A 30-nucleotide hybridizing overlap should be plenty to insure an effective covalent attachment without a high-temperature requirement to melt single strands before hybridization, which can be more difficult to do inside a flow cell.

**First Experiments (ENS, Paris)**

The streptavidin functionalized flow cell was placed onto the objective of the magnetic tweezers system using an oil immersion lens at 100x magnification.

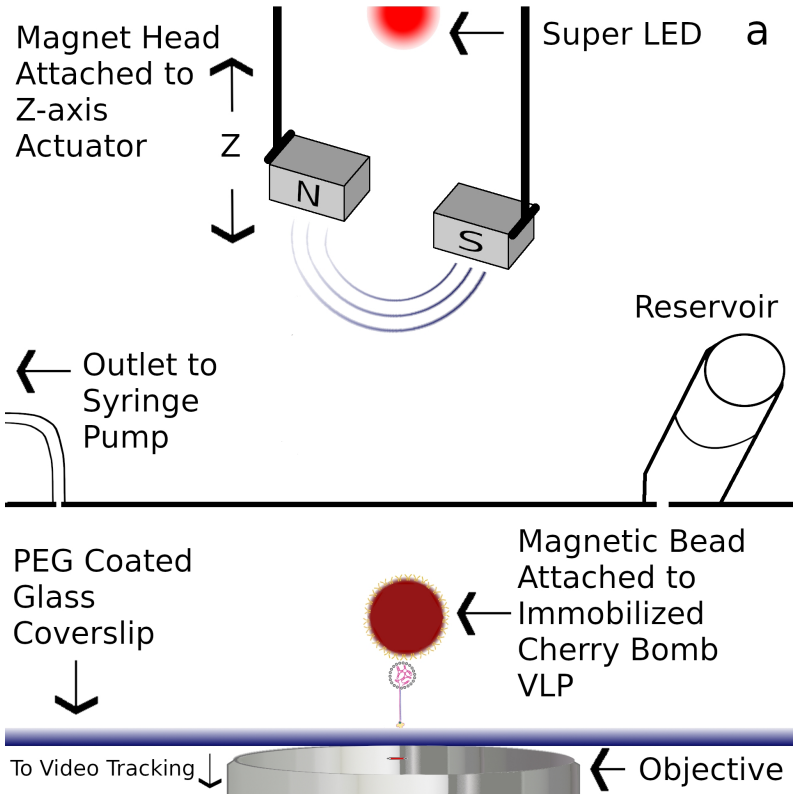
Magnet Head
Attached to
Z-axis
Actuator
Z
N
S
Super LED
a
Reservoir
Outlet to
Syringe
Pump
PEG Coated
Glass
Coverslip
Magnetic Bead
Attached to
Immobilized
Cherry Bomb
VLP
To Video Tracking
Objective

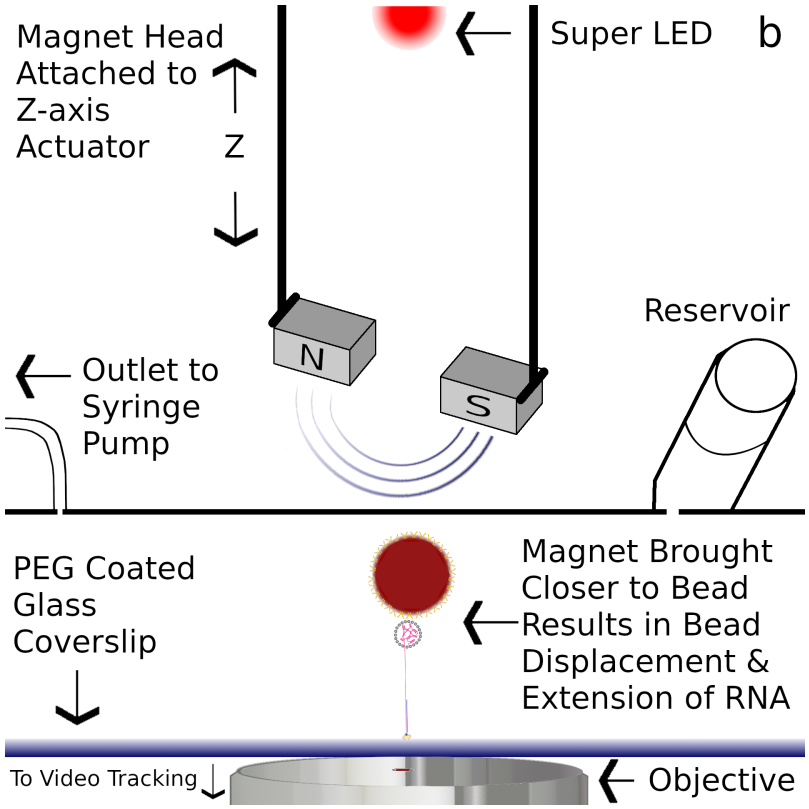
Magnet Head
Attached to
Z-axis
Actuator
Z
N
S
Super LED
b
Reservoir
Outlet to
Syringe
Pump
PEG Coated
Glass
Coverslip
Magnet Brought
Closer to Bead
Results in Bead
Displacement &
Extension of RNA
To Video Tracking
Objective

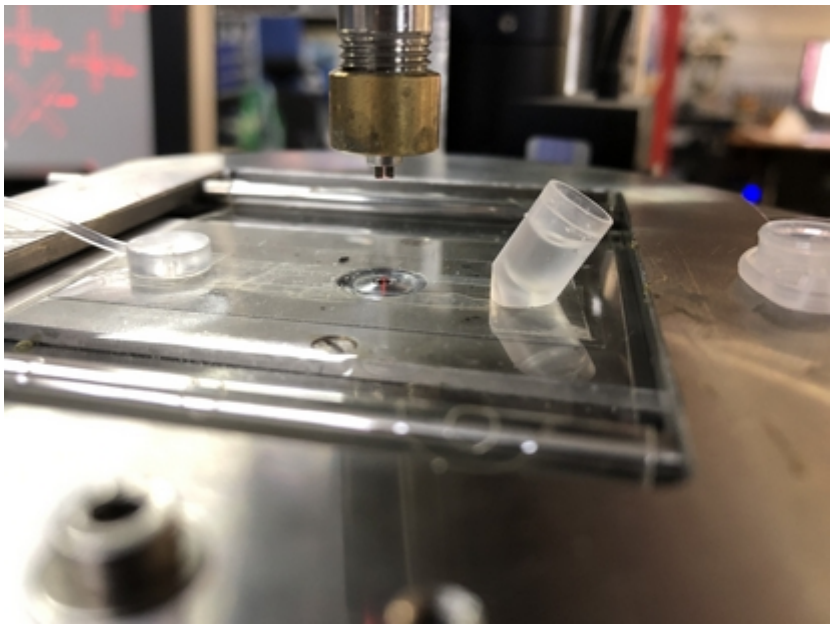

**Figure 2. a-c. a)** Cartoon depicting magnetic tweezers apparatus. Flow cell containing cherry bomb VLPs with magnetic beads attached to a glass coverslip by streptavidin. **b)** When the dual magnet head is brought closer to the flow cell, an increase in force is felt by the super-paramagnetic beads (2.8 micrometer anti-capsid-protein antibody functionalized carboxylate Dynabeads, M280, Thermofisher) which may result in RNA being pulled out of the capsid and an extension in the magnetic bead height relative the surface of the coverslip can be measured. **c)** A photograph of the magnetic tweezer instrument's stage and dual magnetic head. The flow cell for the experiment is on top of the stage/objective of the microscope with a reservoir inlet on the right and the outlet valve on the left is attached to a syringe pump, not shown. The instrument has a digitally-controlled actuator, which allows for precise movement of the dual magnet head, a red Super LED shown from above, and a 100x 1.4 NA objective connected to a CCD camera which allows the illuminated beads to be observed and bead movements

over time can be recorded potentially in parallel. The two magnets at the end of the copper looking cylinder at the top of the image are placed directly above the region of interest in the flow cell containing the sample/beads for measurement. The force is felt most strongly on the line that is normal to the flow cell surface and splits the two magnets. Images of the beads are taken by the CCD camera at a frame rate which can be set from 30-100 Hz.

Magnetic beads with a carboxylic acid functionalized surface were covalently attached to anti-capsid protein monoclonal antibodies (a gift from Professor Mark Young, Montana State University), using EDC and Sulfo-NHS chemistry to attach surface-exposed amines of the antibody.

For the pulling experiments, the cherry-bomb capsids were introduced by pipetting the solution into a reservoir on the flow cell and by pulling vacuum from the other side of the flow chamber with a syringe pump at a rate of 10 μL/min for 5 minutes and then the sample in the flow cell chamber was then incubated for 1 hour at room temperature at a 0.6 nM final concentration of the cherry bomb construct in a low divalent cation RAB (0.5 mM magnesium chloride instead of 5mM) in 0.1% bovine serum albumin and 0.05% sodium azide. The volume of the flow cell chamber is approximately 40-50 uL. After a wash of 150 uL of RAB* buffer (does not contain magnesium chloride), 1 uL of magnetic beads (washed and diluted four fold in RAB* from stock concentration) was directly injected into the flow chamber (bypassing the reservoir). Magnesium was not used once magnetic beads were to be introduced to prevent magnetic bead clumping which occurs in magnesium ion containing buffers (especially if $[Mg^{2+}]$ is greater than about 0.5 mM). Beads were concentrated under

magnetic force over a region of the flow cell such that by releasing the magnetic force, beads could be incubated over cherry bomb containing regions of the flow cell. After a 10 minute incubation, magnetic beads were washed away using a syringe pump and the remaining beads in the field of view were the subject of the experimental force pulling.

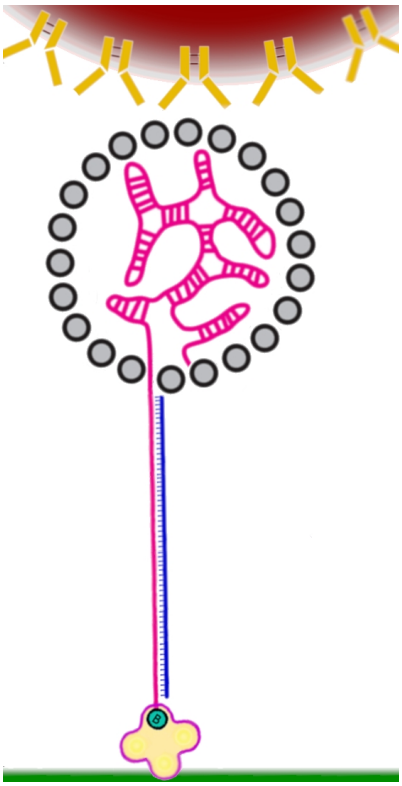

**Figure 3.** Biotinylated B1 RNA Cherry Bomb construct attached to a surface of a streptavidin-functionalized coverslip with an antibody-coated 2.8 micrometer Dynabead (top, which are brownish red with yellow antibodies). Cherry bomb is denoted with grey spheres marking the capsid, pink is the RNA and blue is the DNA handle. Streptavidin is the yellow diamond shaped object attached to a glass coverslip in green.

Usually, force was applied either by increasing of a force ramp, such that for 2-4 seconds the magnet was lowered 50 micrometers at a time, or starting a fixed estimated

force that could be set between 10-50 piconewtons of force involving slow ramps upwards to a high force and if seeing something interesting in the bead dynamics, then quickly dropping the force to below 5 piconewtons (low force condition) to confirm if we are observing a capsid-bound magnetic bead. The latter procedure was useful to figure out how much force would be necessary to observe a change in the capsid dynamics. Often we would leave the sample under constant force for the period of 2-3 minutes, then the force was dropped to below 5 piconewtons for 30 seconds to a minute. Then a new slow ramp up to the higher force (the ramp would take 5-15 seconds depending on how high the force was brought up to by moving the magnet at a slow 0.01-0.05 mm per second).

In the trace below, shown in figure 4, is the red curve which is the estimated applied force to the magnetic beads in piconewtons (right y axis), the yellow curve represents the relative bead height displacement in micrometers (left y axis) and the x axis is time in seconds. The yellow line represent the position of the bead at any frame (the frame rate is set to 30 Hz) and specifically reports on z-height of the bead with reference to the flow cell glass coverslip surface. For reference, the cherry bomb construct attached to a flow cell and a magnetic bead is inset as a cartoon in the bottom left of the trace. The red trace represents the force, and the constant force (horizontal) lines are made thicker in red for easier visualization and interpretation. Variance in the force should be very minimal, thermal effects do not contribute much to relative magnet position when the force is set to a fixed level.

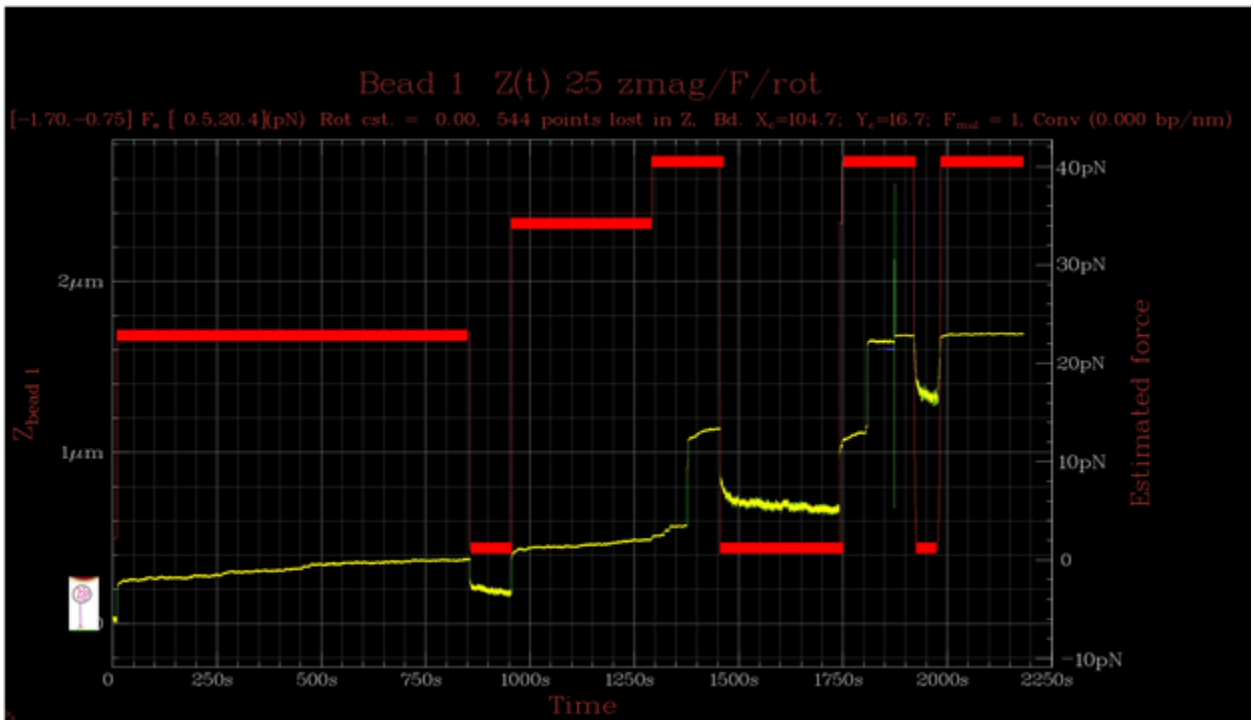


**Figure 4.** This magnetic tweezer trace of the cherry bomb capsid VLP has an extension difference of nearly 1.7 micrometers. A brief analysis of the force extension curve suggests that single-stranded RNA may be being pulled as the forces and extension response have characteristics of the unzipping of double stranded regions of nucleic acid (data not shown). Indeed, an extended RNA base, under sufficient force, is close to 0.6 nanometers, then a length of 1.7 micrometers is potentially possible for B1 RNA (~3200 nucleotides long). Interestingly, if you release the force from 20 piconewtons you see some interesting events around 1950, 2250 and 2400 seconds. We are wondering if part of the curve could be resulting in a refolding of RNA after the release of force by withdrawing the magnet, but it is unlikely that the capsid is still intact after the ~1375 second abrupt transition (where the yellow trace makes a vertical step). Inset in the bottom left hand corner is a cartoon schematic of the virus like particle attached to a

magnetic bead, at approximately the scale representative of the trace height of ~150 nm near the beginning of the experiment.

Our data suggest that RNA is being pulled since we are observing abrupt extension transitions when the force is kept constant, at ~1375, 1800 and 1875 seconds. We observe an end to the yellow extension curve because the bead had been pulled off of the tether, potentially through the streptavidin-biotin interaction but it is possible that this loss of the magnetic bead could also have occurred by pulling off a capsid protein from the capsid.

**Second set of experiments (UCLA): covalent linkage of magnetic beads to capsids.**

In an attempt to decrease the number of non-covalent interactions in the cherry bomb pulling system, a new approach was attempted using a DNA tether that keeps the capsid away from the surface of the glass coverslip.

To attach the magnetic beads to the capsid, we decided to make an activated carboxylate coated magnetic dynabead (2.8 micrometers in diameter) that had a EDC/sulfo-NHS activated functionalization. This resulted in a dynabead with a NHS group available for interacting with the capsid directly via reacting with the primary amines of the lysine groups present on the capsid shell. Since the flow cell already has the DNA tethers attached reagents were sequentially introduced into the flow cell. First, streptavidin was incubated followed by a wash of RAB* buffer, then biotinylated B1 cherry bomb VLPs were incubated within the Streptavidin-DNA-PEG glass coverslip functionalized flow cell. Finally, a buffer change into a 20 mM sodium bicarbonate buffer

was done (pH 7.5) to introduce the sulfo-NHS dynabeads into the flow chamber where they could react with the lysines present on the immobilized cherry bomb capsid. The flow rate was done at approximately 10 uL/min for all experiments.

**Surface preparation**

Much of the challenge using magnetic tweezers involves surface functionalization, cleanliness, and characterization. Using a modified strategy outlined in Schlingman et al[88], #1.5 glass coverslips were cleaned using a concentrated KOH and ethanol solution in a coverslip glass jar overnight. Once the slides had been cleaned, glass coverslips in the glass jar were drained from the ethanol KOH solutionwere washed by treatment with 100% acetone and sonicated for 10 min in a bath sonicator. Subsequent washes were done with ethanol then coverslips were allowed to dry using argon gas. A 1% (w/v) silane-PEG(3kda)-NHS (Nanocs) in 100% DMSO was made to minimize  hydrolysis of the NHS esters. Approximately 30 uL of solution was pipetted onto the cleaned, dry glass coverslips, with a second coverslip carefully aligned above the first to sandwich the solution and cover the entire surface of both coverslips. This is allowed to incubate for one hour at room temperature and then the coverslips are rinsed with dd$H_2O$ and rinsed with 20 mM sodium bicarbonate buffer pH 7.2.

To assemble a flow cell, precut double-sided tape was laid down on top of the dried NHS-PEG coated coverslip to then allow for precut mylar sheets to be laid down on top with two holes to allow for an inlet and outlet at either end of the flow cell and effectively forming a sealed system (except for the inlet outlet ports). Once the coverslips, and mylar sheet had been sealed together by removing air bubbles present

in the double sided tape by gentle horizontal motion with downward pressure using the dull side of a razor blade, the outlet port and inlet reservoir was attached using ~ 1 cm square piece of double-sided tape that has a precut 2 mm hole in the center. Making sure these two attachments are attached efficiently also requires a bit of pressing to remove any extra air. Below is a picture of the completed flow cell with the inlet reservoir on the right and outlet port connected to a long piece of tubing that terminates in a 1 or 3 mL syringe such that the reservoir containing samples or buffer can be introduced at a slow reproducible rate using a syringe pump. At the top of the image the two small magnets attached to the cylinder above is the key part part of the magnetic tweezer apparatus as these magnets can be raised or lowered to decrease or increase the effective force that the magnetic microspheres can feel inside the flow chamber. DNA was attached to the NHS functionalized cell as mentioned above.

**Operation of magnetic tweezers and sample introduction.**

Once the flow cell had been assembled, capsids and DNA handles were introduced. This introduction needs to be done relatively quickly after finishing the NHS-PEGylated coverslips, unless the coverslips are immediately frozen after formation. Magnetic tweezer setup was a custom build by Dr. Duyoung Min, based on similar instrument setups from design of Vincent Croquette and David Bensimon at the Ecole Normale Superieure. A light microscope with a moveable x-y stage and a retractable dual magnet head which can be moved vertically by an actuator (stepper motor) to impart different magnetic forces onto the flow cell containing the super-paramagnetic beads. Custom labview software was used to control movement of stage and dual

magnet head height, and record bead positions in x, y and z dimensions. Data was saved in CSV format and plotted using matplotlib and python[89].

**Results of second set of experiments (UCLA, with Bowie Lab)**

Below is a representative trace of the experiment done at UCLA using the 1 kb DNA tether to extend the capsid away from the glass surface and potentially abrogate issues with magnetic beads non-specifically interacting with the glass coverslip functionalized surface.

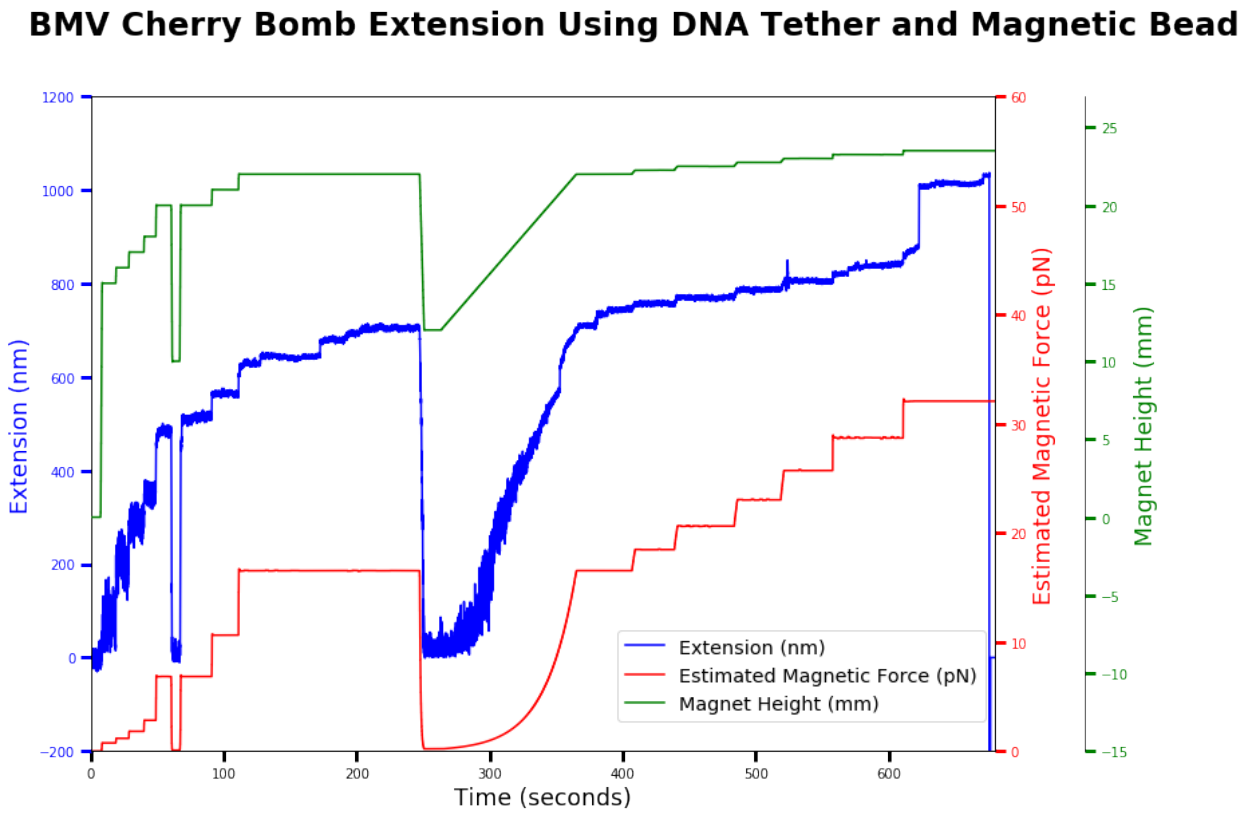


**Figure 5.** The curve above displays the trace of the extension in nanometers of the RNA being pulled out of the cherry bomb capsid construct (denoted in blue), versus the

time on the x axis, and overlaid are the traces of the estimated magnetic force (in red) produced by varying the magnet height (in green) closer to or away from the surface of the flow cell where the magnetic beads are bound to the capsid covalently.

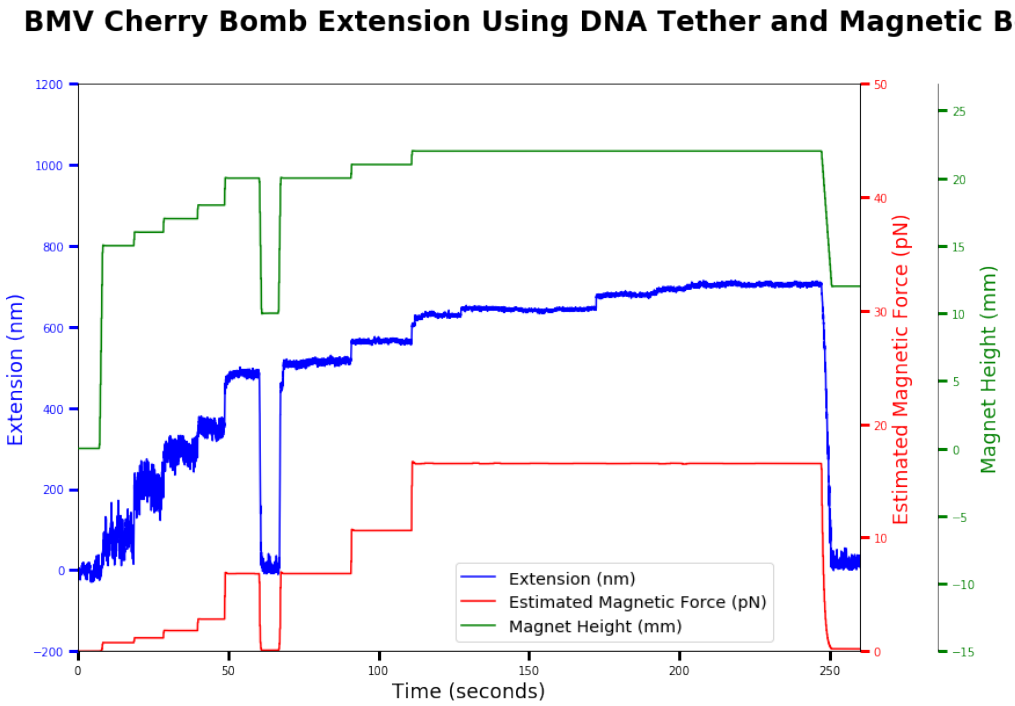


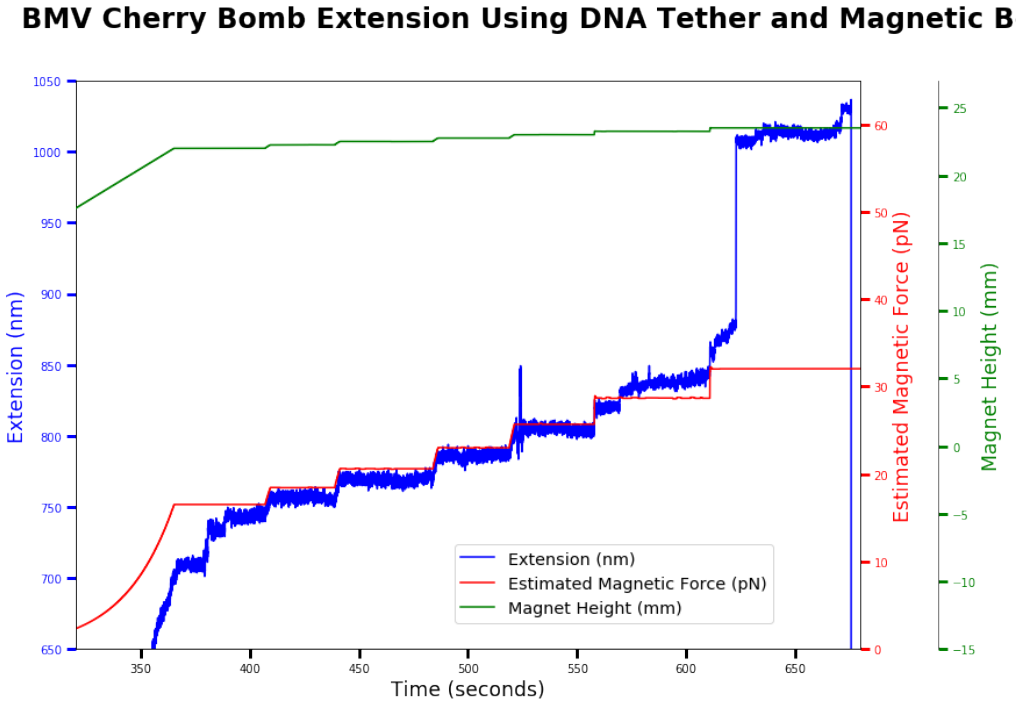

**Figure 6. a and b.** These two figures are a division of the single-molecule magnetic tweezer trace of figure 5 above into its **a)** early and **b)** late time points, namely to focus on low and high estimated magnetic forces being applied to the magnetic bead, respectively.

From figure 6a we are interpreting that we are mostly observing the straightening of the DNA tether from the beginning of the trace at 0 seconds until 110 seconds where the force applied is 12 pN or less. The DNA tether should be ~ 300 nm long, plus another ~150 nm of the cherry bomb complex and ~20-30 nm for the 3kda PEG functionalization of the glass coverslip. We are approaching ~500 nm of extension which is close to the 570 nm of initial extension observed in the trace at a fixed force of 12 pN. In figure 6b, we see some rather large jumps as observed in figure 4. Interestingly some of these jumps are from 10-40 nm, up to a 130 nm jump at the 620 second time point. Could this final jump be a disassembly event? Further experiments are underway to unravel this question.

**Discussion**

From figure 6b) we can observe that in the high force regime (>30 pN) that extensions of the RNA can occur while the force is fixed, these extensions are on the order of 10-150 nm. While it remains early in our process of running these experiments, we interpret these displacements as RNA being ratcheted out of the capsid, and we are looking forward to using other strategies that complement these measurements to verify this. One idea is to introduce RNases that can result in the RNA being degraded and

therefore under low enough forces, we expect the tethers to break as RNA has already been pulled out of the capsid. Another possibility is to cross-link the capsid together with a change to look only at RNA being pulled out without capsid disassembly at all. Together these experiments will reveal the subtle nature of this viral capsid, and potentially new insights into physical and biological constraints of the dynamics of the capsid.

## Chapter 6

### ssRNA Undergoes Single-Molecule Compaction in the Presence of Polyvalent Cations

Liya Oster, Richard W. Sportsman, Ana Luisa Duran-Meza, Charles M. Knobler and William M. Gelbart

### Abstract

In the presence of polyvalent cations, the phosphate backbone of double-stranded DNA (dsDNA) undergoes a single-molecule, first-order phase transition called condensation, best visualized by the presence of DNA toroid for sufficiently long dsDNA molecules (>40kbp). In dsDNA condensation, when 90% of the phosphate backbone is neutralized by positive charges, the dsDNA compacts into tightly wound toroids. In this study we examine the effects of increasing concentrations of spermine, a cation with a 4+ charge in solution, on the effective size of long ssRNAs (>3knt). Our results suggest

a fundamental difference in the physical phenomenon of single-stranded nucleic acids and double stranded DNA interacting with polyvalent cations. Analytical ultracentrifuge data was gathered to more accurately determine sedimentation coefficients of spermine-RNA complexes. Results indicate that ssRNAs do not undergo a condensation event analogous to the condensation of DNA. Instead, long ssRNAs undergo a continuous compaction as the spermine to ssRNA charge ratio increases.

## Introduction

The condensation of double-stranded (ds) DNA by polyvalent ions was first demonstrated by Gosule and Schellman[90] who wondered if the packaging of the 39.9 kb DNA of the T7 phage into the preformed capsid was aided by condensation induced by the trivalent polyamine spermidine, which is present in cells. In *in vitro* experiments they found that the DNA underwent an abrupt, apparently cooperative decrease in size with increasing spermidine concentration; a similar phenomenon was observed with the tetravalent polyamine spermine, but at a lower concentration. Later studies demonstrated that the collapse is a first-order transition in which polyvalent ions with charges of 3+ or greater induce attractive interactions between the like-charged worm-like random coils resulting in precipitates of the DNA, which in sufficiently long polymers have toroidal or rod-like structures (see the review by Bloomfield[91]). This condensation phenomenon is distinct from the continuous increase in density of individual polymers resulting from the adsorption of counterions, which reduces intrachain repulsions, but does not result in interchain attraction; we term this *compaction*.

The effect of polyvalent ions on dsRNA is less clear. With the exception of an equimolar mixture of homopolymer polyA+polyU, 25 bp dsRNAs were not found to be condensed by polyvalent ions under conditions where comparable length dsDNAs aggregated and precipitated[92]. Similarly, thermodynamic and optical measurements showed that three 280bp homopolymer mixtures, polyI+polyC, polyC+polyG and polyA+polyU were compacted by polyamines[93]. Much less is known about the effect of polyvalent ions on *ss*RNA. It has been shown by measurements of the sedimentation rate that Turnip Yellow Mosaic Virus (TYMV) RNA is compacted by spermine[94] and that the packaging of this 6300 nt-long RNA into 28-nm diameter capsids is enabled by its interaction with spermidine[95]. It is not known, however, if this is the result of condensation. In this study, we compare the effects of increasing concentrations of spermine on a long ssRNA and dsDNA by two methods, spectroscopic measurements of concentration after centrifugation and measurements of sedimentation measurements in the ultracentrifuge. We determine that unlike the dsDNA, the ssRNA does not condense, undergoing instead a continuous increase in density.

**Materials and Methods**

Long (5,300 nt) ssRNA was obtained from the pRDCT7B1B3 plasmid described by Cadena-Nava et al.[7] which was linearized with EcoRI and *in vitro* transcribed using the ThermoFisher MEGAscript™ Kit. To ensure all the transcripts were of the same length, the RNA was loaded onto the central wells of a 1% agarose gel, flanked on either side by aliquots that were stained with ethidium bromide. Using the labeled RNA

bands as a ruler, we excised the unstained RNA from the gel, and extracted the RNA from the gel by gel electroelution into a dialysis bag. The extracted RNA was then washed 5x in TE buffer (10 mM Tris-HCl, pH7.5; 1 mM EDTA) using a 100kDa Amicon® Ultra-0.5 Centrifugal Filters spun at 7000 rcf at 4℃ for 10 minutes, with each spin greater than a 10-fold change in volume, resulting in a buffer/solute exchange of ~100,000 fold.

Centrifugation experiments similar to those detailed in Raspaud, 1998[96] were performed on RNA and DNA with a variety of spermine:nucleic acid charge ratios, but with a key difference of using a lower concentration of RNA and DNA and fluorescence as a readout. These conditions were used to prefer only single molecule compaction and not a multi-nucleic acid aggregate. In these experiments, nucleic acid was incubated in TE buffer, which was degassed by bath sonication and argon sparging with increasing concentrations of spermine hydrochloride (Sigma-Aldrich) for 1 hour at 4℃; this was done to avoid the oxidation of spermine. The RNA concentration was 2.5 µg/mL, and the total volume of each solution was 200 µL. Each RNA sample was then centrifuged for 7 minutes at 4℃ and 11,000 rcf. For the DNA samples, the total volume was 250 µL with a concentration of 4 µg/mL, and was centrifuged at 18,000 rcf for 15 minutes. The top 50 µL of supernatant was then extracted and put on a black opaque 96-well plate and diluted 2x with TE buffer. SYBR Gold nucleic acid intercalating dye was added to visualize the presence or absence of RNA in solution. The fluorescence of samples before and after centrifugation was determined using a Tecan Infinite M1000 Pro plate reader, and each supernatant (top 50 µL of post-centrifugation sample) fluorescence reading was normalized to its pre-centrifugation sample. For both

samples, the samples fluorescence intensity measurements were normalized against the nucleic acid before centrifugation. This ratio of post- to pre-centrifugation is then multiplied by 100% to display the change in the concentration of the nucleic acid as a percentage of starting concentration.

Change in sedimentation coefficient (S) of RNA with spermine was measured using an analytical ultracentrifuge (AUC). The concentration of the RNA in these experiments was 8 µg/mL RNA, with a total of 400 µL of solution to maximize signal without being too concentrated to minimize the chance of RNA and spermine forming multi-RNA aggregates. 5317-nucleotide long B1B3 RNA was used in AUC experiments from Cadena-Nava et. al[7].The buffer was 10 mM Tris-HCl, pH 7.5. The centrifugation speed and time was adjusted each run to account for the change in sedimentation velocity of each RNA and spermine sample. AUC data was also gathered for dsDNA (10mM Tris, 8.3µg/mL) under increasing spermine concentrations to compare the profile of DNA condensation under increasing spermine conditions to the profile of RNA compaction under the same spermine and solution concentrations.

To further understand the results from analytical ultracentrifugation, we also measured the hydrodynamic radius of B1B3 RNA using dynamic light scattering (Zetasizer Nano ZS).

**Results**

Data for the supernatant experiments adapted from Raspaud[96] for DNA and RNA are shown in figure 1a and 1b, respectively.

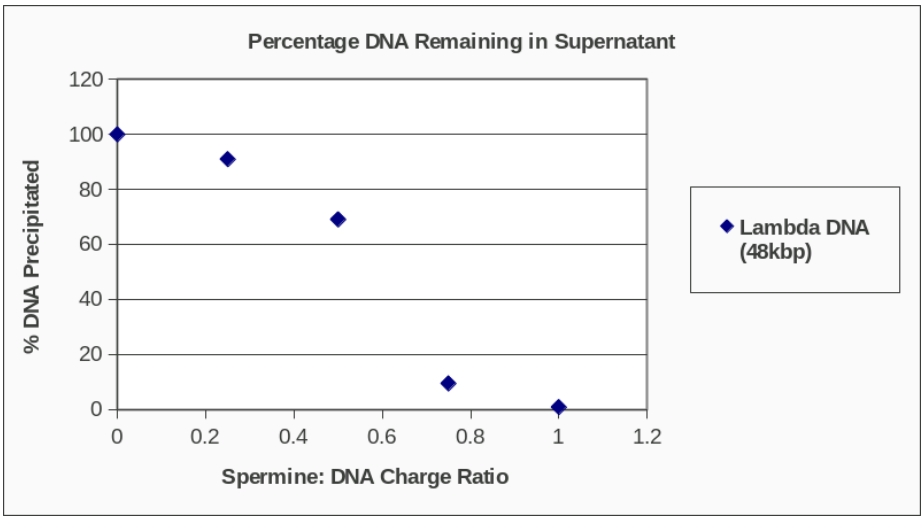


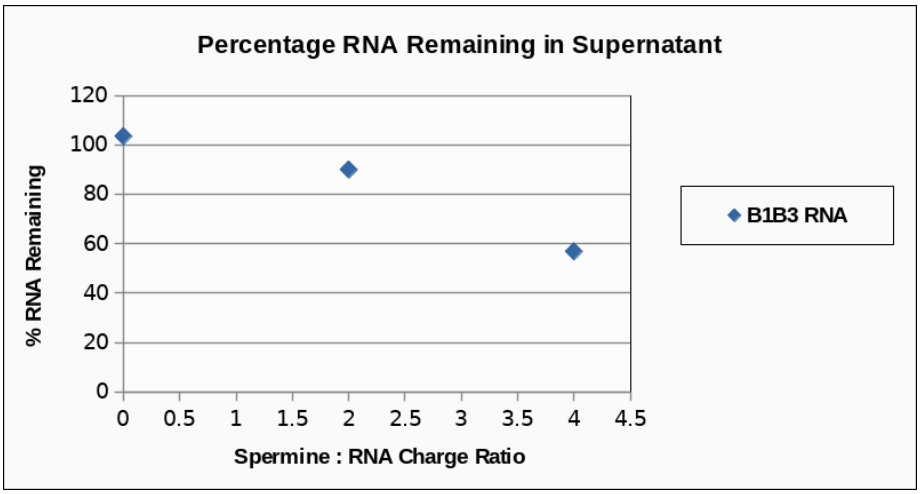


**Figure 1. a and b.** a) Condensation of DNA as measured by centrifugation of DNA following incubation with spermine for 1 hour at 4C in TE buffer, pH 7.5. From the 250 uL samples, DNA was centrifuged at 18,000 rcf for 15 minutes, and the top 50 uL of supernatant was pipetted for analysis in a 96 well black plate. b) RNA compaction by the presence of spermine for 1 hour at 4C in TE buffer, pH 7.5. 250 uL of sample was then centrifuged at 11,000 RCF for 7 minutes at 4C; a lower centrifugal force and lesser time was elected because the spermine to RNA charge ratio range was much higher

than the spermine to DNA ratios and therefore, precaution was taken to minimize aggregation in solution. Using a TECAN Infinite M1000 fluorescent plate reader.

Analytical ultracentrifugation data of B1B3 RNA and DNA with increasing concentrations of polyvalent cations are displayed in figures 2 and 3a and 3b, respectively. As the concentration of spermine increases to stoichiometric charge balance of the negatively charged phosphate backbone of the RNA, the sedimentation coefficient of the RNA increases continuously. In contrast, the sedimentation coefficient of dsDNA upon increasing spermine concentration results in a discontinuous change between the charge ratios of 0.75:1 and 1: 1 spermine to RNA charge ratio, in agreement with previous literature.

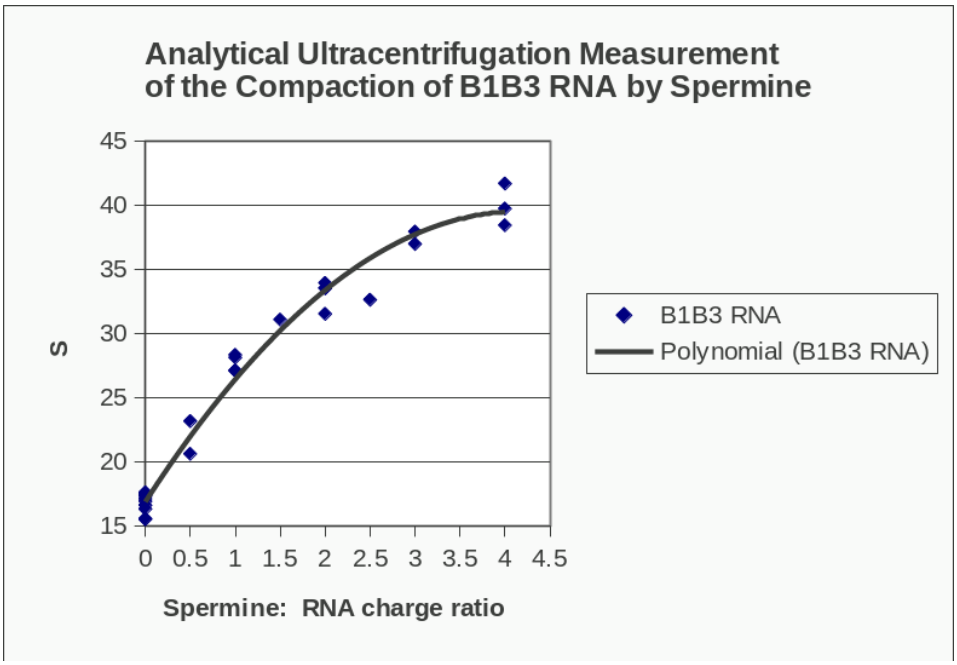


**Figure 2**. The plot above shows the increase in Svedbergs of the B1B3 RNA (~5300 nt long) as a function of spermine to RNA charge ratio. Using a polynomial fit illustrates

that there appears to be a maximum that the observed S rate approaches once a certain spermine to RNA ratio is reached.

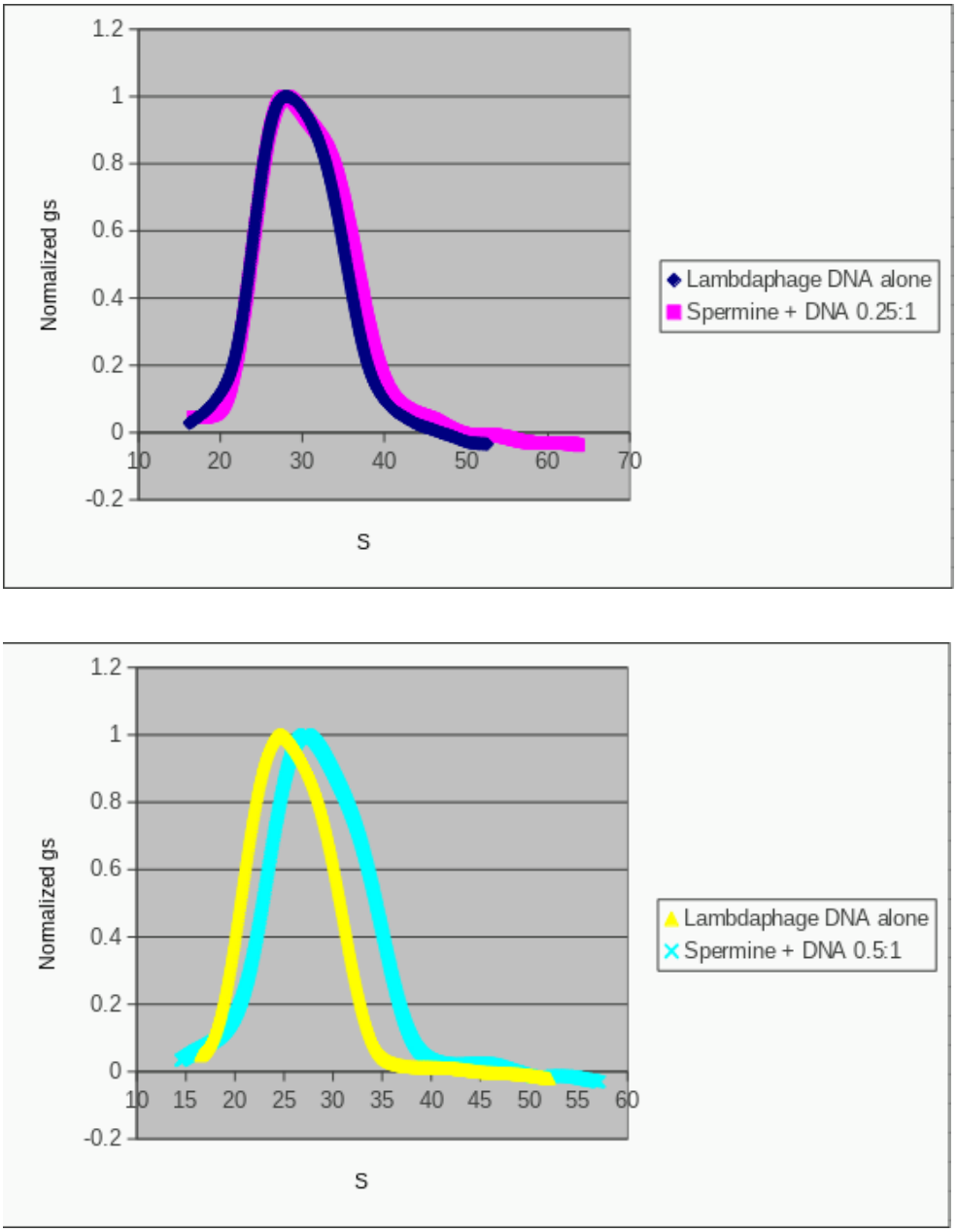


**Figure 3. a and b.** AUC measurements of spermine compaction of DNA. As DNA is compacted by the presence of the polyvalent cation, its sedimentation rate changes, shifted to a higher number (DNA without spermine is labeled in yellow). Because of the

limitation of DNA forming toroids and multi-DNA aggregates at higher spermine to DNA charge ratios, 0.25:1 and 0.5:1 DNA to spermine charge ratios are the only samples which have meaningful data as higher ratios of spermine to DNA result in precipitation of the DNA in the centrifuge within minutes of beginning the AUC experiment (the AUC measurement can take up to a couple of hours). Variability due to run to run differences in sample preparation could be the reason these two graphs show different initial s values, therefore a comparison only from the same sample, namely its control lambda DNA and the experimental condition should be compared. This *change* in gs due to spermine can be compared from one sample to another.

The continuous profile of the RNA compaction by spermine was confirmed by dynamic light scattering measurements, these results are shown below. These data suggest a trend of the RNA becoming more compact up to about a 2:1 ratio, larger ratios were not attempted at the time of the measurements. Distributions in the measurement precision is not as tight as to be expected, but experiments are being repeated.

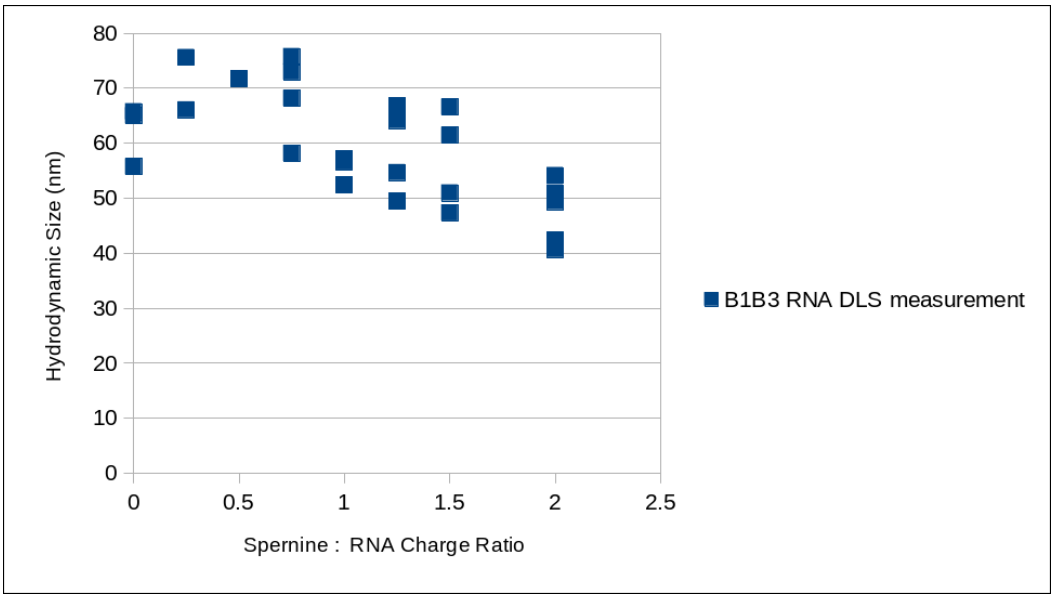


**Figure 4.** B1B3 RNA (~5300nt) was compacted with spermine in TE buffer at 4 Celsius at various spermine to RNA charge ratios. Using a 40 uL sample in a cuvette, the dynamic light scattering measurement was made using the Malvern Zetasizer Nano ZS DLS instrument. Multiple measurements were taken, samples with a polydispersity index of 0.15 or lower were plotted.

***In vitro* encapsidation of spermine-pre-condensed B1B3 RNA into a BMV capsid**

Data for spermine pre-RNA compaction for subsequent *in vitro* self-assembly are shown below. These experiments required packaging RNA with BMV WT Capsid protein using a quick two step assembly method. 5300 nt B1B3 RNA at 0.03 m/mL was incubated with 0.144 mg/mL BMV capsid protein in RNA Assembly buffer (RAB: 50 mM Tris-HCl, 50 mM NaCl, 5 mM $MgCl_2$ 10 mM KCl) for one hour at room temperature. To each 100 uL of solution, 1 uL of 1.08 M acetic acid was mixed rapidly, without introducing bubbles, to change the pH to approximately 4.75. Samples were analyzed by a native agarose gel and negative stain EM resulting in particles similar to WT

capsids. In the spermine to RNA charge ratio of 2:1, spermine was introduced into the RAB buffer mixing with RNA first, then adding capsid protein 30 minutes later for the one hour incubation as noted earlier in this paragraph. The pH change was done as before and results of the two different assemblies were compared. EM images from both assays were analyzed by counting the number of multiplet capsids, namely how many capsid appear to be single capsid, doublet capsid, triplet and quadruplet. This assay may not be able to discern chance capsids ordering on the grid next to each other versus true multi-capsid aggregates.

Results from this self-assembly assay suggest that spermine can play a role in compacting RNA inside a capsid, to a certain degree, but further higher concentrations of spermine should be tried to see if a shift in a distribution of multiplets to singlets can be increased. Indeed, we are trying concentrations of spermine ~50 micromolar, but higher amounts do occur inside cells up to 1 mM.[98]

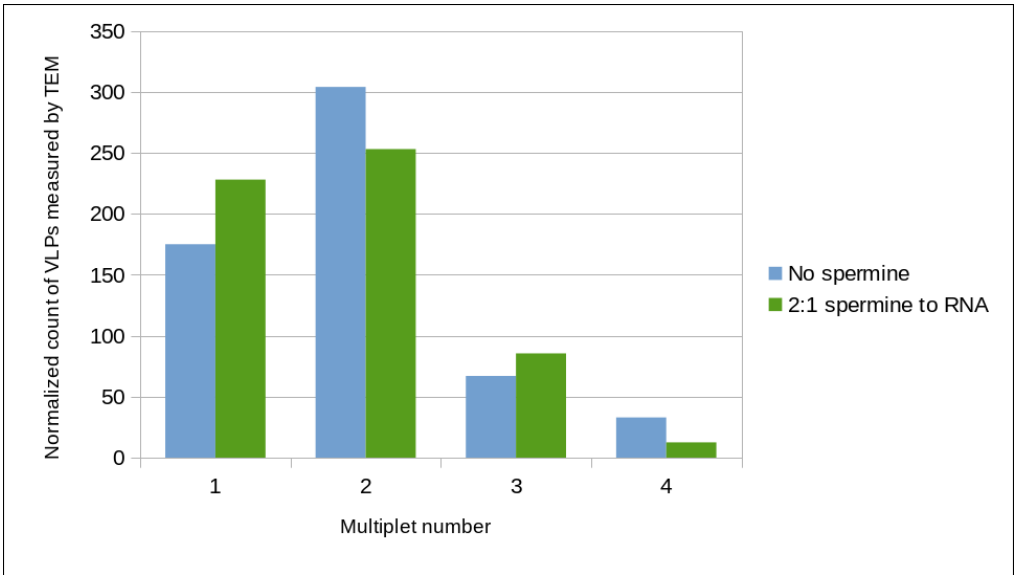


**Figure 5.** B1B3 RNA at 30 nM concentration is pre-compacted with or without 24 micromolar spermine in RNA assembly buffer pH 7.2 for 60 minutes at room

temperature. Sample was then incubated with 4.8 mass equivalents of BMV capsid protein for 30 minutes at room temperature then 1.1 M acetic acid was added to a final self-assembly reaction concentration of 0.01 M. Samples are then diluted 20 fold in VSB buffer and deposited onto a 400 mesh carbon- and parlodion coated copper grid and stained with 2% uranyl acetate for TEM imaging. Figure show results from particle picking (For 2:1 spermine to RNA charge ratio VLP assemblies, number of capsid species counted was = 508, for no spermine assemblies 579 singlet and multiplet species were counted). Plotted is the amount of singlet, doublet, triplet and quadruplet particles that *appear* in the resultant TEM images. Y-axis is normalized to account for difference between total number of particles picked between control and spermine experimental conditions (so what appears is a normalization of 579/508 multiplied to each number counted in the 2:1 spermine sample).

**Discussion**

In solutions of high polyvalent cation concentration, dsDNA undergoes a first-order phase-transition-like event that causes the DNA to spontaneously compact into tightly-wound toroids. In this study, we have begun to examine the effects of polyvalent cations on long ssRNAs and compare the profile of ssRNAs vs dsDNAs in the presence of spermine concentrations. Unlike dsDNA, ssRNA does not undergo a DNA condensation-like transition, and instead compacts continuously in the presence of spermine. The compaction of ssRNA under increasing spermine conditions can be seen from the continuous curves measured from analytical ultracentrifugation and dynamic light scattering.

ssRNA has a very different secondary and tertiary structure than dsDNA because of ssRNA's ability to fold and base pair with itself while retaining some single-stranded character with "stem loops" terminating double-stranded "stem" regions and "bulges" acting as junctions/branch points of the RNA secondary structure. dsDNA has a persistence length of ~150 bp, and when significantly long dsDNA (>20,000 bp) is in the presence of sufficiently high amounts of polyvalent cation, the rigid and highly negatively charged nature of the DNA can be overcome resulting in curved and condensed toroidal form of the DNA which is thermodynamically favored due to hexagonal close packing of the DNA strands present in the DNA toroid. DNA condensation is a result of the onset of an effective self-attraction of different parts of the dsDNA molecule that are mediated by the polyvalent cation "bridging" the DNA strands, in addition to screening the self-repulsion of the dsDNA and forcing the DNA into a curved state.

Though RNA does not condense, the spermine has a significant effect on the sedimentation coefficient of the RNA. The sedimentation coefficient of the 4:1 spermine:RNA charge is about 2.5 times greater than the sedimentation coefficient of the RNA on its own.

ssRNA has a much shorter persistence length than DNA, is a more flexible molecule, and can be treated as a branched polymer because of its secondary structure. When ssRNA folds in on itself, it forms rigid regions in the structure, called duplexes, that are about 5-10 base pairs in length, and single-stranded loops. The duplex length may not be sufficiently long to promote the same sort of energetically favorable condensed state in RNA as in DNA. Additionally, spermine may bind

differently to *short* duplexed RNA than to *short* duplexed DNA such that condensation effects by polyvalent cations are not observed (Katz *et al.* [92]). For long enough, normal composition ssRNA (i.e. RNA with ranges of 15-30% composition of each base, not possessing long tracts of single base regions), its secondary structure will be presented that exists in about 50% single-stranded and 50% in base paired form.[97] Because of this, the RNA's compact properties and interactions with spermine and with its self-interactions are fundamentally different from dsDNA and spermine. We argue that RNA is being compacted at a single-molecule level; this is partially due to the decrease in self-repulsion with the adsorbed spermine playing this role, along with the RNA-spermine complex becoming more dense and less mobile, as the spermine makes the RNA less prone to fluctuations from the thermal energy accessible in the system, therefore contributing to its compact state.

## Chapter 7

## Summary

Our studies have elucidated how virus-host interactions occur *in vitro* with regard to a co-translational delivery mechanism whereby the genome of positive-sense-RNA virus is made accessible to the ribosomal machinery without necessarily being accompanied by disassembly of the protective capsid. We have done this with a combination of in vitro (cell-free) translation measurements, and two different “fishing” experiments in which the 5’-end of the packaged RNA genome is caught fluctuating outside its capsid: in the first case the RNA end is biotinylated so that it will be bound by streptavidin outside the capsid, and in the second case the 5’-capped end is bound by purified initiation factor proteins. We have also prepared virus-like particles in which capsid protein self-assembles around the viral RNA with its 5’-end constrained to be outside the capsid by a long complementary oligo; using the resulting duplex as a handle, we have performed single-particle magnetic tweezer experiments in which the

force required to pull the RNA out of its capsid is measured as a function of length. These results provide preliminary confirmation for the possibility of a virus remaining intact until it can hand over its ready-to-translate RNA genome to the protection of the ribosomal machinery that will synthesize its protein gene products. All of the experiments involve contribute to understanding how RNA viruses have evolved to balance the need for capsid stability – to ensure *protection* of the genome, with the equally important need for capsid *in*stability – to ensure *accessibility* of the genome to its host's ribosomal machinery. Intriguingly, this may help us understand new ways to combat RNA viruses by inhibiting initial translation of their genomes from within the capsid.

We hope in future studies to complete characterization of the fluctuation of viral RNA out of its capsid by translation initiation factors, using structural methods like CryoEM to reveal the details of this dynamical interaction. Further, our studies addressing the conformational state of the RNA in the capsid – including the use of polyvalent cations to pre-compactify the RNA before the *in vitro* self-assembly procedure – opens up possibilities for the packaging of larger amounts of genetic information in virus-like particles formed from the capsid protein of CCMV and BMV. We posit that this method will provide an important platform for research groups and gene delivery companies looking for effective ways to package RNA genes in "clean", monodisperse, biocompatible, protective (protein) cages.

## Bibliography


1. Gelbart WM, Knobler CM. Pressurized Viruses. *Science*. 2009;323(5922):1682-1683. doi:10.1126/science.1170645

2. Bancroft JB, Hiebert E. Formation of an infectious nucleoprotein from protein and nucleic acid isolated from a small spherical virus. *Virology*. 1967;32(2):354-356. doi:10.1016/0042-6822(67)90284-X

3. Bancroft JB, Hills GJ, Markham R. A study of the self-assembly process in a small spherical virus formation of organized structures from protein subunits in vitro. *Virology*. 1967;31(2):354-379. doi:10.1016/0042-6822(67)90180-8

4. Fraenkel-Conrat H, Williams RC. RECONSTITUTION OF ACTIVE TOBACCO MOSAIC VIRUS FROM ITS INACTIVE PROTEIN AND NUCLEIC ACID COMPONENTS. *Proc Natl Acad Sci*. 1955;41(10):690-698. doi:10.1073/pnas.41.10.690

5. Takahashi WN, Ishii M. The formation of rod-shaped particles resembling tobacco mosaic virus by polymerization of a protein from mosaic- diseased tobacco leaves . *Phytopathology*. 1952;42:690-691.

6. Canady MA, Tsuruta H, Johnson JE. Analysis of rapid, large-scale protein quaternary structural changes: time-resolved X-ray solution scattering of Nudaurelia capensis ω virus (NωV) maturation. *J Mol Biol*. 2001;311(4):803-814. doi:10.1006/jmbi.2001.4896

7. Cadena-Nava RD, Comas-Garcia M, Garmann RF, Rao ALN, Knobler CM, Gelbart WM. Self-Assembly of Viral Capsid Protein and RNA Molecules of Different Sizes: Requirement for a Specific High Protein/RNA Mass Ratio. *J Virol*. 2012;86(6):3318-3326. doi:10.1128/JVI.06566-11

8. Biddlecome A, Habte HH, McGrath KM, et al. Delivery of self-amplifying RNA vaccines in in vitro reconstituted virus-like particles. *PLOS ONE*. 2019;14(6):e0215031. doi:10.1371/journal.pone.0215031

9. Restrepo-Hartwig MA, Ahlquist P. Brome Mosaic Virus Helicase- and Polymerase-Like Proteins Colocalize on the Endoplasmic Reticulum at Sites of Viral RNA Synthesis. *J VIROL*. 1996;70:9.

10. Smirnyagina E, Lin NS, Ahlquist P, Virol J. The polymerase-like core of brome mosaic virus 2a protein, lacking a region interacting with viral 1a protein in vitro, maintains activity and 1a selectivity in RNA replication. *J VIROL*.:9.

11. Rao ALN. Molecular Studies on Bromovirus Capsid Protein III. Analysis of Cell-to-Cell Movement Competence of Coat Protein Defective Variants of Cowpea Chlorotic Mottle Virus. :11.

12. Bamunusinghe D, Seo J-K, Rao ALN. Subcellular Localization and Rearrangement of Endoplasmic Reticulum by Brome Mosaic Virus Capsid Protein. *J Virol*. 2011;85(6):2953-2963. doi:10.1128/JVI.02020-10

13. Speir JA, Munshi S, Wang G, Baker TS, Johnson JE. Structures of the native and swollen forms of cowpea chlorotic mottle virus determined by X-ray crystallography and cryo-electron microscopy. *Structure*. 1995;3:63-78.

14. Wilson TMA. Cotranslational disassembly of tobacco mosaic virus in vitro. *Virology*. 1984;137(2):255-265. doi:10.1016/0042-6822(84)90217-4

15. Roenhorst JW, Verduin BJM, Goldbach RW. Virus-ribosome complexes from cell-free translation systems supplemented with cowpea chlorotic mottle virus particles. *Virology*. 1989;168(1):138-146. doi:10.1016/0042-6822(89)90412-1

16. Bakker SE, Ford RJ, Barker AM, et al. Isolation of an Asymmetric RNA Uncoating Intermediate for a Single-Stranded RNA Plant Virus. *J Mol Biol*. 2012;417(1-2):65-78. doi:10.1016/j.jmb.2012.01.017

17. Garmann RF, Sportsman R, Beren C, Manoharan VN, Knobler CM, Gelbart WM. A Simple RNA-DNA Scaffold Templates the Assembly of Monofunctional Virus-Like Particles. *J Am Chem Soc*. 2015;137(24):7584-7587. doi:10.1021/jacs.5b03770

18. Krupovic M, Koonin EV. Multiple origins of viral capsid proteins from cellular ancestors. *Proc Natl Acad Sci*. 2017;114(12):E2401-E2410. doi:10.1073/pnas.1621061114

20. Rose AS, Bradley AR, Valasatava Y, Duarte JM, Prlić A, Rose PW. NGL viewer: web-based molecular graphics for large complexes. Valencia A, ed. *Bioinformatics*. 2018;34(21):3755-3758. doi:10.1093/bioinformatics/bty419

21. Tama F, Brooks CL. The Mechanism and Pathway of pH Induced Swelling in Cowpea Chlorotic Mottle Virus. *J Mol Biol*. 2002;318(3):733-747. doi:10.1016/S0022-2836(02)00135-3

22. Gopal A, Zhou ZH, Knobler CM, Gelbart WM. Visualizing large RNA molecules in solution. *RNA*. 2012;18(2):284-299. doi:10.1261/rna.027557.111

23. Brisco M, Hull R, Wilson TMA. Swelling of isometric and of bacilliform plant virus nucleocapsids is required for virus-specific protein synthesis in vitro. *Virology*. 1986;148(1):210-217. doi:10.1016/0042-6822(86)90416-2

24. Caspar DL, Klug A. Physical principles in the construction of regular viruses. *Cold Spring Harb Symp Quant Biol*. 1962;27:1-24. doi:10.1101/sqb.1962.027.001.005

25. Hinnebusch AG. The scanning mechanism of eukaryotic translation initiation. *Annu Rev Biochem*. 2014;83:779-812. doi:10.1146/annurev-biochem-060713-035802

26. Mayberry LK, Dennis MD, Leah Allen M, et al. Expression and Purification of Recombinant Wheat Translation Initiation Factors eIF1, eIF1A, eIF4A, eIF4B, eIF4F, eIF(iso)4F, and eIF5. In: *Methods in Enzymology*. Vol 430. Elsevier; 2007:397-408. doi:10.1016/S0076-6879(07)30015-3

27. Friedland DE, Wooten WNB, LaVoy JE, Hagedorn CH, Goss DJ. A Mutant of Eukaryotic Protein Synthesis Initiation Factor eIF4E $_{K119A}$ Has an Increased Binding Affinity for both m $^{7}$ G Cap Analogues and eIF4G Peptides $^{\dagger}$. *Biochemistry*. 2005;44(11):4546-4550. doi:10.1021/bi047645m

28. Niedzwiecka A, Marcotrigiano J, Stepinski J, et al. Biophysical Studies of eIF4E Cap-binding Protein: Recognition of mRNA 5′ Cap Structure and Synthetic Fragments of eIF4G and 4E-BP1 Proteins. *J Mol Biol*. 2002;319(3):615-635. doi:10.1016/S0022-2836(02)00328-5

29. Ma W, Saccardo A, Roccatano D, et al. Modular assembly of proteins on nanoparticles. *Nat Commun*. 2018;9(1):1489. doi:10.1038/s41467-018-03931-4

30. Garmann RF, Comas-Garcia M, Gopal A, Knobler CM, Gelbart WM. The Assembly Pathway of an Icosahedral Single-Stranded RNA Virus Depends on the Strength of Inter-Subunit Attractions. *J Mol Biol*. 2014;426(5):1050-1060. doi:10.1016/j.jmb.2013.10.017

31. Alam SB, Rochon D. Evidence that Hsc70 Is Associated with Cucumber Necrosis Virus Particles and Plays a Role in Particle Disassembly. Simon AE, ed. *J Virol*. 2017;91(2):e01555-16, /jvi/91/2/e01555-16.atom. doi:10.1128/JVI.01555-16

32. Pitulle C, Kleineidam RG, Sproat B, Krupp G. Initiator oligonucleotides for the combination of chemical and enzymatic RNA synthesis. *Gene*. 1992;112(1):101-105. doi:10.1016/0378-1119(92)90309-D

33. Lee J, Vogt CE, McBrairty M, Al-Hashimi HM. Influence of Dimethylsulfoxide on RNA Structure and Ligand Binding. *Anal Chem*. 2013;85(20). doi:10.1021/ac402038t

34. Douglas T. Viruses: Making Friends with Old Foes. *Science*. 2006;312(5775):873-875. doi:10.1126/science.1123223

35. Liepold L, Anderson S, Willits D, et al. Viral capsids as MRI contrast agents. *Magn Reson Med*. 2007;58(5):871-879. doi:10.1002/mrm.21307

36. Prasuhn, Jr. DE, Yeh RM, Obenaus A, Manchester M, Finn MG. Viral MRI contrast agents: coordination of Gd by native virions and attachment of Gd complexes by azide–alkyne cycloaddition. *Chem Commun*. 2007;(12):1269-1271. doi:10.1039/B615084E

37. Malyutin AG, Easterday R, Lozovyy Y, et al. Viruslike Nanoparticles with Maghemite Cores Allow for Enhanced MRI Contrast Agents. *Chem Mater*. 2015;27(1):327-335. doi:10.1021/cm504029j

38. Datta A, Hooker JM, Botta M, Francis MB, Aime S, Raymond KN. High Relaxivity Gadolinium Hydroxypyridonate−Viral Capsid Conjugates: Nanosized MRI Contrast Agents [1]. *J Am Chem Soc*. 2008;130(8):2546-2552. doi:10.1021/ja0765363

39. Wu M, Sherwin T, Brown WL, Stockley PG. Delivery of antisense oligonucleotides to leukemia cells by RNA bacteriophage capsids. *Nanomedicine Nanotechnol Biol Med*. 2005;1(1):67-76. doi:10.1016/j.nano.2004.11.011

40. Wu M, Brown WL, Stockley PG. Cell-Specific Delivery of Bacteriophage-Encapsidated Ricin A Chain. *Bioconjug Chem*. 1995;6(5):587-595. doi:10.1021/bc00035a013

41. Brown WL, Mastico RA, Wu M, et al. RNA Bacteriophage Capsid-Mediated Drug Delivery and Epitope Presentation. *Intervirology*. 2002;45(4-6):371-380. doi:10.1159/000067930

42. Destito G, Yeh R, Rae CS, Finn MG, Manchester M. Folic Acid-Mediated Targeting of Cowpea Mosaic Virus Particles to Tumor Cells. *Chem Biol*. 2007;14(10):1152-1162. doi:10.1016/j.chembiol.2007.08.015

43. Azizgolshani O, Garmann RF, Cadena-Nava R, Knobler CM, Gelbart WM. Reconstituted plant viral capsids can release genes to mammalian cells. *Virology*. 2013;441(1):12-17. doi:10.1016/j.virol.2013.03.001

44. Aljabali AAA, Shukla S, Lomonossoff GP, Steinmetz NF, Evans DJ. CPMV-DOX Delivers. *Mol Pharm*. 2013;10(1):3-10. doi:10.1021/mp3002057

45. Wang Q, Lin T, Johnson JE, Finn MG. Natural Supramolecular Building Blocks. *Chem Biol*. 2002;9(7):813-819. doi:10.1016/S1074-5521(02)00166-7

46. Dixit SK, Goicochea NL, Daniel M-C, et al. Quantum Dot Encapsulation in Viral Capsids. *Nano Lett*. 2006;6(9):1993-1999. doi:10.1021/nl061165u

47. Kostiainen MA, Kasyutich O, Cornelissen JJLM, Nolte RJM. Self-assembly and optically triggered disassembly of hierarchical dendron–virus complexes. *Nat Chem*. 2010;2(5):394-399. doi:10.1038/nchem.592

48. Chen C, Daniel M-C, Quinkert ZT, et al. Nanoparticle-Templated Assembly of Viral Protein Cages. *Nano Lett*. 2006;6(4):611-615. doi:10.1021/nl0600878

49. Maye MM. En route to patchy superlattices. *Nat Nanotechnol*. 2013;8(1):5-6. doi:10.1038/nnano.2012.244

50. Strable E, Finn MG. Chemical Modification of Viruses and Virus-Like Particles. In: Manchester M, Steinmetz NF, eds. *Viruses and Nanotechnology*. Vol 327. Berlin, Heidelberg: Springer Berlin Heidelberg; 2009:1-21. doi:10.1007/978-3-540-69379-6_1

51. Patel KG, Swartz JR. Surface Functionalization of Virus-Like Particles by Direct Conjugation Using Azide−Alkyne Click Chemistry. *Bioconjug Chem*. 2011;22(3):376-387. doi:10.1021/bc100367u

52. Pokorski JK, Steinmetz NF. The Art of Engineering Viral Nanoparticles. *Mol Pharm*. 2011;8(1):29-43. doi:10.1021/mp100225y

53. Pokorski JK, Breitenkamp K, Liepold LO, Qazi S, Finn MG. Functional Virus-Based Polymer–Protein Nanoparticles by Atom Transfer Radical Polymerization. *J Am Chem Soc*. 2011;133(24):9242-9245. doi:10.1021/ja203286n

54. Gupta SS, Raja KS, Kaltgrad E, Strable E, Finn MG. Virus–glycopolymer conjugates by copper(i) catalysis of atom transfer radical polymerization and azide–alkyne cycloaddition. *Chem Commun*. 2005;(34):4315. doi:10.1039/b502444g

55. Smith JC, Lee K-B, Wang Q, et al. Nanopatterning the Chemospecific Immobilization of Cowpea Mosaic Virus Capsid. *Nano Lett*. 2003;3(7):883-886. doi:10.1021/nl025956h

56. Steinmetz NF, Lomonossoff GP, Evans DJ. Cowpea Mosaic Virus for Material Fabrication: Addressable Carboxylate Groups on a Programmable Nanoscaffold. *Langmuir*. 2006;22(8):3488-3490. doi:10.1021/la060078e

57. Blum AS, Soto CM, Wilson CD, et al. Cowpea Mosaic Virus as a Scaffold for 3-D Patterning of Gold Nanoparticles. *Nano Lett*. 2004;4(5):867-870. doi:10.1021/nl0497474

58. Young M, Debbie W, Uchida M, Douglas T. Plant Viruses as Biotemplates for Materials and Their Use in Nanotechnology. *Annu Rev Phytopathol*. 2008;46(1):361-384. doi:10.1146/annurev.phyto.032508.131939

59. Gillitzer E, Willits D, Young M, Douglas T. Chemical modification of a viral cage for multivalent presentation. *Chem Commun*. 2002;(20):2390-2391. doi:10.1039/b207853h

60. Raja KS, Wang Q, Gonzalez MJ, Manchester M, Johnson JE, Finn MG. Hybrid virus-polymer materials. 1. Synthesis and properties of PEG-decorated cowpea mosaic virus. *Biomacromolecules*. 2003;4(3):472-476. doi:10.1021/bm025740+

61. Klem MT, Willits D, Young M, Douglas T. 2-D Array Formation of Genetically Engineered Viral Cages on Au Surfaces and Imaging by Atomic Force Microscopy. *J Am Chem Soc*. 2003;125(36):10806-10807. doi:10.1021/ja0363718

62. Suci PA, Kang S, Young M, Douglas T. A Streptavidin−Protein Cage Janus Particle for Polarized Targeting and Modular Functionalization. *J Am Chem Soc*. 2009;131(26):9164-9165. doi:10.1021/ja9035187

63. Li F, Chen Y, Chen H, et al. Monofunctionalization of Protein Nanocages. *J Am Chem Soc*. 2011;133(50):20040-20043. doi:10.1021/ja207276g

64. Stephanopoulos N, Liu M, Tong GJ, et al. Immobilization and One-Dimensional Arrangement of Virus Capsids with Nanoscale Precision Using DNA Origami. *Nano Lett*. 2010;10(7):2714-2720. doi:10.1021/nl1018468

65. Rothemund PWK. Folding DNA to create nanoscale shapes and patterns. *Nature*. 2006;440(7082):297-302. doi:10.1038/nature04586

66. Strable E, Johnson JE, Finn MG. Natural Nanochemical Building Blocks: Icosahedral Virus Particles Organized by Attached Oligonucleotides. *Nano Lett*. 2004;4(8):1385-1389. doi:10.1021/nl0493850

67. Wang D, Capehart SL, Pal S, et al. Hierarchical Assembly of Plasmonic Nanostructures Using Virus Capsid Scaffolds on DNA Origami Templates. *ACS Nano*. 2014;8(8):7896-7904. doi:10.1021/nn5015819

68. Rogers WB, Manoharan VN. Programming colloidal phase transitions with DNA strand displacement. *Science*. 2015;347(6222):639-642. doi:10.1126/science.1259762

69. Mirkin CA, Letsinger RL, Mucic RC, Storhoff JJ. A DNA-based method for rationally assembling nanoparticles into macroscopic materials. *Nature*. 1996;382(6592):607-609. doi:10.1038/382607a0

70. Pfeiffer P, Herzog M, Hirth L. Stabilization of Brome Mosaic Virus. *Philos Trans R Soc B Biol Sci*. 1976;276(943):99-107. doi:10.1098/rstb.1976.0100

71. Mukherjee S, Pfeifer CM, Johnson JM, Liu J, Zlotnick A. Redirecting the Coat Protein of a Spherical Virus to Assemble into Tubular Nanostructures. *J Am Chem Soc*. 2006;128(8):2538-2539. doi:10.1021/ja056656f

72. Cherry Bomb. https://en.wikipedia.org/wiki/Cherry_bomb.

73. Hurst SJ, Lytton-Jean AKR, Mirkin CA. Maximizing DNA Loading on a Range of Gold Nanoparticle Sizes. *Anal Chem*. 2006;78(24):8313-8318. doi:10.1021/ac0613582

74. Jung S, Yi H. An Integrated Approach for Enhanced Protein Conjugation and Capture with Viral Nanotemplates and Hydrogel Microparticle Platforms via Rapid Bioorthogonal Reactions. *Langmuir*. 2014;30(26):7762-7770. doi:10.1021/la501772t

75. Eber FJ, Eiben S, Jeske H, Wege C. Bottom-Up-Assembled Nanostar Colloids of Gold Cores and Tubes Derived From Tobacco Mosaic Virus. *Angew Chem Int Ed*. 2013;52(28):7203-7207. doi:10.1002/anie.201300834

76. Yi H, Rubloff GW, Culver JN. TMV Microarrays: Hybridization-Based Assembly of DNA-Programmed Viral Nanotemplates. *Langmuir*. 2007;23(5):2663-2667. doi:10.1021/la062493c

77. Hohn T. Role of RNA in the assembly process of bacteriophage fr. *J Mol Biol*. 1969;43(1):191-200. doi:10.1016/0022-2836(69)90088-6

78. Kler S, Wang JC-Y, Dhason M, Oppenheim A, Zlotnick A. Scaffold Properties Are a Key Determinant of the Size and Shape of Self-Assembled Virus-Derived Particles. *ACS Chem Biol*. 2013;8(12):2753-2761. doi:10.1021/cb4005518

79. Liu N, Peng B, Lin Y, et al. Pulling Genetic RNA out of Tobacco Mosaic Virus Using Single-Molecule Force Spectroscopy. *J Am Chem Soc*. 2010;132(32):11036-11038. doi:10.1021/ja1052544

80. Smith DE, Tans SJ, Smith SB, Grimes S, Anderson DL, Bustamante C. The bacteriophage φ29 portal motor can package DNA against a large internal force. *Nature*. 2001;413(6857):748-752. doi:10.1038/35099581

81. Annamalai P, Rao ALN. Replication-independent expression of genome components and capsid protein of brome mosaic virus in planta: A functional role for viral replicase in RNA packaging. *Virology*. 2005;338(1):96-111. doi:10.1016/j.virol.2005.05.013

82. Garmann RF, Comas-Garcia M, Koay MST, Cornelissen JJLM, Knobler CM, Gelbart WM. Role of Electrostatics in the Assembly Pathway of a Single-Stranded RNA Virus. *J Virol*. 2014;88(18):10472-10479. doi:10.1128/JVI.01044-14

83. Singh' I, Helenius A. Role of Ribosomes in Semliki Forest Virus Nucleocapsid Uncoating. *J VIROL*. 1992;66:10.

84. Qu X, Wen J-D, Lancaster L, Noller HF, Bustamante C, Tinoco I. The ribosome uses two active mechanisms to unwind messenger RNA during translation. *Nature*. 2011;475(7354):118-121. doi:10.1038/nature10126

85. Liu N, Chen Y, Peng B, et al. Single-Molecule Force Spectroscopy Study on the Mechanism of RNA Disassembly in Tobacco Mosaic Virus. *Biophys J*. 2013;105(12):2790-2800. doi:10.1016/j.bpj.2013.10.005

86. Strick T, Allemand J-F, Croquette V, Bensimon D. Twisting and stretching single DNA molecules. *Mol Biol*. 2000:26.

87. Chada N, Sigdel KP, Gari RRS, Matin TR, Randall LL, King GM. Glass is a Viable Substrate for Precision Force Microscopy of Membrane Proteins. *Sci Rep*. 2015;5(1):12550. doi:10.1038/srep12550

88. Schlingman DJ, Mack AH, Mochrie SGJ, Regan L. A new method for the covalent attachment of DNA to a surface for single-molecule studies. *Colloids Surf B Biointerfaces*. 2011;83(1):91-95. doi:10.1016/j.colsurfb.2010.11.002

89. Hunter JD. Matplotlib: A 2D Graphics Environment. *Comput Sci Eng*. 2007;9(3):90-95. doi:10.1109/MCSE.2007.55

90. Gosule LC, Schellman JA. Compact form of DNA induced by spermidine. *Nature*. 1976;259(5541):333-335. doi:10.1038/259333a0

91. Bloomfield VA. DNA condensation by multivalent cations. *Biopolymers*. 1997;44(3):269-282. doi:https://doi.org/10.1002/(SICI)1097-0282(1997)44:3<269::AID-BIP6>3.0.CO;2-T

92. Katz AM, Tolokh IS, Pabit SA, Baker N, Onufriev AV, Pollack L. Spermine Condenses DNA, but Not RNA Duplexes. *Biophys J*. 2017;112(1):22-30. doi:10.1016/j.bpj.2016.11.018

93. Kabir A, Suresh Kumar G. Targeting Double-Stranded RNA with Spermine, 1-Naphthylacetyl Spermine and Spermidine: A Comparative Biophysical Investigation. *J Phys Chem B*. 2014;118(38):11050-11064. doi:10.1021/jp5035294

94. Mitra S, Kaesberg P. Interaction of polyamines with turnip yellow mosaic virus RNA. *Biochem Biophys Res Commun*. 1963;11(2):146-151. doi:10.1016/0006-291X(63)90082-2

95. Cohen SS, Greenberg ML. Spermidine, an intrinsic component of turnip yellow mosaic virus. *Proc Natl Acad Sci*. 1981;78(9):5470-5474. doi:10.1073/pnas.78.9.5470

96. Raspaud E, Olvera de la Cruz M, Sikorav J-L, Livolant F. Precipitation of DNA by Polyamines: A Polyelectrolyte Behavior. *Biophys J*. 1998;74(1):381-393. doi:10.1016/S0006-3495(98)77795-1

97. Yoffe AM, Prinsen P, Gopal A, Knobler CM, Gelbart WM, Ben-Shaul A. Predicting the sizes of large RNA molecules. Proc Natl Acad Sci. 2008;105(42):16153-16158. doi:10.1073/pnas.0808089105

98. Russell DH, Buchrach U. Clinical Relevance of Polyamines. CRC Crit Rev Clin Lab Sci. 1982;18(3):261-311. doi:10.3109/10408368209085073